Mechanistic Models of Anti-HIV Microbicide Drug Delivery

by

Yajing Gao

Department of Biomedical Engineering
Duke University

Date:_____

Approved:

_____
David F. Katz, Supervisor

_____
Stefan Zauscher

_____
George A. Truskey

_____
Fan Yuan

_____
Kim A. Woodrow

Dissertation submitted in partial fulfillment of
the requirements for the degree of Doctor
of Philosophy in the Department of
Biomedical Engineering in the Graduate School
of Duke University

2016

ABSTRACT

Mechanistic Models of Anti-HIV Microbicide Drug Delivery

by

Yajing Gao

Department of Biomedical Engineering
Duke University

Date:_____

Approved:

_____
David F. Katz, Supervisor

_____
Stefan Zauscher

_____
George A. Truskey

_____
Fan Yuan

_____
Kim A. Woodrow

An abstract of a dissertation submitted in partial fulfillment of the requirements for the degree of Doctor of Philosophy in the Department of Biomedical Engineering in the Graduate School of Duke University

2016

Abstract

A new modality for preventing HIV transmission is emerging in the form of topical microbicides. Some clinical trials have shown some promising results of these methods of protection while other trials have failed to show efficacy. Due to the relatively novel nature of microbicide drug transport, a rigorous, deterministic analysis of that transport can help improve the design of microbicide vehicles and understand results from clinical trials. This type of analysis can aid microbicide product design by helping understand and organize the determinants of drug transport and the potential efficacies of candidate microbicide products.

Microbicide drug transport is modeled as a diffusion process with convection and reaction effects in appropriate compartments. This is applied here to vaginal gels and rings and a rectal enema, all delivering the microbicide drug Tenofovir. Although the focus here is on Tenofovir, the methods established in this dissertation can readily be adapted to other drugs, given knowledge of their physical and chemical properties, such as the diffusion coefficient, partition coefficient, and reaction kinetics. Other dosage forms such as tablets and fiber meshes can also be modeled using the perspective and methods developed here.

The analyses here include convective details of intravaginal flows by both ambient fluid and spreading gels with different rheological properties and applied

volumes. These are input to the overall conservation equations for drug mass transport in different compartments. The results are Tenofovir concentration distributions in time and space for a variety of microbicide products and conditions. The Tenofovir concentrations in the vaginal and rectal mucosal stroma are converted, via a coupled reaction equation, to concentrations of Tenofovir diphosphate, which is the active form of the drug that functions as a reverse transcriptase inhibitor against HIV. Key model outputs are related to concentrations measured in experimental pharmacokinetic (PK) studies, e.g. concentrations in biopsies and blood. A new measure of microbicide prophylactic functionality, the Percent Protected, is calculated. This is the time dependent volume of the entire stroma (and thus fraction of host cells therein) in which Tenofovir diphosphate concentrations equal or exceed a target prophylactic value, e.g. an EC_{50}.

Results show the prophylactic potentials of the studied microbicide vehicles against HIV infections. Key design parameters for each are addressed in application of the models. For a vaginal gel, fast spreading at small volume is more effective than slower spreading at high volume. Vaginal rings are shown to be most effective if inserted and retained as close to the fornix as possible. Because of the long half-life of Tenofovir diphosphate, temporary removal of the vaginal ring (after achieving steady state) for up to 24h does not appreciably diminish Percent Protected. However, full steady state (for the entire stromal volume) is not achieved until several days after ring

insertion. Delivery of Tenofovir to the rectal mucosa by an enema is dominated by surface area of coated mucosa and whether the interiors of rectal crypts are filled with the enema fluid. For the enema 100% Percent Protected is achieved much more rapidly than for vaginal products, primarily because of the much thinner epithelial layer of the mucosa. For example, 100% Percent Protected can be achieved with a one minute enema application, and 15 minute wait time.

Results of these models have good agreement with experimental pharmacokinetic data, in animals and clinical trials. They also improve upon traditional, empirical PK modeling, and this is illustrated here. Our deterministic approach can inform design of sampling in clinical trials by indicating time periods during which significant changes in drug concentrations occur in different compartments. More fundamentally, the work here helps delineate the determinants of microbicide drug delivery. This information can be the key to improved, rational design of microbicide products and their dosage regimens.

Contents

List of Tables

List of Figures

Acknowledgements

I would like to thank Dr. David Katz for his advice and support over the years. We have almost daily conversation about research, food, geography, and among other things Duke basketball. I would also like to thank my committee members, Dr. Stefan Zauscher, Dr. George Truskey, Dr. Fan Yuan, and Dr. Kim Woodrow for their guidance in completion of this dissertation.

Special thanks to members of the Katz lab, including perennial members Jennifer Peters, Michael DeSoto, and Marcus Henderson, all of whom have put up with me over the years. Especially Jenny who performed the rheological experiments, made wonderful illustrations, and kept the entire lab running. A number of undergraduate students have helped me with the project, Meng Kang, Sophia Chang, and Andrew Yuan, who is an expert at batch processing and plotting gigabytes of data. I also had great conversations and company with other cohorts who have worked in the lab, including Jason Chen, Cami Parrish, Tejen Shah, Melisa Kim, Debbie Xie, Andrew Lynch, Morgan Simons, Aubrey Presnell, and Alan Sze. And finally to the other Ph.D. students whose work this dissertation is based on. Sarah Kieweg for her work on squeezing flow and general gel rheology, Anthony Geonnotti for his model of Cyanovirin and work on the vaginal ring, Bonnie Lai for her model of viral transport in gels, and Oranat Chuchuen for her work on transport properties of Tenofovir.

I also would like to acknowledge the collaborators who have worked with me or whose work inspired this dissertation: Dr. Andrew Szeri with his lab members Su Chan Park, Savas Tasoglu, Kelsey MacMillan, and Claire Funke at UC Berkeley, for their work on the elastic squeezing flow problem; Dr. Kim Woodrow at the University of Washington for her work on creating drug delivering fiber meshes; Dr. Patrick Kiser at Northwestern University for his work on creating microbicide vaginal rings. Dr. Kate Guthrie at Brown University for her on user perception of vaginal gels; Dr. Lisa Rohan at University of Pittsburgh for her work on formulating microbicide gels; Dr. Anthony Ham at ImQuest BioSciences for his work on creating microbicide tablets; Dr. Craig Hendrix, Dr. Laura Ensign and their groups at Johns Hopkins University for their work on the DREAM project to create a microbicide containing rectal enema; Dr. Adam Wax and his lab at Duke University for creating the Confocal Raman method to measure Tenofovir transport; Dr. Lisa Rohan and Dr. Kuo Yang at UNC-Chapel Hill for their work on measuring Tenofovir through mass spec and PK modeling; Dr. Nick Cogan, Dr. Yousuff Hussaini, and Angela Jarrett at Florida State University for their collaborative work on creating a sensitivity analysis for the vaginal transport model.

My graduate study is possible with grants from NIH RO1 HD 072702 and U19 AI 077289. I would like to thank all the great teachers I've had for their knowledge and encouragement, in particular Dr. Myra Halpin who started my path in research. And finally thanks to my friends and family for their support in finishing this dissertation.

1. Introduction

Topical microbicides for women are important tools in the fight against the HIV epidemic. Products based on different drugs and delivery systems (e.g. gels, intravaginal rings, films and suppositories) are in various stages of development. Most Phase 3 trials of microbicide products have failed to date, and poor user adherence, indicating product use, has been a major factor attributed to such failures[44, 61]. There is evidence that a vaginal gel containing the antiretroviral drug Tenofovir can significantly reduce the sexual transmission rate of HIV provided it is applied as indicated and that greater adherence to the dosage regimen results in greater anti-HIV efficacy[45].

Microbicide product success is dependent on such adherence, together with satisfactory drug delivery by a product. It is striking that microbicide product design to date has been based almost entirely on empirical approaches to evaluate drug delivery. Overall, the prevailing philosophy has been to create products in which "more drug is better," provided the products are safe and stable. For vaginal microbicide gels (to date the most evaluated delivery system), gel volumes have been chosen to be as high as believed will be tolerated by users, and therefore, the failures of adherence for the recent microbicide gel trials were attributed in part to the messiness of these high volume gels.

As the microbicide field moves forward, it seeks to fill in gaps in the methods used in product conception, design and development. Deterministic mathematical

modeling of the microbicide drug delivery process can help fill one of these gaps. Modeling can relate properties of a microbicide product, together with those of its host environment and dosage regimen, to details of drug delivery, i.e. pharmacokinetics (PK) and pharmacodynamics (PD). Unfortunately there has been very little such modeling in the microbicide field, with the exception of the work undertaken in the Katz research group. The goal of this Ph.D. thesis is to extend and broaden this work, and to make it as relevant and usable as possible to the microbicide community overall. Previous studies in the Katz lab emphasized vaginal microbicide gels, and their spreading and coating of the vaginal mucosa in particular[52]. Only in the two instances was the mass transport of drugs analyzed: interacting co-diffusion of HIV virions and Cyanovirin molecules[29] (a lectin that binds key proteins on the viral envelope) and transport of Dapivirine (an antiretroviral reverse transcriptase inhibitor) from an intravaginal ring to the surface of the vaginal mucosa[28]. This work focuses on the mass transport of leading microbicide drug Tenofovir to the vaginal mucosa.

The first problem is a mathematical model of diffusion of Tenofovir from a gel coating layer down into the mucosal epithelium and the stroma (where Tenofovir primarily acts) and then into the bloodstream[25]. Results of this work provide an initial biophysical understanding of the roles played by drug transport properties and the histology of the host environment in drug delivery. Importantly, the model simulated

the measurement of drug concentrations obtained in a mucosal biopsy, which is a staple of PK studies. There are many limitations to the interpretation of the mass averaged concentration measured in a biopsy, and the model helps describe and interpret them. It was also applied to study effects of variation in the thickness of the epithelial layer, which occurs throughout the menstrual cycle.

The next problem is the role of gel spreading in Tenofovir delivery to the vaginal mucosal tissue. First, a model of the fluid mechanics of gel spreading process is created and accounts for the finite dimensions of the vaginal canal, the fact that one end is closed and the other is open (out from which gel leakage can be computed), and effects of different sites of gel insertion within the canal. Then gel spreading is incorporated into the Tenofovir mass transport model[26]. Further, the mechanism of Tenofovir (TFV) phosphorylation to Tenofovir diphosphate (TFV-DP) in mucosal cells is introduced, with a focus on the CD4+ host cells in the stroma that HIV can infect. TFV-DP is the bioactive form of TFV and has a much longer half-life than TFV. This conversion is a key characteristic of TFV and the model delineates its effect in lengthening the interval after gel insertion when HIV protection may occur. This analysis uses rheological data for three prototype microbicide gels[35] with differing compositions and rheological properties. Gel volume, the size of the vaginal canal, and the site of gel insertion are all varied in realistic ways that span the likely range of conditions in people. The results for

Tenofovir concentrations in the stromal mucosal layer were then referenced to target concentrations believed to be prophylactic against HIV (EC_{50} values that were measured *in vitro*). This analysis marks the first time that results for a PK model for a microbicide were translated to inferences about the resulting PD. Importantly, results of this model demonstrated that reducing vaginal microbicide gel volume does not necessarily compromise the predicted effectiveness of the gel.

Then, the next problem is analysis of Tenofovir delivery by an intravaginal ring (IVR), a type of drug delivery vehicle that is currently of great interest. While gel application would need to be episodic, or "on demand" in relation to sexual activity, delivery by an IVR (that remains within the vaginal canal for many weeks) would be continuous and, therefore, not coitally dependent. Notably, a contraceptive IVR (NuvaRing) is currently available commercially. This analysis addresses how characteristics of the IVR (most importantly its drug release rate) together with characteristics of the vaginal environment (dimensions of the canal, thickness of the epithelial layer, presence and flow of vaginal fluid) govern Tenofovir delivery and also effectiveness against HIV.

In addition to the vagina, sexual transmission of HIV can occur in the rectum. There is increasing interest in rectal application of microbicides because many people, men who have sex with men (MSMs) and also heterosexual populations practice

receptive anal intercourse (RAI). Rectal gels and enemas are currently being developed to deliver microbicide drugs, and Tenofovir is the leading such drug. Thus, a model of microbicide distribution is created for drug delivery model in the rectum. The rectal anatomy and histology are quite different from those of the vagina. The rectal canal has an approximately circular cross sectional area while the vaginal lumen is flat, almost rectangular. More importantly, the rectal mucosal architecture is quite different. The vaginal epithelium is stratified squamous with multiple layers of cells, while the rectal epithelium is columnar and contains a single layer of cells. The rectal mucosa contains a mosaic of approximately cylindrical crypts and the epithelial layer warps around the surface with a thinner stroma below the epithelium compared with that of the vaginal mucosa. The model incorporates these rectal features and creates the first deterministic look at microbicide drug delivery in the rectum and how it compares with that in the vagina. The first analysis is for a rectal enema that creates a perfect coating of the rectal mucosa (similar to the first vaginal gel transport model developed here). Results so far demonstrate a much more rapid transport of Tenofovir in the rectal stroma. Enemas are attractive as a drug delivery modality because of their low viscosity, which would promote rapid spreading along the canal. However, a major factor in the success of an enema drug delivery system will be its retention time before expulsion. The initial results of the model show how important this retention time is to Tenofovir delivery.

1.1 Topical Microbicides and Modeling

Approximately 35 million people worldwide are infected with HIV[41], of whom 68% reside in Sub-Saharan Africa. Despite international programs in education and prevention, new infections continue to occur at an alarming rate. The epidemic disproportionally affects women, with 13 women infected for every 10 men[32]; this disparity is in part due to a higher risk of contracting HIV from receptive vaginal intercourse than from insertive vaginal intercourse(8 per 10,000 vs. 4 per 10,000). New methods of prevention are needed to curb the epidemic. Traditional education and prevention methods focus on safe sex practices such as abstinence, faithfulness and condom use[9]. Condom use has been a proven method for prevention of HIV; however, the choice of use is primarily contingent on the man, leaving the woman with little choice in protection[30]. Clearly, new methods of protection that can be used by women will lead to reduction in new HIV infections and will empower women to make their own choices about their sexual health.

Topical microbicides have emerged as a potential new tool in preventing new HIV infections[6, 42, 84]. Microbicides are delivered locally to tissue that will most likely be infected, and act by either neutralizing the virus before it enters host cells or by preventing the onset of infection in those cells[80, 95]. Candidate microbicides have had a disappointing record in clinical trials to date[44]. Success of a product in trials depends

upon good user adherence as well as good drug delivery. Poor user adherence has been attributed to failure in two recent trials[59, 73]. Further, there is a limited understanding of how properties of a product and its drug, the dosage regimen, and the host environment govern drug delivery. This is in part due to very limited modeling of the drug delivery process. In traditional compartmental PK modeling, the body is divided into simple homogeneous compartments, with transfer coefficients deduced by fitting the model to clinical data[91]. This approach is not compatible with the full biophysics and chemistry of microbicide mass transport and is inherently inaccurate for vaginal and rectal microbicide delivery. It does not give information on the efficacy of the microbicide, nor can it predict the effects of different delivery vehicles, dosage regimens or of physiological variability in the host environment.

Modeling of the microbicide mass transport process through a more mechanistic approach will help drug designers and manufacturers make more accurate and informed decisions in product design and evaluation. A mechanistic approach should use the underlying transport mechanisms such as fluid mechanics, diffusion, and chemical kinetics to build an accurate model of the drug delivery process.

1.2 Clinical Trials and Microbicide Delivery Vehicles

Currently there are several types of microbicide delivery vehicles proposed for delivery of drugs into the vagina. These include gels, rings, films, meshes, and

tablets[19]. In addition to delivering a pharmacokinetically active concentration to the local vaginal environment, the dosage forms need to be acceptable to women so that they will adhere to the prescribed dosage regimens[63]. The different dosage forms offer a range of drug loading and release rates, which will lead to a variety of design choices depending on the active pharmaceutical ingredient, desired dosage interval, and user preference.

Vaginal gels are the furthest along in terms of development, with multiple phase III trials already completed. The gels are usually composed of a hydrophilic polymer that is mostly water with the active pharmaceutical ingredient dissolved within the polymer network. The gel is then applied through an applicator once or twice per day to the vaginal canal. The first completed phase III trial[46], CAPRISA 004, instructed the women to use the gel before and after sex. The trial demonstrated that a 4 mL 1% Tenofovir gel is effective at preventing new HIV infections compared to the placebo. However a second trial[59], VOICE, which instructed the women to apply the same gel once a day, did not show protection compared with the placebo. A third trial involving Tenofovir, called FACTS, used the same dosage regimen as CAPRISA 004 but failed to show adequate protection[44]. As noted above, it is believed that failures in VOICE and FACTS were due, to a significant extent, to poor user adherence in those trials. Recent analyses of data from VOICE showed that for the subset of participants documented to

have applied the gel as instructed there was a significant reduction in sexually transmitted HIV[59]. This finding together with that from CAPRSIA 004 showed that greater efficacy in reduction of HIV transmission was associated with greater adherence to designated gel application[31].

Vaginal rings are another candidate dosage form for microbicide delivery. A number of rings are already approved for use as contraceptives[23]. The rings are made of a rubbery polymer with matrix of drug that can be delivered to the vaginal canal over an extended period of time, on the order of weeks to months[57]. Rings have the potential to be easy to use and long lasting, which will greatly increase user adherence. A recently completed study called ASPIRE showed promising results for a ring delivering the microbicide Dapivirine in reducing the incidence of new HIV infections[4]. Current studies are focusing on the design of rings to deliver multiple drugs over an extended period of time. These include rings that can deliver both a contraceptive as well as microbicide drug[16].

Films, suppositories, and fiber meshes are the other potential choices for microbicide delivery vehicles. Dissolving films containing microbicides have been shown to quickly release drugs that can reduce the rate of infection *in vitro[1, 36]*. Films may be preferable to gels because they will not leak, and their ease of use may lead to greater adherence[22]. Vaginal suppositories and tablets are another class of delivery

vehicles that are being evaluated in *in vivo* as well as in *in vitro* studies[17]. Fiber mesh microbicide delivery systems are also being developed[5, 11]. An attractive feature of them is that different drugs could be loaded into each fiber. By controlling fiber composition and drug loading, controlled asynchronous release of drugs could be achieved[12].

1.3 Active Pharmaceutical Ingredient in Microbicides

Active Pharmaceutical Ingredients (API) in microbicides can be divided into two sub groups based on their site of action. The first are API's that can disable the HIV virus on contact (i.e. within luminal fluids), and the second are API's that can inhibit viral attack by altering viral interactions with host cells in the body[84]. The first group includes surfactants, antibiotics, acidifying agents and lectins, all of which can disable the viral envelope on contact. The second group includes entry inhibitors, reverse-transcriptase inhibitors, protease inhibitors and integrase inhibitors. These act by either preventing viral entry, conversion of viral RNA to DNA, or subsequent intracellular viral replication.

The first large scale clinical trial of microbicides used nonoxynol-9, a surfactant that has been shown *in vitro* to disable HIV by disaggregating the lipid membrane. However, the trial was unsuccessful because it did not show increased protection against the virus. There is also evidence that a high incidence of vaginal ulcers from

using the surfactant caused an increase in infection[51]. Despite this early setback, other API's have emerged as good microbicide candidates through subsequent trials.

Reverse Transcriptase Inhibitors are once class of API's that have received the most attention for their microbicide properties. This class includes both nucleoside and non-nucleoside analogues that prevent viral RNA from being copied into DNA; this action stops the viral integration process and prevents infection in host cells. Studies have been conducted which showed a Tenofovir Gel[40], Dapivirine Ring[66], UC781 Gel[33], and MIV-150 Ring[82] as promising microbicide products. Clearly, the pharmacological success of these products depends on delivering their API's in sufficient concentrations to host cells in order to prevent infection.

1.3.1 Tenofovir as Microbicide

Tenofovir (TFV), a nucleoside analogue reverse transcriptase inhibitor, is one of the leading microbicide candidates. The most common form of Tenofovir is a pro-drug Tenofovir disoproxil fumarate (Viread) that is taken orally for treatment of HIV and hepatitis B. In its pure form, Tenofovir (Figure 1) is a relatively hydrophilic drug with LogP of 1.5. This allows the drug to dissolve easily in hydrogels and allows good drug delivery through the tissue[13]. The molecular weight of Tenofovir is 287 g/mol, a small molecule which could diffuse across cell membranes and also have a high diffusion coefficient driven by thermal energy from Stokes-Einstein theory.

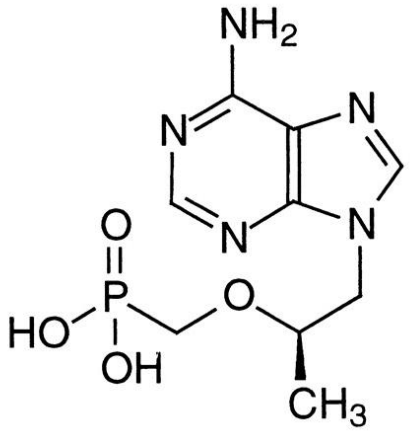

Figure 1: Molecular structure of Tenofovir.

In order to be pharmacokinetically active, a Tenofovir molecule will need to be phosphorylated twice within host cells to Tenofovir diphosphate (TFV-DP). Tenofovir diphosphate (Figure 2), and by extension Tenofovir, have many unique features that are attractive in microbicide applications. First, while TFV is free to move and is transported in and out of cells, TFV-DP cannot leave cells as readily. Second, TFV-DP has an extremely long intra-cellular half-life[38] on the order of days compared with TFV, which is on the order of hours. And third, despite the slow rate of decay, TFV-DP formation rate is surprisingly fast. The steady state level that is proportional to applied TFV concentration can be achieved a few hours after initial TFV dose[78]. The long half-life combined with the ability to stay within host cells, allow TFV-DP to stay active potentially many days after the initial dose. This retention will allow an easier dosing

schedule that people are more likely to follow compared to a more frequent dosage regimen.

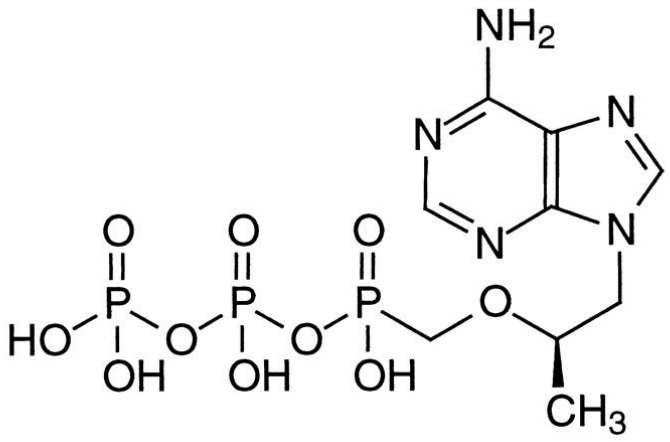

Figure 2: Molecular structure of Tenofovir diphosphate.

1.4 Vaginal Geometry

The human vaginal canal extends from the introitus to the fornix and ranges in length from 10 to 15 cm[7, 72]. In a resting state, the walls of the vaginal canal are collapsed, the width is around 2.5 cm, meaning that the cross section is approximately rectangular with height that is a few hundred microns in order to accommodate ambient vaginal fluid[69]. The walls of the canal exhibit an elastic squeezing force that is dependent on the local wall displacement from its resting state[49, 85, 88, 89]. This relationship is taken as linear. Consequently, gel insertion creates an elastic restoring force the total value of which is proportional to the applied gel volume. The modulus of

elasticity in the vaginal canal can be measured directly[62]. For example, a gel volume of 3.5 mL creates a squeezing force of about 1 lbf, or 4 Newtons.

The vaginal mucosa contains two layers, the epithelium and the stroma (Figure 3). The upper layer, epithelium contains stratified squamous epithelial cells with varying thickness depending on the phase of the menstrual cycle, which is typically around 200 microns[71]. The lower stroma layer contains connective tissue, vasculature, and host cells susceptible to HIV infection. It is typically about 2 to 3 mm thick[79]. The vasculature in the stroma is believed to be about 10% of the total volume. Drug delivered to the tissue will typically be cleared by this vasculature.

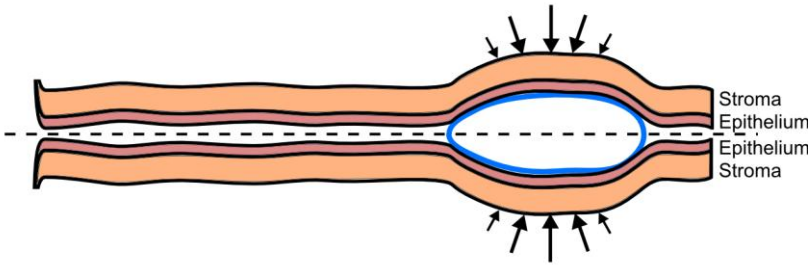

Figure 3: Vaginal geometry with introitus to the left and cervix to the right. The blue bolus is a gel with squeezing force indicated by arrows.

1.5 Pharmacokinetic Models

Traditional pharmacokinetic (PK) models use a black box compartment approach to predict drug concentration and distribution in the body[74, 91]. Drug concentration in each compartment is assumed to be homogeneous, with transfer coefficients and/or elimination coefficients. These coefficients are found by fitting experimental PK data to

the model, typically data from measurements for concentration vs. time in different compartments. For example, a number of experimental pharmacokinetic studies have been conducted for the Tenofovir gel[40, 78]. Data were processed to compute key, traditional PK parameters such as C_{max} (maximum concentration), t_{max} (time to maximum concentration), and AUC (area under the curve of concentration vs. time plot). Unfortunately, these compartmental models make many key assumptions that are not accurate in a complex vaginal delivery system[34]. The first is an assumption of first or zeroth order absorption of drug. This assumption is good for intravenous or some oral dosage forms, but might be too simple in other physiological models. The second is an assumption of instantaneously uniform distribution in each compartment. This assumption is good for small compartments or ones with active transport like the blood, but it fails for a large tissue compartment that does not equilibrate in a short period of time. The third assumption is first order transport kinetics between compartments. This behavior is often observed in homogeneous compartments that have well defined boundaries, but in the vaginal environment, our mechanistic modeling shows that both the second and third assumptions break down. In addition to the inaccuracies of the assumptions in the PK models, they are also limited by the fact that they contain many parameters that are difficult to measure directly even under controlled conditions, e.g. drug transport rates between interior compartments. These must be obtained, often as

part of multi-parametric data fitting from results of in vivo studies in animals and humans which can be full of uncontrolled variability (this has been a major limitation of microbicide PK studies).

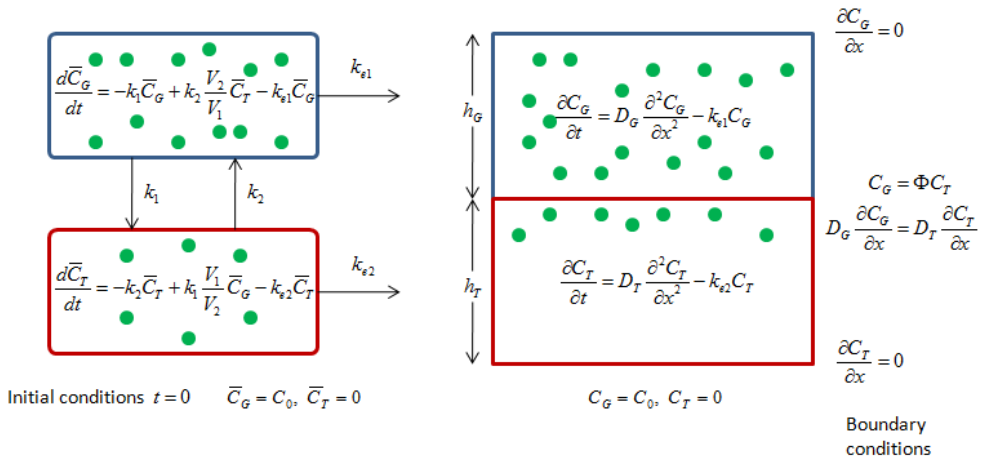

Figure 4: Diagram of classic PK model (left) and mechanistic PK model (right). The model is a simple two compartment one. It could characterize drug transport from a gel layer into a homogeneous tissue specimen.

Deterministic (or mechanistic) transport models that directly embody physical and chemical processes are inherently more accurate than the empirical compartmental models (Figure 4). They are not constrained by the assumptions used in classic PK models. Most of the parameters in the mechanistic models can be computed or measured directly. These models can give comparative and predictive power when dosage forms or anatomical dimensions change. Models of vaginal microbicide

transport will need to incorporate drug transport within multiple compartments, including the lumen, layers of the mucosa, and the circulatory system to capture a complete rendition of the drug delivery process. Mechanistic models can accomplish this.

1.5.1 Comparison between Classic and Mechanistic PK Model

A simple comparison can be made between the two models to show whether the approaches can yield similar results when modeling the same system. The mechanistic model with physically based parameters can be taken as the input to the empirical model. The output of the mechanistic model is a time and space dependent concentration profile. The result can then be averaged to yield the concentration in each compartment over time which can be fitted into the empirical model. In the simple two compartment model (Figure 4) the unknowns of the empirical model are the two internal kinetic transfer rates k_1 and k_2; the other parameters like volume and rates of elimination are the same as the mechanistic model. The unknowns are then fitted to the average concentrations here for the tissue compartment. The gel compartment is less interesting due to fast diffusion in the mechanistic model yielding an approximately homogeneous concentration distribution similar to the classic PK model. A fit to the two curves is achieved by the classic least squares method, which minimizes the sum of the squares of residual at each time point.

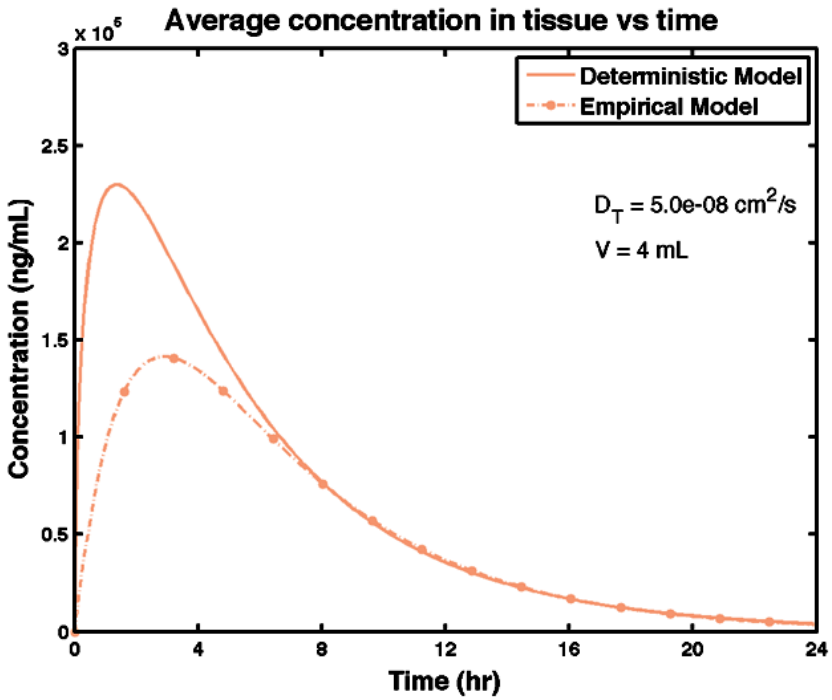

Figure 5: Classic PK (empirical) model fitted to mechanistic PK (deterministic) model in the tissue for a two compartment problem

The result of the comparison between the models is shown in (Figure 5). The two curves are fairly different due to the inability of the classic PK approach to model the deterministic problem. The two models fit well after approximately 7 hours, but the PK model fails to capture the behavior at short times, notably the peak concentration predicted by the classic PK model is 40% lower than the value predicted by the deterministic model.

1.5.2 Multivariate Optimization in Parameter Space (MOPS) Approach

One problem with using the classic least square approach is that what humans may perceive as being a good fit might be different than the normal approach in sum of the squares of residuals. As an alternative, the data can be fitted in the parameter space (for parameters k_1 and k_2) instead of the output data. This new method termed Multivariate Optimization in Parameter Space, or MOPS will attempt to minimize the distance between an ideal set of parameters k_1 and k_2 in the space for which the parameters exists.

For each time point there are two differential equations in the classic PK model and two unknowns k_1 and k_2. However, due to the mass transfer from gel to tissue being simply the negation of the transfer in the opposite direction, there is one degree of freedom, so if taking the equation for the tissue, the solution to the unknowns k_1 and k_2 form a linear subspace (Equation 1).

$$\frac{d\overline{C}_T}{dt} = -k_2 \overline{C}_T + k_1 \frac{V_1}{V_2} \overline{C}_G - k_{e2} \overline{C}_T$$

Equation 1

Note the equation above is valid for each time point. It involves taking the time derivative of concentration, which might not be feasible for real data that is sparse. In an ideal situation where the classic PK model fit perfectly with the mechanistic PK model,

the lines for the solution of k_1 and k_2 would be expected to cross at a single point. However, since the two models cannot agree exactly, there is no straight forward method of finding the best solution. Similar to the method of least square fit, the best solution can be defined as the one which minimizes the distance between the optimal solution and that of the lines in parameter space. The distance D between a point (x, y) and a line $ax + by + c = 0$ is given by (Equation 2).

$$D = \frac{|ax + by + c|}{\sqrt{a^2 + b^2}}$$

Equation 2

This method can be graphically represented below in (Figure 6). Each blue line is the line of possible solutions in parameter space k_1 and k_2 at each time point. The red dot is the optimized solution for which the sum of the distance to each line is minimized.

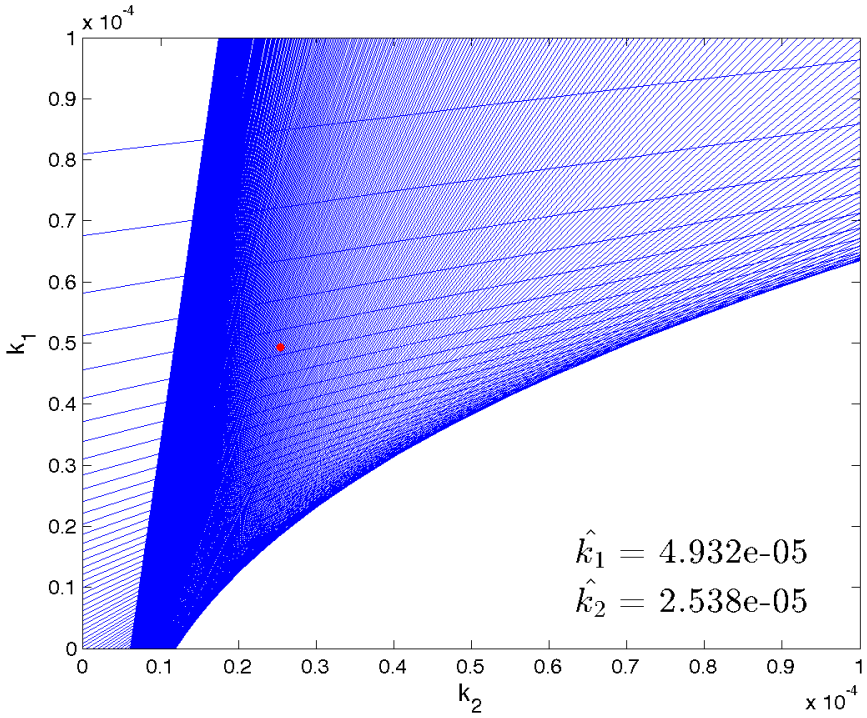

Figure 6: Graphical representation of MOPS approach, each line is possible solution at different time point, the red dot is the optimal solution.

The MOPS method can be scaled to other dimensions for problems with more than two compartments. In general, each additional compartment introduces two variables and one additional equation. Each set of equation can be separated where they define a line of the two particular transport parameter.

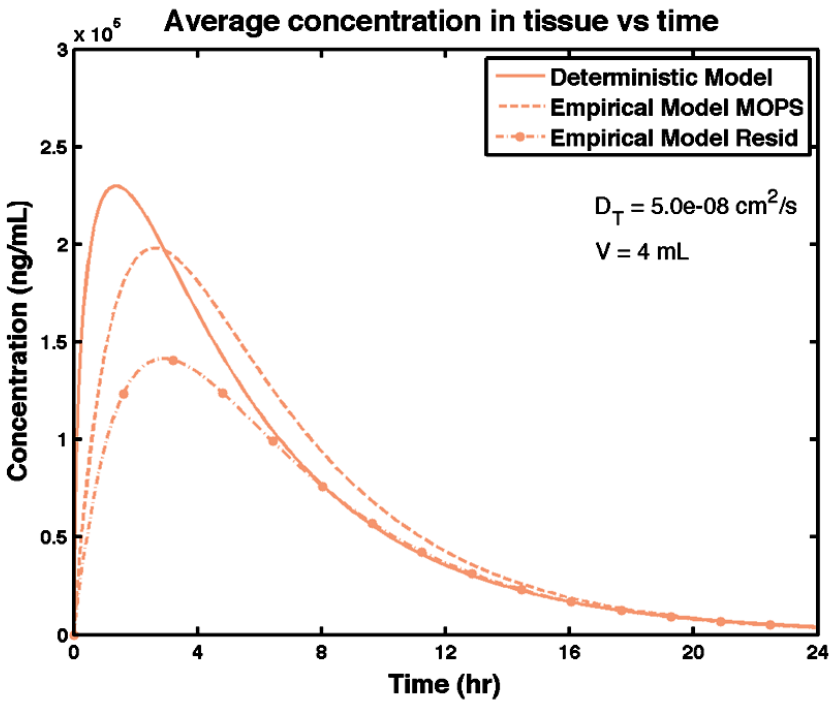

Figure 7: Comparison between a residual and MOPS fit to the empirical model with the deterministic model

The result of the MOPS approach can be compared with the least squares residual fit (Figure 7). This new approach more closely matches the classic PK measure C_{max}, t_{max} and AUC as well as a visually closer fit. This is partly due to human perception of distance between two lines as the orthogonal distance compared to the least square approach, which is a measure of the vertical distance. For lines that have a high slope like the initial rise in concentration of the PK curve, a perceptively close distance will have a large residual in the least squares approach.

1.6 Diffusion and Transport Theory

Diffusion is one of the most fundamental modes of drug transport. The transport of molecules can be thought of as being driven by a concentration gradient or as being based on the random motion caused by thermal energy. In both cases, a diffusion equation (Equation 3) can be derived for the concentration of particles or species over time and space[91]. Indeed the diffusion equation can be seen in various disciplines across science. In general, it describes any random non-specific movement of a species (usually chemical molecules or heat) over time. The diffusion equation is even found in the solution to the Schrödinger equation[65].

$$\frac{\partial C}{\partial t} = D\frac{\partial^2 C}{\partial x^2}$$

Equation 3

In the diffusion equation (Equation 3), the change of local concentration C over time t is proportional to the product of the diffusion coefficient D and the Laplacian of the concentration over space, e.g. x in one dimension. The concentration defined here and throughout the dissertation is a point variable, but it is also a local volume average over intracellular and extracellular drug. For example, tenofovir is found within and outside of cells, but its phosphorylation product Tenofovir diphosphate is only found inside cells. Our definition of concentration can be related to what is measured in a homogenized tissue biopsy, and this enables us to compare predictions of our modeling

with experimental PK data (see below). Because Tenofovir diphosphate is not found outside of cells, the value computed here is proportional to the local number density of cells. Values of Tenofovir diphosphate concentration that are prophylactic against HIV are obtained in various ways, and may reflect either intracellular or total tissue concentrations. By applying the simple proportionality between our predicted values of Tenofovir diphosphate concentrations within cells and in whole tissue, our results can be related to both types of measurements.

The diffusion coefficient can in principle vary in both time and space, but is generally assumed to be a constant in each medium over time. Once again, the diffusion coefficient here is defined as a point average value within each compartment. Transport through cells and around cells might occur at different rates, and the value here is an effective average of transport on a mini-macro scale. Computational estimates of the diffusion coefficient for a free molecule in a liquid medium can be made using Stokes Einstein theory (Equation 4).

$$D = \frac{kT}{6\pi\eta r}$$

Equation 4

In Equation 4, the diffusion coefficient D is given by the Boltzmann's constant k, the absolute temperature T, the viscosity of the liquid η, and the radius of the diffusing molecule r. Most of the variables in the equation can be easily determined. For

example, the viscosity of a liquid can be directly measured by a viscometer or rheometer, and for common liquids, it can also be found in a table (as a function of temperature). The radius of the molecule can be experimentally measured, e.g. via dynamic light scattering, but only for molecules that are larger than 10 nanometers. For smaller molecules, the radius can be estimated using computational chemistry models. The diffusion coefficient in media such as tissue can be estimated from permeability assays.

$$P = \frac{\Phi D}{\Delta x}$$

Equation 5

The permeability P of a membrane or any homogeneous material is related to the diffusion coefficient D by the partition coefficient Φ and the thickness of the membrane Δx (Equation 5). The partition coefficient here and throughout this thesis is defined between two compartments as the equilibrium ratio of the two concentration values at steady state. The diffusion coefficient can be derived by experimentally measuring the permeability and the partition coefficient. Permeability experiments contain two compartments, a donor and a receiver that sandwiched a membrane. If the donor and receiver compartments are sufficiently large, then at early times in the experiment, the transport across the membrane can be assumed to be at quasi steady state. The permeability of the membrane is then directly proportional to the diffusion

coefficient and inversely proportional to the thickness of the membrane. The partition coefficient is the ratio of solubility between the fluid compartment and the membrane. High solubility in the membrane equates to higher effective permeability. This approach to measuring the diffusion coefficient of molecules in tissue breaks down if the tissue is not homogeneous in the direction of drug transport. For example, if drug is diffusing through the layers of the epithelium and stroma (which have different structures), its rate of diffusion will be different in those two layers. This is not captured in a traditional permeability experiment. For our problem of microbicide drug transport into tissue, the Katz group is addressing this by developing and applying confocal Raman spectroscopy to measure drug concentration profiles in the epithelial and stromal layers of tissues[15]. Those data are processed to deduce diffusion and partition coefficients relevant to each layer[14].

Convection can also be an important factor in drug transport. In the vagina, vaginal fluid flow can give rise to a convective flow of drug. In the blood stream, convective transport is also significant. The Péctlet number given in Equation 6 is the ratio of transport by convection to the transport by diffusion. The Péctlet number Pe is defined by the quotient of the length scale l times the velocity v to the diffusion coefficient D. If the number is sufficiently larger than one, convection dominates; if it is less than one, then diffusion dominates.

$$Pe = \frac{lv}{D}$$

Equation 6

Drug transport between and within compartments can sometimes be modeled as kinetic rate processes. The most commonly used is the elimination of drug via the kidney or liver. The rates are usually first order, not only because they are the most often observed, but also because the kinetics are linear and captures the most salient features of the elimination process. Because first order kinetics is linear in concentration, as are both convective and diffusive transport, it can be useful in dimensional analysis of the problem and also can be used for more advanced methods such as linear time invariant systems theory.

1.7 Numerical Methods

Partial differential equations (PDE) that comprise the system of transport equations are difficult to solve directly. The two most common numerical methods are finite difference and finite element analysis. Finite element methods are typically used when tackling more complex geometry and need dedicated software packages to solve, while finite difference methods are for simpler problems and can be transformed to computationally simple forms.

Finite difference methods can be classified as either explicit or implicit. The explicit method computes the forward difference with respect to time using the solution

at the current time point. The implicit solution uses backward difference to solve the system of equations given by the unknown future time point. Explicit methods have the advantage of being faster, but might be numerically unstable, while implicit methods are computationally slower but always stable. Given that the diffusion equation is a parabolic PDE, and does not contain and singularities, the convergence criteria are well defined for the explicit method.

$$\frac{C_i^{n+1} - C_i^n}{\Delta t} = D\frac{C_{i+1}^n - 2C_i^n + C_{i-1}^n}{\Delta x^2}$$

Equation 7

The explicit finite difference method for the diffusion equation (Equation 3) is shown above (Equation 7). The concentration C has superscript indicating the time step, and subscript indicating the discretized position. The time derivative with time step Δt is equal to the diffusion coefficient D times the central difference of the second derivative with respect to spacing Δx. Using von Neumann stability analysis, this equation can be shown to be stable if the diffusion coefficient times the time step divided by the square of the spacing is less than or equal to one half (Equation 8).

$$\frac{D\Delta t}{\Delta x^2} \leq \frac{1}{2}$$

Equation 8

Numerically, the spacing of the points is typically fixed, while the time step varies to achieve the desired stability and convergence. Convergence can be tested by using incrementally smaller time steps. In order to find a convergent solution, typical time steps are orders of magnitude smaller. The finite difference method converts the PDE to a series of Ordinary Differential Equations (ODE), which can be solved numerically using MATLAB's built in ODE solver such as the Runge-Kutta 4,5 method. The Runge-Kutta method is an adaptive algorithm. The adaptive step size is attractive because it limits both the error by using smaller step sizes and can also speed up the algorithm when smaller step sizes are not needed.

The boundary conditions of the diffusion equation can be of three types. The first is a concentration boundary condition, the second a no flux boundary condition, and the third a continuous boundary condition. Concentration boundary conditions are used whenever the boundary is assumed to have a constant concentration. In the finite difference method, this condition can be implemented simply by setting once of the neighboring concentration values in Equation 7 to the boundary concentration. The no flux boundary is used when the drug is physically unable to pass through a barrier. The flux at the boundary is zero, so if this boundary condition is substituted in Equation 7 it is equivalent to setting both the right and left concentrations to the same value (Equation 9).

$$\frac{C_i^{n+1} - C_i^n}{\Delta t} = 2D \frac{C_{i+1}^n - C_i^n}{\Delta x^2}$$

Equation 9

The continuous boundary condition for an internal boundary between two compartments is more complex. The boundary has to satisfy two conditions: first there is equal flux in and out of both compartments. And second the concentrations at the boundary are related by the partition coefficient between them. The solution is similar to the concentration boundary condition, except the concentration at the boundary is recomputed at each time step.

$$C_{i+1} = \frac{\frac{D_1 C_{i-1}}{\Delta x_1} + \frac{D_2 C_{j+1}}{\Delta x_2}}{\frac{\Phi D_1}{\Delta x_1} + \frac{D_2}{\Delta x_2}} \qquad \text{(a)}$$

$$C_{j-1} = \frac{\frac{D_1 C_{i-1}}{\Delta x_1} + \frac{D_2 C_{j+1}}{\Delta x_2}}{\frac{D_1}{\Phi \Delta x_1} + \frac{D_2}{\Delta x_2}} \qquad \text{(b)}$$

Equation 10

The concentration values used for calculating the differential equation at points C_i of the first compartment and C_j of the second compartment are in Equation 10. The diffusion coefficient and the spacing for each compartments are $D_1, D_2,$ and $\Delta x_1,\ \Delta x_2$. The partition coefficient between C_{i+1} and C_{j-1} is Φ.

2. Mass Transport of Drug in the Vaginal Mucosa

2.1 Introduction

Vaginal gels are currently the leading dosage form for the delivery of microbicides for women. The success of these products will depend on both good user adherence and the ability of the product to deliver a prophylactic amount of drug to the intended target in the appropriate time frame. The first phase III trial (CAPRISA 004) of a microbicide gel loaded with 1% Tenofovir showed a reduction in new HIV infections[46]. However two follow-up trials (VOICE and FACTS)[44, 59] both showed negative result in the ability to reduce infection. One major difference between the trials is the recommended dosing protocol, while CAPRISA 004 and FACTS used a before and after sex dosing, the VOICE trial suggested a daily dosage regimen. Of course the difference in dosing protocol cannot completely explain the results of these trials, as CAPRISA 004 was successful while FACTS failed both with the same before and after sex dosage regimen. The failure of the two studies has been partially attributed to poor user adherence. When correcting for adherence, the data showed that greater adherence in the CAPRISA 004 study resulted in a higher level of protection against HIV. Adherence alone is not the complete story on drug efficacy, presently knowledge of the pharmacokinetics and distribution of drug is very limited, thus understanding of how

different dosage forms and dosage regimens effect the time and space distribution of the drug will be a key in the design of microbicide products.

This chapter will present the first work in mechanistic modeling of drug distribution in the vaginal environment by a microbicide gel. The gel delivery system is chosen primarily due to the large number of data from studies that are available, but this method can be extended to other dosage forms as well. This extension is possible because the same fundamental principles of mass transport are the same with varying parameters depending on the particular drug, environment, and dosage form. In the subsequent chapters this analysis will be extended to model the delivery of microbicide drugs by a vaginal ring and the delivery of microbicides to a rectal environment.

Tenofovir, one of the leading microbicide candidates, acts by inhibiting reverse transcriptase, which is a necessary enzyme in HIV replication. Other candidate drugs like dapivirine, MIV 150, and IQP-0528 also are reverse transcriptase inhibitors. However, Tenofovir is unique in that it has to be converted to Tenofovir diphosphate in order to be biologically active. This extra intracellular step has benefits including a long half-life of the diphosphate form, but it also presents a challenge in modeling and measurement of Tenofovir PK. It is believed that while Tenofovir can be transported in and out of cells quickly, once converted to the diphosphate form, it does not readily leave the host cells. Studies have shown there to be a linear correlation between the

Tenofovir that is present in tissue and the Tenofovir diphosphate measured in cells[78]. The overall effect of Tenofovir diphosphate on Tenofovir transport is assumed to be small. This assumption is due to both the small proportion of Tenofovir being converted to the diphosphate form (approximately 5% of total Tenofovir is converted to the diphosphate form), small host cell density in the stroma (approximately 10% of total stromal volume), and the relative speed of conversion of Tenofovir to the diphosphate form compared to the time scale of interest (less than an hour compared with over a day). In fact after Tenofovir diphosphate has already been saturated within each cell, no more Tenofovir is expected to be consumed in the formation of new Tenofovir diphosphate, which means there will be no bearing on transport of Tenofovir. In PK studies, tissue concentrations of Tenofovir and sometimes Tenofovir diphosphate are measured via biopsies. These biopsies homogenize the entire tissue collected, and thus cannot distinguish between intracellular and extracellular Tenofovir. More over biopsies cannot provide a spatial distribution of the Tenofovir being measured. But due to the ubiquitous nature of biopsy measurements, they are still valuable in determining the presence of drugs in tissue and can be checked with predictions from PK models.

The first model of vaginal drug distribution will be incorporating the mechanistic processes of drug delivery in the gel, epithelium, stroma, and blood compartments. There have been relatively few studies of human PK data for a 1% Tenofovir gel. The

two studies that contain pharmacokinetic data of Tenofovir and Tenofovir diphosphate are the CONRAD study[78] and MTN-001[40]. In the CONRAD study, data were obtained at 0.5, 1, 2, 4, 6, 8, or 24 hours post either a single dose or a twice daily dose. The MTN-001 study used a daily dosing protocol and samples were collected 3 and 6 weeks after the first dose. These two human PK studies will be used as references to some of the parameters in the model. The key modeling parameters will be concentration distribution in the gel, tissue, and blood compartments after the initial gel dose. The single dose protocol will gave an accurate measure of the initial uptake of drug as well as the rate of elimination in each compartment. Results in the daily dosing protocol are steady state values of saturation concentration, but it does not provide information on initial Tenofovir uptake.

In this model, the thickness of the epithelial layer and the rate of gel dilution due to vaginal fluid production will be varied to simulate natural changes due to the phase of the menstrual cycle and the onset of menopause. In addition the thickness of biopsies will be varied to mirror real world uncertainties in taking a biopsy sample. The relationship between the measured concentration and depth of biopsy collected will be explored and related to the actual concentration in the stromal layer.

2.2 Materials and Methods

2.2.1 Geometry of the Model

The vaginal canal has an approximately rectangular cross-section in the collapsed state, with a thin height and a width of 2 to 3 cm. The dimensions are variable with a number of factors, including height and weight. Here the total surface area[7, 72] is around 100 cm^2. This is a key parameter in the drug delivery model, since the total volume of gel is divided by the surface to give the value of applied gel thickness. Assuming uniformly distribution of the gel coated over the entire surface area and minimal leakage, then with a 4 mL gel such as those from the CAPRISA 004 and VOICE trials, the total gel thickness would be 800 μm. Since the problem is bilaterally symmetric about the center line of the gel, it is more efficient to compute the half problem. Thus the half-thickness of the gel used in the model is only 400 μm. This length scale is the characteristic dimension in the model because it is much smaller than both the width and the length of the canal. Variations in the other two dimensions have a negligible effect on the overall transport, since vaginal features such as the rugae and other folds are on a bigger length scale than the depth of the epithelial and stromal layers. The problem can now be reduced to a one-dimensional transport model. The analysis here does not address consequences of coitus including semen deposition. In

accord with most gel dosing protocols, the current computational frame work assumes gel application and drug delivery prior to coitus.

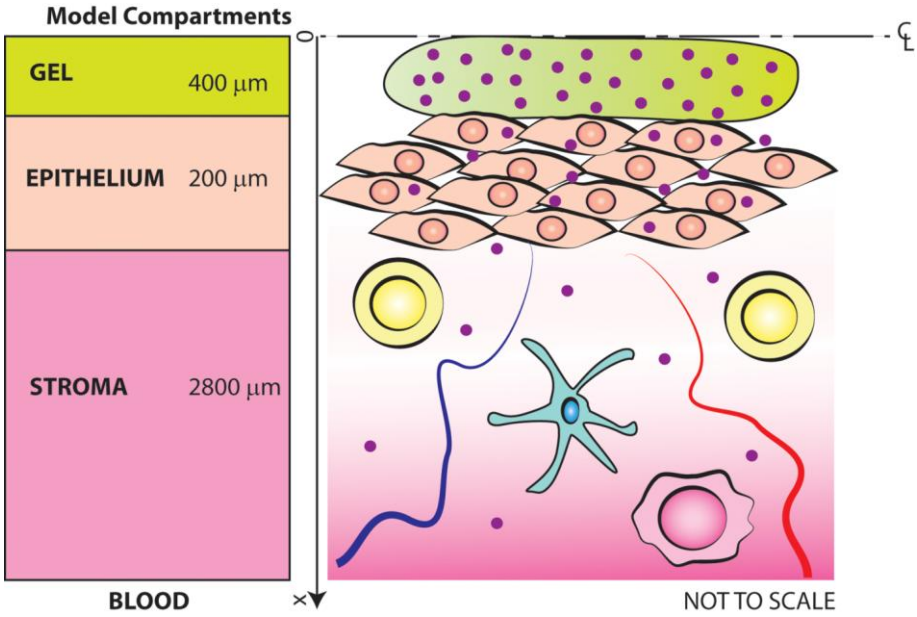

Figure 8: Drawing of the vaginal mucosa with gel layer, epithelium, and stroma. Line of symmetry is indicated on top

A drawing of the model is in Figure 8, the three spatially varying compartments are the gel (400 μm), the epithelium (200 μm), and the stroma (2800 μm). Due to symmetry the model is half of the total gel/tissue problem, only the bottom portion of the gel and tissue is shown, with gel thickness in the model being half of the total. Not in the figure is the blood compartment, which connects in the stroma via the vasculature. The blood compartment is assumed to be a homogeneous due to fast convective flow, with a volume equal to the total volume of distribution for the drug.

2.2.2 Governing Equations for Gel, Epithelium, and Stroma

A system of coupled unsteady diffusion equations can be used to model this one dimensional problem (Equation 11). The three space dependent compartments are the gel, epithelium, and stroma. The symbols C and D denote the local drug concentration and diffusion coefficient, respectively. The subscripts G, E, S, and B denote values in the gel, epithelium, stroma, and blood, respectively. The symbols k_D, k_B, and k_L are first order loss rate constants, characterizing effects of dilution of the gel layer, loss of drug to the vasculature in the stroma, and drug clearance from the blood.

$$\frac{\partial C_G}{\partial t} = D_G \frac{\partial^2 C_G}{\partial x^2} - k_D C_G \quad \text{(a)}$$

$$\frac{\partial C_E}{\partial t} = D_E \frac{\partial^2 C_E}{\partial x^2} \quad \text{(b)}$$

$$\frac{\partial C_S}{\partial t} = D_S \frac{\partial^2 C_S}{\partial x^2} - k_B C_S \quad \text{(c)}$$

Equation 11

Differential equation for the gel layer is in Equation 11a. The presence of ambient vaginal fluid is not included, but instead is assumed to have mixed with the applied gel forming a single homogenous compartment. Mixing effect of a gel with a fluid under shear is expected to be fast, in addition time scale of diffusion for fluid and gel is on the order of seconds. Dilution by ambient fluid over time is accounted by a first order rate

constant[89] k_D. This can be derived by assuming the rate of vaginal fluid production is constant, and the newly created fluid is well mixed into each section of the gel. Then the extra fluid leaving the gel will have the same concentration as the compartment, resulting in a first order reaction rate. The loss of drug is then the fluid production rate times the concentration in the gel. In addition the rate constant k_D also account for loss of drug due to leakage.

Equation 11b is the equation for the epithelium layer. Here the net transport is characterized by a single diffusion coefficient. Although real tissue might not have a perfectly uniform diffusion coefficient, an effective average should be sufficient to describe the transport process across the epithelium. As discussed above, loss of Tenofovir due to conversion into Tenofovir diphosphate is assumed to have a negligible effect. This is due to both the small percentage of total Tenofovir being converted as well as a fast saturation.

Mass conservation equation for the stroma is in Equation 11c. Like the epithelium, transport here is also modeled by a diffusion process. The loss of drug to the vasculature and lymphatic system is modeled as a first order kinetic process with rate constant k_B. This is assuming the distribution of capillaries and lymphatics is uniform throughout the stroma, and in addition the volume fraction of the capillaries is relatively small[79] (about 10%). Due to the large size of the blood compartment, the concentration

in blood is much lower than that of the tissue. In essence the transport of Tenofovir from tissue to blood is just proportional to the tissue concentration instead of a difference in concentration between tissue and blood. Furthermore, the transport of drug from capillaries by to the tissue is negligible.

2.2.3 Boundary and Initial Conditions

The boundary and initial conditions are given in Equation 12.

$$\frac{\partial C_G}{\partial x} = 0 \,@\left(x = 0\right) \tag{a}$$

$$C_G = \Phi_G C_E, D_G \frac{\partial C_G}{\partial x} = D_E \frac{\partial C_E}{\partial x} @\left(x = h_G\right) \tag{b}$$

$$C_E = \Phi_E C_S, D_E \frac{\partial C_E}{\partial x} = D_S \frac{\partial C_S}{\partial x} @\left(x = h_G + h_E\right) \tag{c}$$

$$\frac{\partial C_S}{\partial x} = 0 \,@\left(x = h_G + h_E + h_s\right) \tag{d}$$

$$C_G\left(x,0\right) = C_0 \tag{e}$$

$$C_E\left(x,0\right) = 0 \tag{f}$$

$$C_S\left(x,0\right) = 0 \tag{g}$$

Equation 12

The boundary conditions at both ends of the model are no flux (Equation 12a and Equation 12d). The no flux condition at the edge of the gel layer is due to symmetry. The boundary between the gel and epithelium is continuous with partition coefficient Φ_G

(Equation 12b), likewise the boundary between epithelium and stroma is also continuous flux with partition Φ_E (Equation 12c). The drug is initially in the gel layer with concentration C_0 (Equation 12e) and zero everywhere else (Equation 12f and Equation 12g).

2.2.4 Conservation of Mass Equation for Tenofovir in Blood

Unlike the three other compartments, the blood is assumed to be a well mixed homogeneous compartment. Tenofovir is transported from the stroma to the blood stream through the vasculature. Elimination of the drug from blood is through metabolism in the kidneys, and this is modeled as a first order kinetics with elimination rate k_L. The ordinary differential equation for the blood compartment is in Equation 13, with volume of distribution V_B, and concentration C_B. The mass of drug entering the blood is $\dot{M}_{SB}$, it is derived by the integral of the local stromal concentration over total volume times the kinetic rate k_B.

$$\frac{dC_B}{dt} = \frac{\dot{M}_{SB}(t)}{V_B} - k_L C_B$$

Equation 13

The differential equation in the gel, epithelium, and stroma compartment does not depend on the blood, thus mass transfer coefficient from stroma to blood is decoupled from the blood concentration. The equation for the blood can be solved

independently after obtaining the function $\dot{M}_{SB}$ from the stroma concentration. Equation for the blood from Equation 13 can be integrated using integration by parts to yield an explicit solution in Equation 14.

$$C_B(t) = e^{-k_L t}\int_0^t \frac{\dot{M}_{SB}(\tilde{t})e^{k_L\tilde{t}}}{V_B}d\tilde{t}$$
$$= \frac{\dot{M}_{SB}(t)}{k_L} - \frac{e^{-k_L t}}{k_L}\left[\dot{M}_{SB}(0) + \int_0^t \frac{d\dot{M}_{SB}(\tilde{t})}{dt}e^{k_L\tilde{t}}d\tilde{t}\right]$$

Equation 14

Here the assumption is zero concentration in the blood compartment before initial gel insertion. The expression for concentration in the blood compartment has three terms. The first term is an input term from mass flux, the second term is the effect of initial mass transfer with an exponential decay, and the last term is a weighted time dependent term of the mass transfer rate.

2.2.5 Parameters in the Model

The parameters used in the model are listed in Table 1. The standard values of the epithelial and stroma layer is 200 μm and 2.8 mm respectively[71]. Thickness of the gel layer is 400 μm, which is half of the total from a 4 mL gel due to bilateral symmetry about the centerline for a typical human vaginal canal with surface area of 100 cm^2. Values of the diffusion coefficient in gel can be estimated based on molecular size and Stokes-Einstein theory. Based on the molecular weight of Tenofovir[75] (287 g/mol), the

effective hydrodynamic radius is estimated to be 0.3815 nm (www.molinspiration.com). The resulting diffusion coefficient[91] in water based on the Stokes-Einstein theory is 8.5 x 10^{-6} cm^2/s. Measurement of the diffusion coefficient for molecules in vaginal microbicide gels have been few to date. Diffusion coefficients for fluorescein (molecular weight 322 g/mol) and a 10 kDa dextran were measured in three test gels, one of which is very similar in composition to the clinical Tenofovir gel focused here[27]. The measurements confirmed the accuracy of computed diffusion coefficient in Stokes-Einstein theory. Values of diffusion coefficient in undiluted gel, normalized by the diffusion coefficient in water were 0.68 for fluorescein and 0.57 for dextran. The normalized diffusion coefficient for fluorescein increased to 0.8 after a 1:1 gel dilution with water. On the basis of these data, the value of diffusion coefficient for Tenofovir in gel is 6 x 10^{-6} cm^2/s. Tenofovir permeability has been measured in human cervicovaginal tissue explants with the application of a 1% clinical gel[21, 76]. For a typical tissue thickness of 0.5 mm, the median value for these data gives an estimate of the product of the diffusion coefficient and the partition coefficient to be 5 x 10^{-8} cm^2/sec. Tenofovir is not a hydrophobic drug[81], with relatively high solubility in the tissue, thus the partition coefficient can be taken as unity. Assuming the epithelium and stroma have similar permeability to Tenofovir, the diffusion coefficient for both compartments is then 5 x 10^{-8} cm^2/sec. The volume of distribution for the blood compartment is 75 L[47],

representing the effective volume for the total mass of drug divided by observed blood concentration.

Table 1: Standard values of parameters used in gel model

Parameter	**Symbol**	**Value**	**Reference**
Gel Diffusion Coefficient (cm^2/s)	D_G	6×10^{-6}	[27, 91]
Epithelium Diffusion Coefficient (cm^2/s)	D_E	5×10^{-8}	[21, 76]
Stroma Diffusion Coefficient (cm^2/s)	D_S	5×10^{-8}	[21, 76]
Gel/Epithelium Partition Coefficient	φ_{GE}	1	[81]
Gel Thickness (cm)	h_G	0.04	[78]
Epithelial Thickness (cm)	h_E	0.02	[71]
Stromal Thickness (cm)	h_S	0.28	[71]
Gel Dilution Rate Constant (hr^{-1})	k_D	0.551	[25]
Stroma Blood Transfer Rate Constant (hr^{-1})	k_B	0.122	[25]
Blood Clearance Rate Constant (hr^{-1})	k_L	1.19	[25]
Initial Concentration (ng/mL)	C_0	10^7	[78]
Volume of distribution (L)	V_B	75	[47]

The three additional parameters in the model are the kinetic rate constants for gel dilution/leakage, drug transport to the vasculature and lymphatics in the stroma, and drug clearance from the bloodstream: k_D, k_B, and k_L. There are no direct measurements for k_D and k_B. With oral and intravenous dosing of Tenofovir, or the prodrug Tenofovir disoproxil fumurate, there have been a number of PK studies from which the value of the blood clearance is calculated using standard models[78, 94]. However the value of k_L in the model does not correspond directly to those results because the input parameter from the stroma is different in this model. Consequently, the values of the three rate constants for Tenofovir in our compartmental model were chosen based on first of our results to the PK data for a single dose of 4 mL 1% Tenofovir gel in humans[78]. The study computes standard PK summary parameters and gives plots of Tenofovir concentrations in aspirated vaginal fluid, vaginal biopsies, and blood plasma vs. time after application of single or twice daily dosing. The values of C_{max}, C_{24h}, and *AUC* are given in the table. The three rate parameters are determined by the best fit of the model to the experimental values. Out of the three compartments and three measures given in the study, vaginal fluid aspiration has the most measurement variability. This is due to the fact aspirations might draw differing amounts of fluid in addition to gel that might be present, and does not directly correspond to the gel compartment in this model. Out of the three measures, *AUC*, the area under the curve

gave the least amount of additional information. This is due to the fact pharmacokinetic curves all have similar shape, the information given by both C_{max} and C_{24h} is sufficient to guess the value of the AUC. The fit is achieved by first computing a cost function, defined as the sum of the square of the normalized difference in the four measures of C_{max} and C_{24h} for biopsy and blood. This cost function is then minimized with varying kinetic parameters using the Nelder-Mead Simplex Method in MATLAB[60]. The initial guesses are based on simple models for each parameter: the value of k_D is based on dilution by vaginal fluid production rate with complete mixing, for k_B the value is based on the terminal slope of the data in the tissue compartment since the loss in that compartment is driven by transport to the blood at long times, and the value of k_L is based on the terminal slope of the blood concentration using the same argument. The Tenofovir concentration in biopsy is a volume average for a tissue that is about 2 to 3 mm thick, therefore the simulation of a biopsy in our computations was the spatial average of concentration in the two compartments. The effect of different depth for a biopsy will be explored in the results section.

2.2.6 Numerical Solution of the Equations

The equations were solved using Mathwork's MATLAB software. They are first converted into ordinary differential equations using forward finite difference method. The spatial dimension is discretized into approximately 500 points. The boundary

conditions were rewritten as part of the difference equation. The system of differential equations is then solved using the built-in "ode15s" ordinary differential equation solver for stiff problems. This is due to a large drop in initial concentration at the boundary presents a large derivative when computing the flux. A stiff solver can decrease the computational time by using a smaller order and adaptive step size. Drug concentration in the blood is computed after the main computations, due to the fact the blood is in decoupled from the equation for the stroma. This is achieved by a simple integration of the input term from stromal concentration. Spatial averaged concentration values are computed by integration using the trapezoidal rule on concentration profiles at each time step.

2.3 Results

The fundamental outputs of this model are Tenofovir concentrations as a function of both position (depth) and time in the gel, epithelium, and stroma compartments as well as concentration versus time in the blood. Three dimensional information of time, position, and concentration can be reduced to two dimension by either fixing the time which creates a concentration profile over position, or fixing the position (by averaging) each compartment and plotting the concentration over time. The model can also be used to predict changes due to epithelial thickness over the different phases of the menstrual cycle and the effects of biopsy depth on the measured

concentration. Lastly sensitivity analysis of the model can inform how different contributions of key parameters influence the resulting output of the model.

2.3.1 Drug Concentration Profile at Different Times

The concentration profile of Tenofovir as a function of depth is plotted in Figure 9 at 2, 4, 8, 24, and 48 hours post initial gel insertion. The concentration across the gel layer is nearly constant due to the fact gel diffusion coefficient is about two logs higher than that of the tissue. In fact the concentration profile is a half-parabola due to a quasi-steady condition also due to fast diffusion. The concentration in the tissue layer drops off as a function of depth on the log scale plot. By around 24 hours the concentration is about 2 logs lower than the initial maximum. Over time, gel leakage and dilution becoming increasingly faster than the rate of transport in tissue, as a result tissue concentration is actually lower on the surface compared with a few microns below the epithelium. In this case instead of mass transport into the tissue, the gel and vaginal fluid layer actually facilitates a back flow phenomenon. The drop of concentration in the stroma is very steep. Initially it is about 4 logs every millimeter at 2 hours however by 24 hours the profile is almost flat.

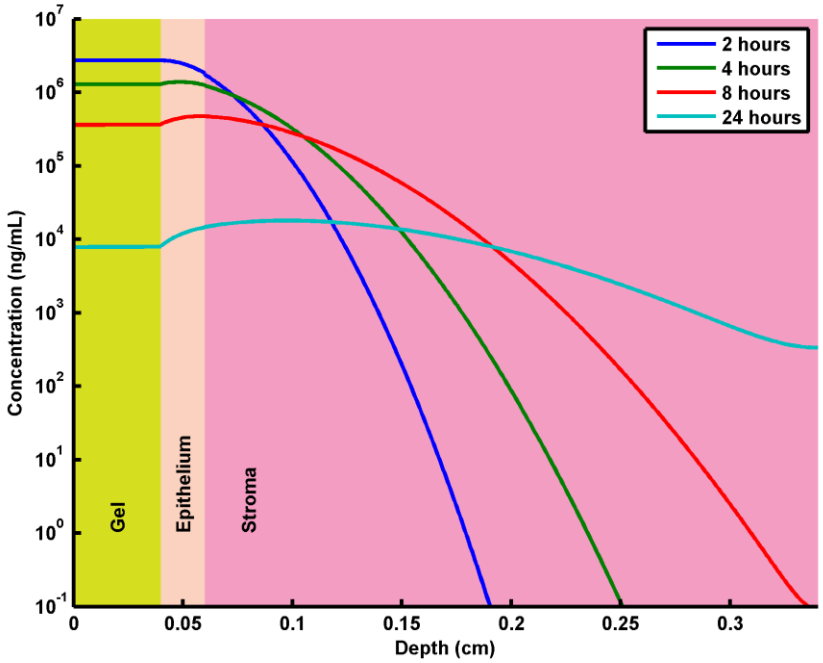

Figure 9: Concentration profiles of Tenofovir in gel and tissue at 2, 4, 8, and 24 hours

2.3.2 Average Concentrations in Compartments vs. Time

Depth averaged concentration of Tenofovir in each compartment on a log scale is plotted in Figure 10. In addition, the simulated biopsy curve is also plotted on the same scale, which is defined as the concentration in a combined epithelial and stromal compartment. The maximum concentration is achieved at around 4 hours for both the tissue and blood plasma with a nearly linear decay after the peak (in log scale, which corresponds to an exponential decay). The concentration if the gel is fairly close to the concentration in the epithelium, due to the small thickness of the epithelial layer and the

relatively flat gradient in both compartments (Figure 9). Going from the gel compartment, the drop off to stroma is about 2 logs, 1.5 logs to simulated biopsy, and about a 5 log drop to the blood. In the stroma the maximum concentration is 1.01 x 10^5 ng/mL, and the concentration at 24 hours is 6.93 x 10^3 ng/mL.

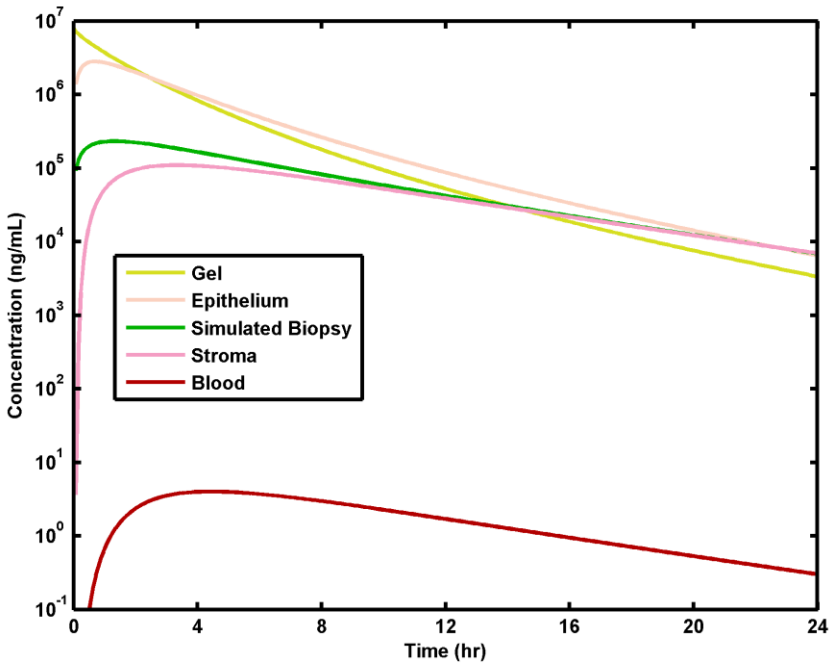

Figure 10: Average concentration over time for each compartment

2.3.3 Pharmacokinetic Summary Measures

A summary of the key pharmacokinetic parameters for the biopsy and blood compartments are presented in Table 2. Corresponding values for human PK data from Schwartz et al[78] study are given in the parenthesis next to the value from the model. The Area Under the Curve or *AUC* values are computed over a 24 hour period, the same

as Schwartz et al. Computational results for the gel compartment is not given here because it does not correspond directly to the experimental values for aspirated vaginal fluid, thus a comparison cannot be made. The computed values for C_{max} and C_{24h} are very close to the experimental data, this is perhaps unsurprising given the model is based on fitting the three kinetic parameters to the C_{max} and C_{24h} for biopsy and blood. However, with four values and only three parameters, there is one less degree of freedom in the fitted parameters, which means the model agreement is not due entirely to the fit. All four parameters showed remarkable agreement in addition to the value of t_{max}, which was not used in the fit shows the validity of the model in predicting human PK results. The result for *AUC* appears to be higher than those of the PK data. This is most likely due to the differences in integration used to compute *AUC*. In the model the time spacing used can be as finely as possible, while in a clinical trial the time points are very sparse and unevenly distributed.

Table 2: Summary pharmacokinetic parameters from the model with comparison to Schwartz et al data in parentheses

	t_{max} (hr)	C_{max} (ng/mL)	C_{24h} (ng/mL)	*AUC* (hr*ng/mL)
Biopsy	1.3 (*2*)	2.32 (*2.2*) x 10^5	6.90 (*7*) x 10^3	1.74 (*0.64*) x 10^6
Blood	4.4 (*4*)	4.01 (*4.0*)	0.301 (*0.3*)	41.8 (*36.4*)

2.3.4 Results for Daily Dosing and BAT24 Dosing

The model can be adapted to multiple dosing strategies by application of a new gel at specified times. The two common dosage regimens are daily dosing and BAT24 dosing. In daily dosing, users apply the gel once every 24 hours regardless of sex. And in BAT24 dosing users are instructed to apply the gel before and after sex, but no more than two in a 24 hour period, practically most users applied the gel up to 3 hours before and 3 hours after sex.

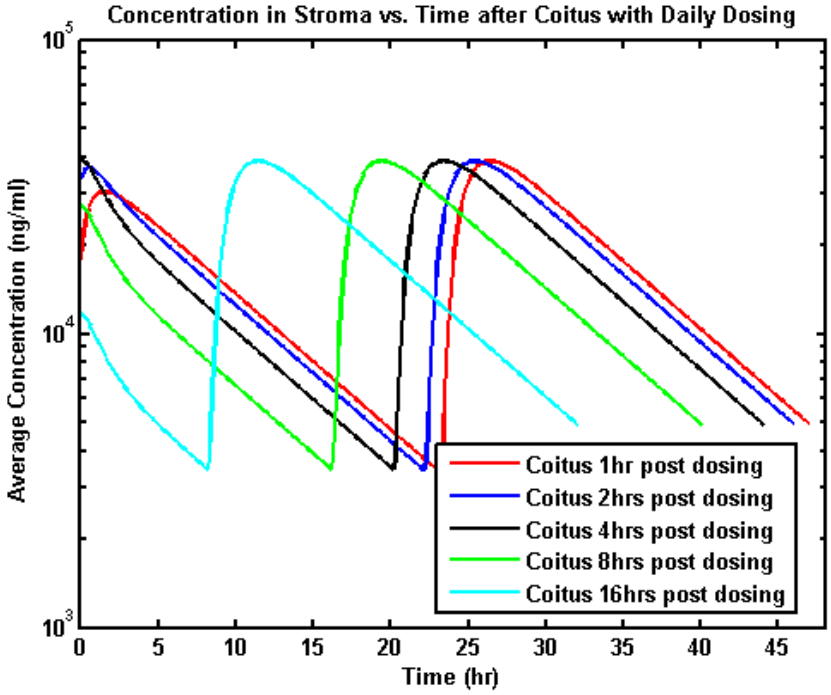

Figure 11: Concentration in stroma with daily dosing, coitus is at time zero

The concentration in stroma under a daily dosing protocol is plotted in Figure 11. This result can be compared with human PK data from the MTN-001 study[40]. The

result show periodic daily dosing does not significantly change the observed average concentration compared with a single dose. There is a considerably large variation in the clinical trials, with concentration differences of up to two logs being very common. The MTN-001 study gave median concentration of 1.13 x 10^5 ng/mL for a biopsy taken at 2, 4, or 6 hours following the most recent dose. In the model the predicted average of simulated biopsy after 0, 2, 4, and 6 hours is 1.28 x 10^5 ng/mL, which is only 13% higher than the median from MTN-001.

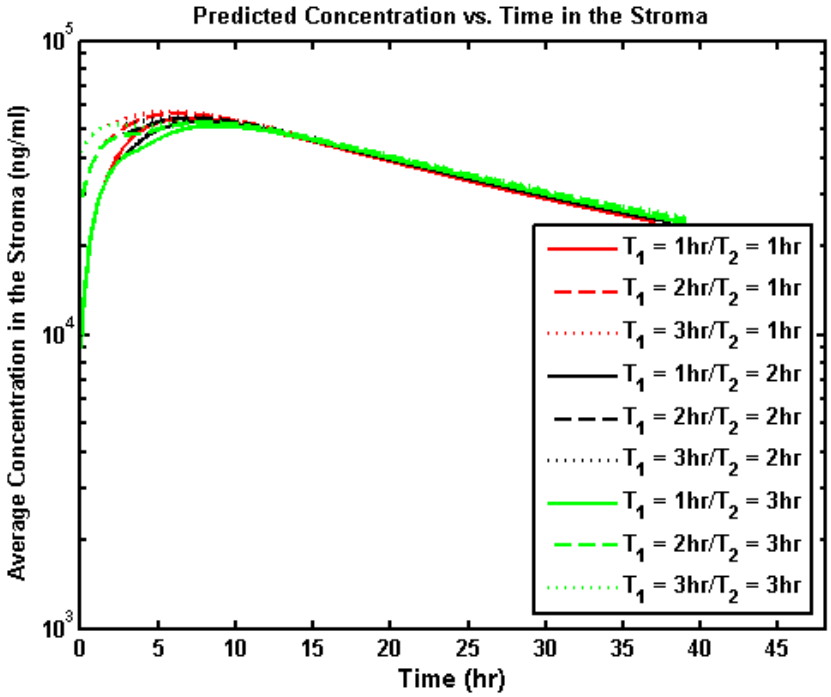

Figure 12: Concentration in stroma with BAT24 dosing, coitus is at time zero

Before and after sex dosing (BAT24) is used in the CAPRISA 004 study, Figure 12 plots the stromal concentration post coitus for a variety of the most common dosing

times. The differences between them are very small, especially when presented on a log scale. The maximum concentration in BAT24 is about 30% higher than daily dosing, and the concentration in the stroma is near the maximum at about 5 hours post coitus. Two successive doses within a few hours of each other cause the decay in concentration to be much slower than daily dosing and a single dose, since the second dose is able to replenish lost drug.

2.3.5 Effects of Variations in Epithelial Thickness

The thickness of human vaginal epithelium varies in response to cyclic variations in levels of women's reproductive hormones[71]. In particular it varies directly with estrogen levels, and is thickest at midcycle. It is also believed the volume of ambient vaginal fluid production varies cyclically and is also highest at midcycle[27]. Since microbicide gels are intended for application throughout the menstrual cycle, it is biologically important to understand possible consequences of cyclic variability in epithelial thickness and vaginal fluid volume on microbicide drug delivery and PK. In principle, a thicker epithelium would delay the arrival of drug molecules to the stroma, and increased volume of ambient vaginal fluid would increase the extent of gel dilution and loss of drug. The model is used to simulate these effects, by changing the rate constant k_D for gel dilution was doubled for a thinner epithelial thickness of 100 μm, and halved for the epithelial thickness of 400 μm.

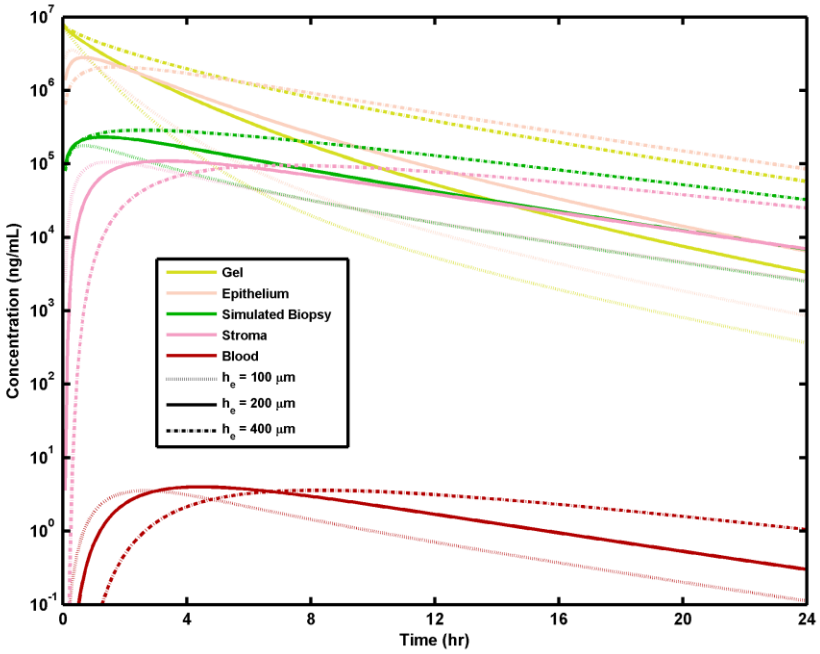

Figure 13: Concentration in compartments with varying epithelial thickness

Concentration in all compartments versus time for three epithelial thicknesses of normal, halved, and doubled are plotted in Figure 13. A table summarizing the key PK parameters is in Table 3. As the epithelial thickness increases the mass transport into the tissue is slower causing a longer t_{max} and a lower C_{max}. Increasing epithelial thickness also causes a decrease in vaginal fluid production. This effect is more pronounced at long times due to the low time constant of dilution, resulting in both the C_{24h} and AUC being higher with increased epithelial thickness.

Table 3: Summary PK parameters in epithelium and stroma with varying epithelial thickness

	t_{max} (hr)	C_{max} (ng/mL)	C_{24h} (ng/mL)	AUC (hr*ng/mL)
Epithelium h_e = 100 μm	0.24	3.55×10^6	8.55×10^2	6.03×10^6
Epithelium h_e = 200 μm	0.72	2.81×10^6	6.48×10^3	1.07×10^7
Epithelium h_e = 400 μm	1.77	2.09×10^6	8.52×10^4	1.79×10^7
Stroma h_e = 100 μm	1.53	1.06×10^5	2.58×10^3	7.04×10^5
Stroma h_e = 200 μm	3.37	1.10×10^5	6.93×10^3	1.10×10^6
Stroma h_e = 400 μm	7.30	9.52×10^4	2.50×10^4	1.41×10^6

2.3.6 Interpreting Biopsy Concentration

Drug concentration measured by a biopsy is the spatial average across the epithelium and the stroma excised by a biopsy punch. The thickness of a biopsy varies in practice, in microbicide trials the thickness is around 3 mm, however values as low as 2 mm are possible. The variation in both the epithelial thickness and biopsy punch thickness can influence the interpretation of the measured drug concentration. A biopsy measurement is intended to relate the activity of the drug at the site of action. Tenofovir is believed to exhibit anti-HIV activity primarily in the stromal layer. Figure 14 shows the ratio of stroma concentration to the measured biopsy concentration under the three different epithelial thicknesses and two different biopsy punch depth. The result show

with a thicker epithelium and at short times the biopsy average over estimate the actual Tenofovir concentration. This is due to most of the drug in a biopsy is concentrated in the epithelium under those conditions. When the epithelium is thin or when the time point approach 24 hours the biopsy average approximates stromal concentration well. With a 400 μm epithelium the measured biopsy average is only about 30% at 4 hours and 80% at 24 hours. With a thinner 2 mm biopsy the ratios are 50% and 95%. For thin epithelium of 200 μm and 100 μm, the ratio is actually greater than 1 due to the backflow concentration gradient from tissue to the fluid observed at long times.

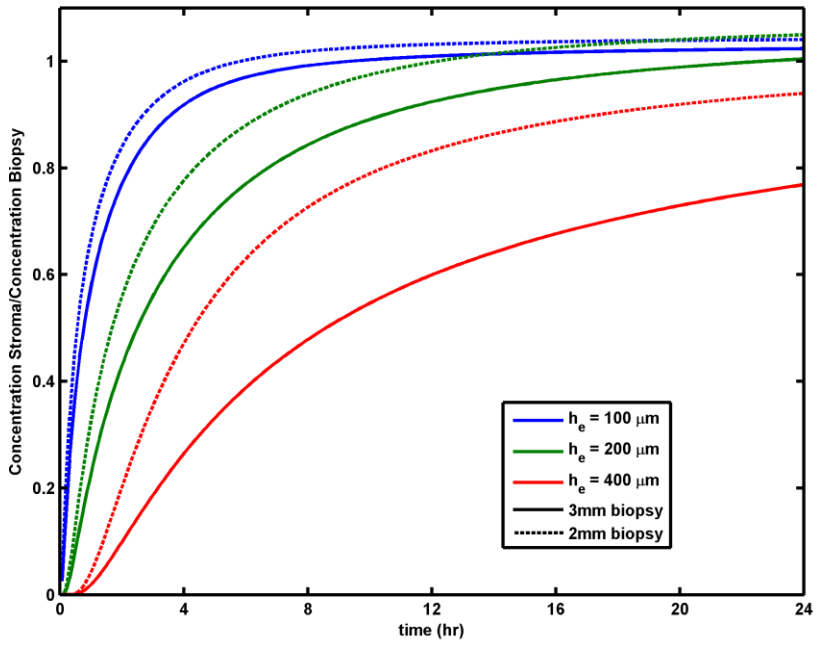

Figure 14: Ratio of stromal concentration to biopsy with varying epithelial and biopsy thickness

2.3.7 Perturbation of Model Parameters

The model of drug transport in vaginal mucosa contains a variety of parameters. They are based on variations in the properties of the drug, the vehicle, dosage regimen, host environment, and in cases of experiments, the variation in data collection. The uncertainty in these parameters contributes to the overall uncertainty of the model predictions. Determining how the magnitude of the parameter uncertainty contributes to the observed variability will allow better understanding of the output. In a typical experiment on vaginal microbicide PK, the results have a large range for each measure, usually on the order of multiple logs for tissue biopsy.

2.3.7.1 Variation in Tissue Diffusion Coefficient

Diffusion coefficient in the tissue is one of the primary factors in drug transport. Differences in diffusion coefficient are expected between individuals as well as in different areas of the tissue in the same individual. The effect of different diffusion coefficient ranging from 0.25, 0.5, 1, 2, 4 times the original value is plotted in Figure 15. For epithelium, stroma, and the blood compartment increasing the diffusion coefficient increases the maximum concentration C_{max} as well as shorten the time to maximum t_{max}, however the concentration at 24 hours C_{24h} is lowered. The effect on maximum concentration for the epithelium is not as pronounced as the other compartments. Effects on the stroma and blood are significant on the log scale. For example with a diffusion

coefficient a quarter of the original both stroma and blood concentrations appears almost flat after reaching the maximum. Concentration at 24 hours drops off in the epithelium more than the stroma or the blood.

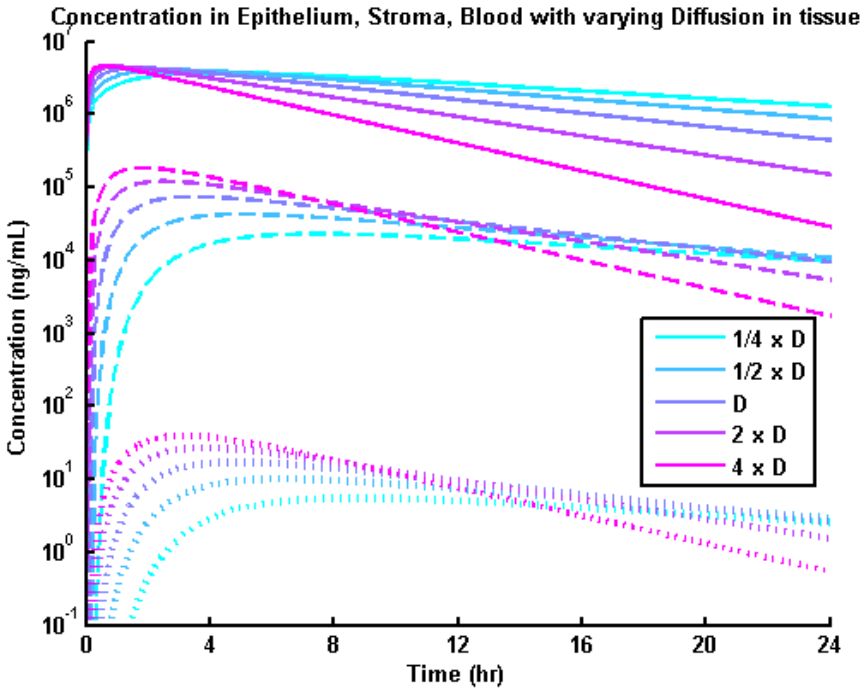

Figure 15: Concentration in compartments with varying tissue diffusion

2.3.7.2 Variation in Partition Coefficient

Partition coefficient between the gel and tissue is dependent on the chemistry of the drug molecule as well as the composition of the gel. It is a measure of the solubility in the gel compared to the solubility in tissue. For a drug with low tissue solubility, the partition coefficient is less than one. Figure 16 plots the concentration versus time with varying partition coefficient from 0.25, 0.5, 1, 2, to 4. For all compartments C_{max} is

increased with increasing partition, however t_{max} stays the same and C_{24h} is at a similar level. Differences in concentration with varying partition coefficient are less than the effect from changing the diffusion coefficient.

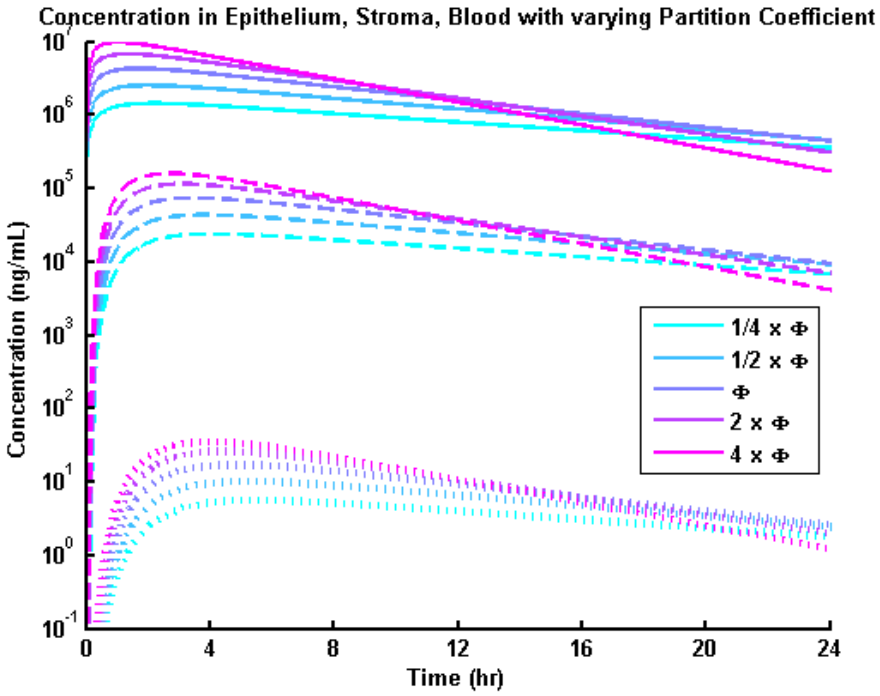

Figure 16: Concentration in compartments with varying partition coefficient

2.3.7.3 Variation in Dilution Constant

The dilution constant in the model is a measure of gel dilution by ambient vaginal fluid and leakage of the gel. Vaginal fluid production varies across women as well as over the course of a single day. Gel leakage is a function of gel composition, volume of ambient fluid, and the size of vaginal canal. Concentration in epithelium, stroma, and blood compartments with varying dilution constant is in Figure 17. The

maximum concentration C_{max} and time to maximum t_{max} is unchanged for all compartments. The concentration at 24 hours C_{24h} is lowered with a higher dilution constant.

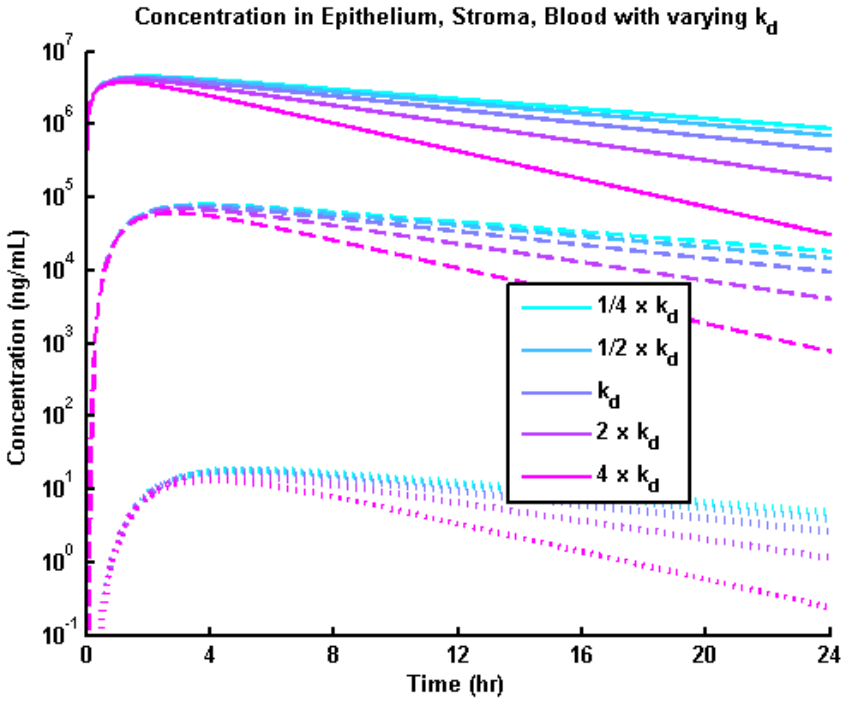

Figure 17: Concentration in compartments with varying dilution constant

2.3.7.4 Variation in Stroma Blood Transfer Constant

Stroma blood transfer constant measures the rate of Tenofovir transport from the stroma to the circulatory system. There are currently no direct ways of measuring this parameter. Like other biological parameters the variability is expected to be high. Concentration variability with different values of the constant is plotted in Figure 18. The changes in concentration for the gel compartment are small, while the biggest

difference is in the stroma. With a higher transport rate the concentration value in the stroma is lowered. The concentration at 24 hours C_{24h} is the most different, variation in the transport constant is clearly visible on the log scale. Surprisingly the changes in the blood compartment is small, most visible change is the time to maximum concentration t_{max}, with a higher transport parameter the time to maximum is shortened. Concentrations at 24 hours in the blood are similar across variations in the blood transfer constant.

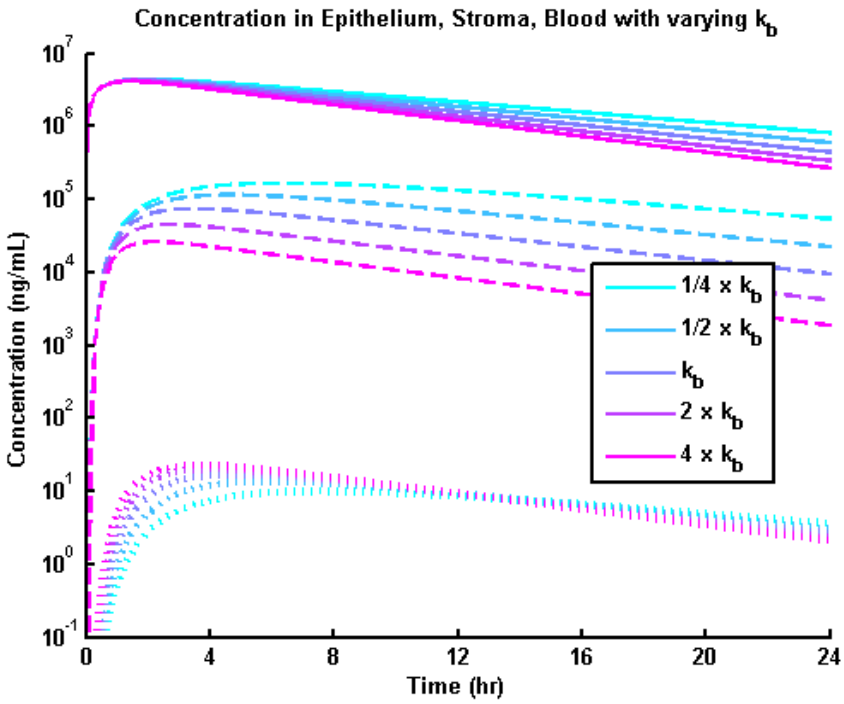

Figure 18: Concentration in compartments with varying stroma blood transfer constant

2.4 Discussion

This is the first mechanistic computational model of drug transport from a vaginal gel to the epithelial and stromal tissue layers of the human vaginal mucosa. The model also include subsequent Tenofovir uptake by the blood stream and lymphatics with the result being a time dependent concentration in the blood compartment. Results of concentration in the tissue are dependent on both space and time. The predictions made by the model were referenced to human PK data in two studies that used a 1% Tenofovir gel at 4 mL. The model and study results agreed well suggesting that this method of modeling can be used to predict results that are not yet measured. This model can be further expanded by including additional factors such as gel spreading and conversion to Tenofovir diphosphate.

Most parameters in the model are based on physical measurements including permeability data. Other parameters such as the three rate constants were found by fitting key PK outputs from a clinical trial with the model. These fits are made using standard algorithms for finding the local minimum of a multivariate function. After experimenting with different initial guesses, the fits all still arrive at the same result. This indicates the parameters found should be a stable local minimum of the cost function, or possibly a global minimum. Predictions based on the fits are very close to the PK measured in clinical trials, with results also comparable to a second trial with the

same gel but using a different dosage regimen. The agreement by itself should not be viewed as full validation of the model, but it is a good starting point in future analysis that test other predictions of the model. Indeed, the model should be helpful in understanding how vaginal delivery of Tenofovir is governed by the various properties of the gel itself, drug loading into the gel, gel volume and coating of the vaginal mucosa, properties of the epithelial and stromal layers, and drug clearance from the blood stream.

A logical follow up of the model is to include the effects on drug transport of gel spreading, which will be explored further in Chapter 4. Gel spreading will introduce a second dimension to the computations, in the direction of gel spreading and depth into the tissue. The analysis will reveal in more detail how gel volume and vaginal properties govern drug delivery. Gel spreading of the Tenofovir gel is fast compared to the 24 hour time scale of drug delivery. It is expected to coat the entire vaginal canal in less than one hour, depending on gel properties as well as insertion position. The perfect coating model here can provide insights of gel composition as it relates to drug delivery independent of spreading. For example, due to the linearity of the model with respect to concentration, all concentration results are proportional to the initial gel concentration level. On the other hand, time dependent factors such as t_{max} do not change with concentration. One way of comparing gel formulations is to conserve the total drug loading, with a different volume of gel. For example, if the volume of the original 4 mL

1% gel is halved, the concentration is increased to 2%. In the stroma the concentration C_{max} increased by 16% with this reduced volume formulation, t_{max} decreased by 26%, C_{24h} decreased by 15% and the *AUC* increased by 1%. This result makes physical sense, as higher initial concentration give a higher maximum concentration, however smaller volume is also depleted faster, decreasing the t_{max} and C_{24h}. Since an equal amount of drug is used, the *AUC* stayed about the same.

Comparison between the two most common dosage regimens also yielded interesting results. The maximum concentration in the stroma for a BAT24 protocol is only slightly higher than daily dosing. However, the drop off in concentration over time is much steeper in the daily dosing case compared to BAT24. Having two doses close to the time of sex offsets the effect of gel dilution during coitus. Clinical trial data showed similar result of marginally higher concentration in multiple dosage regimens compared to a single dose. Although the first two clinical trials with a Tenofovir gel achieved different results with different dosage regimens, a correlation cannot be immediately drawn, since user adherence has proven to be a much bigger factor to success in both trials. Whether differing dosage regimens can lead to greater adherence is yet to be determined.

The transport rate in tissue changes with variation in the epithelial thickness, which is associated with the phases of menstrual cycle. For example, a thicker

epithelium is associated with increased estrogen levels during the mid cycle, which can slow down the rate of Tenofovir transport to the stroma. When the epithelial thickness is doubled from 200 μm to 400 μm, the value of stromal t_{max} more than doubled from 3.4 to 7.3 hours. With a decrease in transport rate, the concentration at 24 hours actually quadrupled from 6.72 x 10^3 ng/mL to 25.0 x 10^3 ng/mL. The clinical significance of this is unclear. However, an increased epithelial thickness at mid cycle will take longer to reach the maximum concentration but is able to sustain concentration levels for a longer time.

The model also gives information about the drug levels measured in a biopsy. Variations in epithelial thickness will change the proportion of drug that is expected to be from the stroma. Since most of the mass of the drug is concentrated near the surface of the tissue, a thicker epithelium will under estimate the amount of drug in the stroma. Another key factor in biopsy is the thickness of excised tissue. This factor is not standardized across microbicide studies, and is rarely mentioned in the results. Once again, due to the fact that drug is concentrated near the surface, a thicker biopsy will only dilute the higher concentration, and thus a thicker biopsy will lead to a lower biopsy concentration even though the tissue sample stayed the same. This difference in sampling creates an additional variable that makes comparison between biopsies of different studies, or even samples from the same study difficult. One way of reducing

this variability is to report the total mass of drug per area of excised tissue. This way a slightly thicker or thinner tissue will have minimal effect on the total mass.

Sensitivity of model parameters will give a better understanding of the intrinsic variability and will predict results from known physiological changes. Here the concentration profile in three different compartments are plotted with varying diffusion coefficient, partition coefficient, dilution constant, or stroma blood transfer constant. Results show that all parameters change concentration profiles uniquely. This observation can be useful in the inverse problem where changes in a particular parameter can be found given variations in the resulting PK data. In particular for short times, only the partition coefficient has a noticeable effect on the epithelial concentration. Both gel dilution and diffusion coefficient affect all compartments but in different ways. Gel dilution is slow acting and the changes are pronounced at long times, while the diffusion coefficient alters the curve at all time points, first by increasing concentration at short times due to fast transport and then by lowering concentration at 24 hours due to faster depletion of drugs. The stroma blood transfer coefficient is unique in that it only significantly affects the stroma compartment, not the blood compartment. This difference is due to the fact that eventually most of the drugs in the stroma will end up in the blood stream, so the rate of this transfer is dictated by the epithelial and gel

compartments. This means by altering the rate constant the only effect would be changing the concentration in the donor to maintain the same mass flux.

2.5 Conclusion

This is the first model of microbicide gel distribution in the vaginal mucosa. The model can help improve understanding of how multiple factors can influence the delivery and efficacy of microbicide gels. The principles used here can be further improved upon and expanded to other drugs and dosage forms. Comparison with existing clinical data showed good agreement with the model predictions. Effects of biological variations in epithelial thickness and vaginal fluid production are explored, which is then related to observed concentration in biopsies. In addition the effects of the two most common dosage regimens are compared in terms of their concentration profile in the stroma. Variability and sensitivity analysis of four other key parameters are also explored with concentrations in three key compartments of epithelium, stroma, and blood. The results here can inform not only the fundamental understanding of drug delivery in the vaginal environment, but also extend the knowledge to gel design and proper dosage regimens that can achieve prophylactic drug concentration in the target mucosa.

3. Gel Spreading in the Vagina

3.1 Introduction

Rheology of microbicide gels can be modeled from the simple to the more complex, e.g. using Newtonian fluid, Power Law, Power Law with yield stress (Herschel-Bulkley), and Carreau with yield stress as constitutive models. Previous work has modeled the spreading of a Herschel-Bulkley fluid being squeezed by a plate[49]. A more advanced model of a Carreau-fluid with yield stress in a channel has been developed[87-89]. This new model can incorporate more realistic dimensions of the vagina. A model of gel spreading in the rectum is also possible using this modeling conceptualization with different geometric details.

Drug is delivered by a vaginal gel primarily through diffusions into the tissue. However, the gel also spreads due to squeezing forces from the vaginal walls. In Chapter 2, the assumption was that the gel coated the entire canal. This assumption may be good for a typical spreading gel over 24 hours, but for transport on a short time scale and for non-spreading, bolus gels, this assumption no longer holds. A model of gel spreading is needed in order to assess the extent of spreading at short times for a typical flowing gel. The spreading model can be useful to help choose the best gel and volume to use in the design of such gel, by metrics related to drug delivered and user acceptability (leakage).

The rate of gel spreading depends on the rheology of the gel. The simplest measure of rheology is viscosity. For simple fluids like water, viscosity is fairly constant with changing temperature. However, the complex polymer networks in a gel exhibit varying viscosities and other rheological behaviors under different flow conditions. Shear thinning is a behavior typical of these polymers, in which the viscosity of the fluid decreases with increasing shear rate. Fluids with this behavior are most simply characterized using the Power Law constitutive model. In addition, a fluid could exhibit a yield stress, where it will resist flow if insufficient external stress is applied. Fluids that are shear thinning and have yield stress can be modeled using the Herschel-Bulkley constitutive model. Furthermore, a third behavior known as zero shear viscosity may occur, in which the viscosity is nearly constant when the shear stress is close to zero. A fluid that has this behavior and is shear thinning can be modeled as a Carreau fluid.

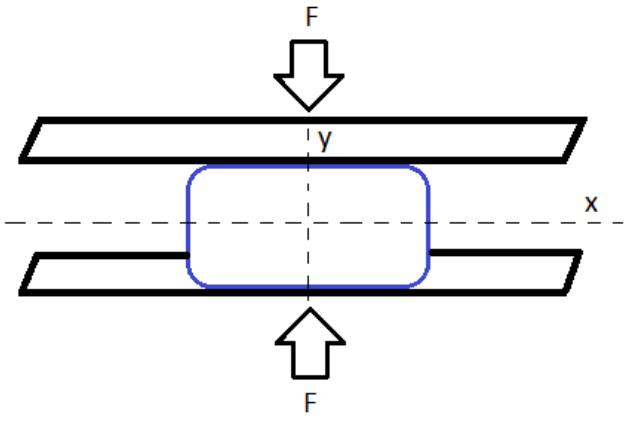

Figure 19: Illustration of squeezing by two plates of a gel in channel geometry with applied force *F*

Previous analysis of gel flow using the Power Law and Herschel-Bukley models in a cylindrical or "hockey puck" geometry was conducted by Sarah Kieweg[48, 49]. The hockey puck model was chosen in part because it is used in the literature for squeezing flow. It represents squeezing as two infinite plates with a cylindrically symmetrical initial condition. This radial model of gel flow was reasonable mathematically due to symmetry, but it is far from captured the geometry of the vaginal canal. A more accurate model would be flow in a channel of approximately fixed width of 2.5 cm (Figure 19). The length of the canal[7, 72] is approximately 10 to 15 cm, the innermost region is the fornix and the outermost opening is the introitus. Based on these dimensions and a gel volume of around 3 mL, the height of the gel is much smaller than either the length or the width. For this derivation, the flow is assumed to be bilaterally symmetric, where the gel can flow out on either end. In the more geometrically realistic model, the fornix is a wall that blocks gel flow, which can be modeled as a half problem of the previous bilateral case.

3.2 Materials and Methods

Three different constitutive models will be used in this analysis. All of them share the same geometry, equations of motion and boundary conditions. However, the results of the flow problem will be different depending on the model. Methods of solving different models will also differ. The simplest model can be solved explicitly,

while the more complex models involve solving a system of equations. The steps for each solution will be outlined in the results section.

3.2.1 Constitutive Equations

The coordinate system for this problem is laid out in Figure 19. Flow in the width direction is assumed to be zero due to symmetry of the initial condition. Flow field is determined by the Navier-Stokes equation. Lubrication theory can be applied due to the height of the gel being much less than the total length during spreading. This leads to a zero pressure gradient in the height dimension (Equation 15).

$$\frac{\partial P}{\partial y} = 0$$

Equation 15

Flow in the x dimension can be simplified by assuming incompressible flow for a liquid and negligible acceleration terms due to small inertial term compared with the viscous term of the equation. This will lead to an equation for the pressure gradient as a function of the change in shear stress over the y dimension (Equation 16).

$$\frac{\partial P}{\partial x} = \frac{\partial}{\partial y}(-\tau)$$

Equation 16

The continuity equation for this problem is given in Equation 17. Once again assuming the fluid is incompressible, the term for changes in density disappears and the result of the equation is zero divergence for velocity.

$$\frac{\partial v_x}{\partial x} + \frac{\partial v_y}{\partial y} = 0$$

Equation 17

The constitutive equation is dependent on the model being used. In a general form the relation can be expressed in terms of the shear rate as a function of shear stress. Most equations for fluid are written in terms of the viscosity or shear stress as a function of shear rate. This relation makes sense in terms of measuring viscosity at a defined shear rate, however in physics terms the shear rate is a response to the applied stress, so the inverse relation is preferred. This generalized relation is in Equation 18.

$$f(\tau) = -\frac{\partial v_x}{\partial y}$$

Equation 18

Finally the fluid flows with an applied external force. This force is a constant that's applied at the walls. Since with lubrication theory the pressure gradient is a function of x position only (Equation 15), integral of pressure at the wall of the fluid yield the total force applied (Equation 19). The coordinate system is setup so that origin bisects both the height and the length in the model (Figure 19), which means the total force is twice the integral of over the half length.

$$F = 2w\int_0^L P dx$$

Equation 19

3.2.2 Boundary Conditions

Boundary conditions are given in Equation 20. The first Equation 20a comes from symmetry condition at the center point, where the flow in the x direction is stagnant. The same is true for Equation 20c in the y direction, where the velocity at the centerline is 0. The no slip boundary condition is in Equation 20b as well as in Equation 20d, the condition is derived from no slip boundary at the wall and the continuity equation. Equation 20e is the boundary condition for velocity at the wall, which is assumed to be uniform with value $\dot{h}$. The pressure boundary condition is in Equation 20f, where the relative pressure at the end of the fluid is 0 (atmospheric). The initial condition to this problem is usually an initial height for the gel h_0.

$$v_x(x=0)=0 \quad \text{(a)}$$

$$v_x(y=h)=0 \quad \text{(b)}$$

$$v_y(y=0)=0 \quad \text{(c)}$$

$$\frac{\partial v_y}{\partial y}(y=h)=0 \quad \text{(d)}$$

$$v_y(y=h)=\dot{h} \quad \text{(e)}$$

$$P(x=L)=0 \quad \text{(f)}$$

Equation 20

3.3 Results

3.3.1 Power Law Fluid

The flow of a Power Law fluid in channel geometry can be adapted from the radial flow model. Both the continuity equation in Equation 17 and the Navier-Stokes equation have been adapted to a rectangular coordinate system. The flow remains two-dimensional with the flow in third depth dimension neglected. Constitutive equation (Equation 18) for a Power Law fluid is shown in Equation 21. Here m and n are the parameters in the Power Law model. The parameter n is the flow behavior index and is related to the shear thinning behavior of the fluid, for a Newtonian fluid the flow behavior index is 1. The parameter m is closely related to viscosity, however its unit is dependent on the value of n. These two parameters are obtained from rheological experiments with varying shear rate by fitting linear regression of log-log plot of viscosity vs. shear rate.

$$\tau = m\left(-\frac{\partial v_x}{\partial y}\right)^n$$

Equation 21

Equation 21 can be plugged into Equation 16 to give the relation between pressure gradient and shear stress. Using the continuity equation from Equation 17, the shear stress can be converted to velocity in the vertical instead of the horizontal direction yielding Equation 22.

$$\frac{\partial P}{\partial x} = m\frac{\partial}{\partial y}\left(\left(x\frac{\partial^2 v_y}{\partial y^2}\right)^n\right)$$

Equation 22

Since the pressure gradient is a function of x only (Equation 15), the expression in Equation 22 can be integrated in the horizontal direction to yield an expression for the vertical velocity. The derivative of vertical velocity can be integrated again to yield the wall velocity boundary condition of Equation 20e. Together with boundary condition of zero pressure at the edge of the flow (Equation 20f) the pressure as a function of position is Equation 23.

$$P = \left(x^{n+1} - L^{n+1}\right)\left(\frac{m}{n+1}\right)\dot{h}^n\left(\frac{2n+1}{n}\right)^n h^{-(2n+1)}$$

Equation 23

Integrating the pressure over the area of the canal would yield the total pressure applied of Equation 19. In this equation, the only unknown is $\dot{h}$ the wall velocity. The terms can be rearranged to Equation 24.

$$\dot{h} = h^{\frac{3n+3}{n}}\left[\frac{F}{\left(\frac{2wm}{n+2}\right)\left(\frac{2n+1}{n}\right)^n\left(\frac{V}{4w}\right)^{n+2}}\right]^{\frac{1}{n}}$$

Equation 24

This equation can be integrated over time to give an explicit expression for the height of the gel as a function of time. This is in Equation 25, and two new constants appear in this expression, p which is the power that the time t is raised to, and G a constant that scales the applied force.

$$h = \left[\left(\frac{1}{h_0} \right)^p + p \left(\frac{F}{G} \right)^{\frac{1}{n}} t \right]^{-\frac{1}{p}} \quad \text{(a)}$$

$$p = \frac{2n+3}{n} \quad \text{(b)}$$

$$G = \left(\frac{2n+1}{4n} \right)^n \left(\frac{m}{8n+16} \right) \left(\frac{V^{n+2}}{w^{n+1}} \right) \quad \text{(c)}$$

Equation 25

The result is similar to that of the radial flow model, with the key difference being the value of the two constants. The result for the radial flow model of the two constants p and G is in Equation 26.

$$p = \frac{3n+5}{2n} \quad \text{(a)}$$

$$G = \left(\frac{2n+1}{2n} \right)^n \left(\frac{\pi m}{n+3} \right) \left(\frac{V}{2\pi} \right)^{\frac{n+3}{2}} \quad \text{(b)}$$

Equation 26

Comparisons can be made for the spreading behavior between the channel and the cylindrical geometry. If the initial height is large or the time of interest is long, then the first term h_0 drops out of the equation, and the spreading as a function of time depends only on the parameter p and a force that is scaled by constant G. The two parameters of p in the channel and radial model can be compared directly. The result is that the power for a radial flow is strictly greater than the channel flow regardless of the value of n and is independent of the channel geometry (for example the width) and other parameters such as the volume and force applied. A greater power parameter p means faster spreading. This makes sense as the radial flow is unconstrained in two dimensions while the channel flow is constrained to flow in a single dimension.

3.3.2 Herschel-Bulkley Fluid

The logical extension to the Power Law model is the Herschel-Bulkley (H-B) model. In the H-B model an additional parameter for yield stress is added to the base Power Law model. Yield stress is a theoretical limit below which the fluid is in static equilibrium. Yield stress behavior is common in many cross-linked polymer systems. For example in hydrogels, the addition of carbopol increases the observed yield stress. This is seen in many candidate microbicide gels, which contain both carbopol and cellulose. The constitutive model is in Equation 27. Shear stress in the problem is no longer continuous, with the stress strain behavior dependent on whether the stress is greater or less than the yield stress.

$$\frac{\partial v_x}{\partial y} = \begin{cases} -\left(\frac{\tau - \tau_0}{m}\right)^{\frac{1}{n}} & \tau \geq \tau_0 \\ 0 & \tau < \tau_0 \end{cases}$$

Equation 27

Starting with Equation 16, if lubrication theory is assumed, the expression can be integrated, and together with the boundary condition in Equation 20d would yield equation Equation 28.

$$\tau = (h - y)\frac{\partial P}{\partial x}$$

Equation 28

Equation 29 is formed by setting Equation 28 equal to the constitutive Equation 27 over the region of fluid that has yielded.

$$(h - y)\frac{\partial P}{\partial x} = m\left(-\frac{\partial v_x}{\partial y}\right)^n + \tau_0$$

Equation 29

From Equation 28, a critical height y_c (Equation 30) can be defined as where the fluid has just begun to yield. Anything above this height is free flowing, while anything below this critical level is static fluid in plug flow. For a flow field where it is flowing everywhere in the fluid, as it is with the case with no yield stress, the critical height is simply the total height.

$$y_c = h - \tau_0 \left(-\frac{\partial P}{\partial x} \right)^{-1}$$

Equation 30

Equation 29 can be integrated to find the velocity in the x direction both above (Equation 31a) and below (Equation 31b) the critical height.

$$v_x = \left[-\left(\frac{-h\frac{\partial P}{\partial x} - \tau_0}{m} \right)^{\frac{n+1}{n}} + \left(\frac{(z-h)\frac{\partial P}{\partial x} - \tau_0}{m} \right)^{\frac{n+1}{n}} \right] \left(\frac{\partial P}{\partial x}\frac{1}{m} \right)^{-1} \left(\frac{n}{n+1} \right) \qquad \text{(a)}$$

$$v_x = -\left(\frac{-h\frac{\partial P}{\partial x} - \tau_0}{m} \right)^{\frac{n+1}{n}} \left(\frac{\partial P}{\partial x}\frac{1}{m} \right)^{-1} \left(\frac{n}{n+1} \right) \qquad \text{(b)}$$

Equation 31

The mass balance equation at each position along the width is given by the vertical squeezing of the gel and the horizontal spreading of the gel in Equation 32.

$$\int_0^h v_x dy = -\dot{h}x$$

Equation 32

Applying velocities in Equation 31 to the mass balance Equation 32 yields an equation relating the pressure gradient to the vertical wall velocity $\dot{h}$ in Equation 33.

$$-\dot{h}x=-\left(\frac{\partial P}{\partial x}\frac{1}{m}\right)^{-1}\left(\frac{n}{n+1}\right)\left[\left(\frac{-h\frac{\partial P}{\partial x}-\tau_0}{m}\right)^{\frac{n+1}{n}}\left(h-\tau_0\left(-\frac{\partial P}{\partial x}\right)^{-1}\right)-\right.$$
$$\left.\left(\frac{-h\frac{\partial P}{\partial x}-\tau_0}{m}\right)^{\frac{2n+1}{n}}\left(\frac{n}{2n+1}\right)\left(\frac{\partial P}{\partial x}\frac{1}{m}\right)\right]-\left(\frac{-h\frac{\partial P}{\partial x}-\tau_0}{m}\right)^{\frac{n+1}{n}}\left(\frac{\partial P}{\partial x}\frac{1}{m}\right)^{-1}\left(\frac{n}{n+1}\right)\tau_0-\left(\frac{\partial P}{\partial x}\right)^{-1}$$

Equation 33

The above equation can be simplified and non-dimensionalized into Equation 34a, where X (Equation 34b) is the non-dimensional pressure gradient, and S_n (Equation 34c) is the non-dimensional wall velocity.

$$0=\left(\frac{n+1}{n}\right)\left(\frac{x}{L}\right)S_n X^2-\frac{n+1}{2n+1}\left(-X-1\right)^{\frac{2n+1}{n}}-\left(-X-1\right)^{\frac{n+1}{n}} \quad \text{(a)}$$

$$X=\frac{h}{\tau_0}\frac{\partial P}{\partial x} \quad \text{(b)}$$

$$S_n=\frac{L\left(-\dot{h}\right)m^{\frac{1}{n}}}{h^2\tau_0^{\frac{1}{n}}} \quad \text{(c)}$$

Equation 34

No simple explicit solution exists for the non-dimensionalized pressure gradient in Equation 34a. However asymptotically with large and small X, the last term is small compared to the first two. By neglecting the last term in the equation, the pressure gradient can be solved explicitly, this reduces to Equation 35.

$$X = -1 - \left(\frac{2n+1}{n}\right)^n \frac{mx^n\left(-\dot{h}\right)^n}{\tau_0 h^{2n}}$$

Equation 35

The pressure gradient in Equation 35 can be integrated once to yield the pressure, and plugged into the force equation in Equation 19. The result is the unknown wall velocity $\dot{h}$ as a function of the known parameters in the problem. Unlike the Power Law fluid, a Herschel-Bulkley fluid here does not contain an explicit solution of height as a function of time, but rather an ordinary differential equation for height that can be solved numerically as an initial value problem in Equation 36.

$$\dot{h} = -\left(Fh - \tau_0 L^2\right)^{\frac{1}{n}} \left[\left(\frac{2n+1}{n}\right)^n \frac{2wmL^{n+2}}{(n+2)h^{2n}}\right]^{-\frac{1}{n}}$$

Equation 36

3.3.3 Carreau-like Fluid

A Carreau fluid is an improvement to the Power Law model[88]. It contains three parameters, in addition to the two from the Power Law model it has one additional parameter that capture the shoulder at low shear rates of the log-log viscosity vs. shear rate data observed for certain materials. This parameter is called the zero shear viscosity (m_0), it is a correction to the Power Law model where instead of an infinite viscosity at zero shear stress, the viscosity is now at a defined value. Similar to the Herschel-Bulkley model, a yield stress can also be introduced here. The constitutive equation is given in

Equation 37, where depending on whether the applied stress is greater than the yield stress the fluid is either in the yielding or unyielding region. Unlike the previous models where the shear stress is defined as a function of shear rate, here a "Carreau-like" fluid has similar characteristics to a Carreau fluid but with shear rate as a function of shear stress. This leads to an explicit relationship where the stress causes the strain.

$$\frac{\partial v_x}{\partial y} = \begin{cases} \frac{\tau - \tau_0}{m_0} + \left(\frac{\tau - \tau_0}{m} \right)^{\frac{1}{n}} & \tau \geq \tau_0 \\ 0 & \tau < \tau_0 \end{cases}$$

Equation 37

Integrating Equation 16 with respect to y gives a simple expression for pressure. From Equation 15, it is clear that the pressure gradient is a function of x only. The shear stress is simply the pressure gradient times y. Using Equation 18 which relates a generic stress strain relation and then plugging it into the continuity equation in Equation 17 yields Equation 38.

$$\frac{\partial}{\partial x}\left(- f\left(\frac{\partial P}{\partial x} y \right) \right) = -\frac{\partial^2 v_y}{\partial y^2}$$

Equation 38

This expression can be integrated twice with respect to y with the top boundary having vertical velocity of $\dot{h}$, which becomes Equation 39.

$$\int_0^h \int_y^h f\left(\frac{\partial P}{\partial x}\tilde{y}\right) d\tilde{y} dy = -\dot{h}$$

Equation 39

In the above expression, the double integral can be reduced to a single integral graphically. The region of integration is a triangle over the region bounded by y and $\tilde{y}$, because the integrand is a function of $\tilde{y}$ only, this triangle region can be reduced to y times the integrand. Once again, define a critical y value at which the fluid has just yielded (Equation 40). Then the single integral is given in Equation 41.

$$y_{crit} = \frac{\tau_0}{\frac{\partial P}{\partial x}}$$

Equation 40

$$\int_{y_{crit}}^h y\left(\frac{\frac{\partial P}{\partial x}y - \tau_0}{m_0}\right) + y\left(\frac{\frac{\partial P}{\partial x}y - \tau_0}{m}\right)^{\frac{1}{n}} - y_{crit}\left(\frac{\frac{\partial P}{\partial x}y - \tau_0}{m_0}\right) - y_{crit}\left(\frac{\frac{\partial P}{\partial x}y - \tau_0}{m}\right)^{\frac{1}{n}} dy = -\dot{h}x$$

Equation 41

The above expression can be integrated again to yield a relation between the pressure gradient as a function of position and the vertical wall velocity $\dot{h}$ in Equation 42.

$$g\left(\frac{\partial P}{\partial x}\right) = x = -\frac{1}{\dot{h}}\left[\frac{1}{3}\frac{1}{m_0}\left(\frac{\partial P}{\partial x}h^3 - \tau_0 y_{crit}^2\right) - \frac{\tau_0}{m_0}h\left(h - y_{crit}\right) + \frac{\left(\frac{\frac{\partial P}{\partial x}h - \tau_0}{m}\right)^{\frac{2n+1}{n}}}{\left(\frac{\frac{\partial P}{\partial x}}{m}\right)^2\left(\frac{2n+1}{n}\right)}\right]$$

Equation 42

This is the effective Reynolds equation for the problem. The force equation is given by Equation 19 as an integral of pressure. Here, an explicit relation between the pressure or pressure gradient and position is not known. Instead, Equation 42 gives a simple inverse relation where the position x is a function of the pressure gradient. The integral of the pressure gradient can be shown to be equivalent to an integral of the inverse function over the same volume in Equation 43. Here the function g is the inverse function on the right hand side of Equation 42.

$$\frac{F}{2w} = \int_0^L \int_x^L \frac{\partial P}{\partial x} d\tilde{x}\, dx = \int_0^{\frac{\partial P}{\partial x}(x=L)} \frac{1}{2}L^2 - \frac{1}{2}\left[g(y)\right]^2 dy$$

Equation 43

Numerically the solution to height as a function of time can be found by integrating $\dot{h}$ over time. The value of $\dot{h}$ at each time point is governed by integrating the pressure gradient of Equation 42 constrained to the force condition of Equation 43. The first step is to guess a value of $\dot{h}$ at each time point, Equation 42 would give the

pressure gradient from 0 to L, and then this pressure gradient is plugged into Equation 43 to see whether it satisfies the applied force. This process is repeated until a desired tolerance on $\dot{h}$ for that time point is achieved.

3.3.4 Fitting Rheological Parameters

Rheological properties of hydrogels are complex. They cannot be determined by simple viscometer, which only measures the viscosity when the fluid is assumed Newtonian with a low viscosity. A rheometer on the other hand is able to measure a wide range of viscosities, and more importantly is able to do so under a variety of applied stress or shear. The results can be fit to a constitutive model of the fluid for parameters in the model.

Measurements are typically made under body temperature of 37°C in order to simulate the environmental condition a gel is under for most of the flow. Temperature dependence in the properties of a gel has been proposed to control gel spreading. For example, the gel can have a faster rate of spreading at a low temperature when the gel is initially inserted, and a slow rate of spreading at body temperature in order to avoid leakage. Spreading of the pluronic gel is plotted here as area coated as a function of time in Figure 20. A hydrogel is more than 90% water, so the thermal diffusivity is expected to be similar at 0.143×10^{-2} cm^2/s. The characteristic time for a gel measuring 0.1 cm thick is determined by squaring the length and dividing by the diffusivity, which gives a time of around 7 seconds. In the plot, the gel has already reached 35°C at 9 seconds. This

result implies the change from room to body temperature can be considered almost instantaneous.

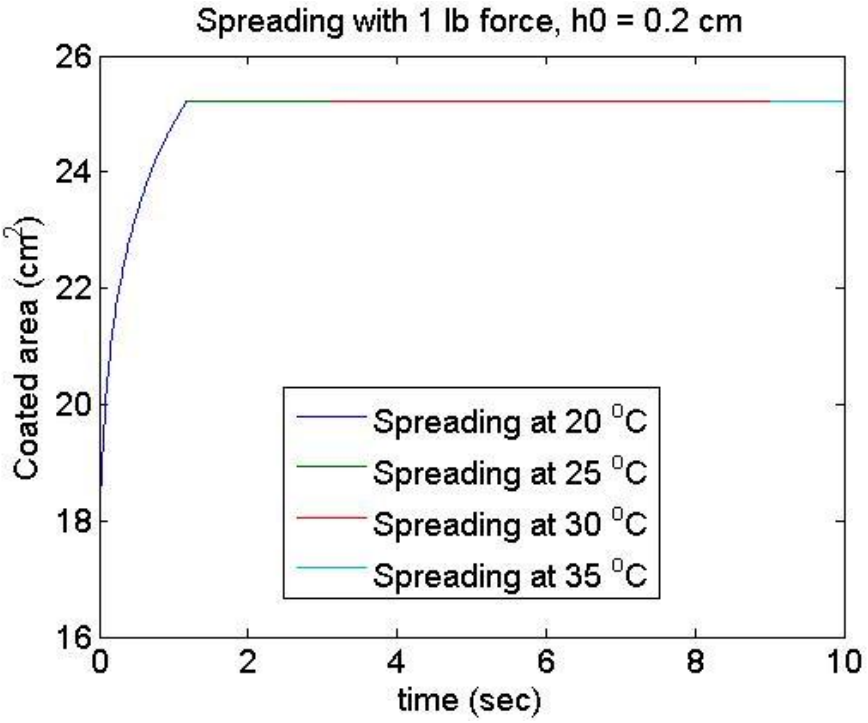

Figure 20: Coated area of a pluronic gel

Two ways of measuring shear stress and shear rate in a rheometer are by either a stress controlled or a strain controlled protocol. The strain controlled protocol are typically used in regions of high shear, while the stress controlled protocol are used in the low shear regions. This is because in the high shear region, if a set stress is applied for a low viscosity gel the gel might shear at a rate higher than the designed limit of the machine, limiting the number of useful data in the experiment. On the other hand, if the gel is highly viscous, in low shear regions a strain controlled protocol is hard to achieve especially when yield stress is present. The yield stress of a fluid usually confounds

experimental stress strain relation. Without accounting for the yield stress, viscosity values at low shear rates will approach infinity since as the shear rate approaches zero the apparent stress stays constant. One way of measuring yield stress is using a stress relaxation experiment[55]. The experiment works by first shearing the gel under constant stress and then stopping the applied stress to measure the residual stress over time, the final time point when the stress settled down to a minimum is used for the yield stress. This is not the only way to measure yield stress, but the method can gave more consistent results compared to the oscillatory method.

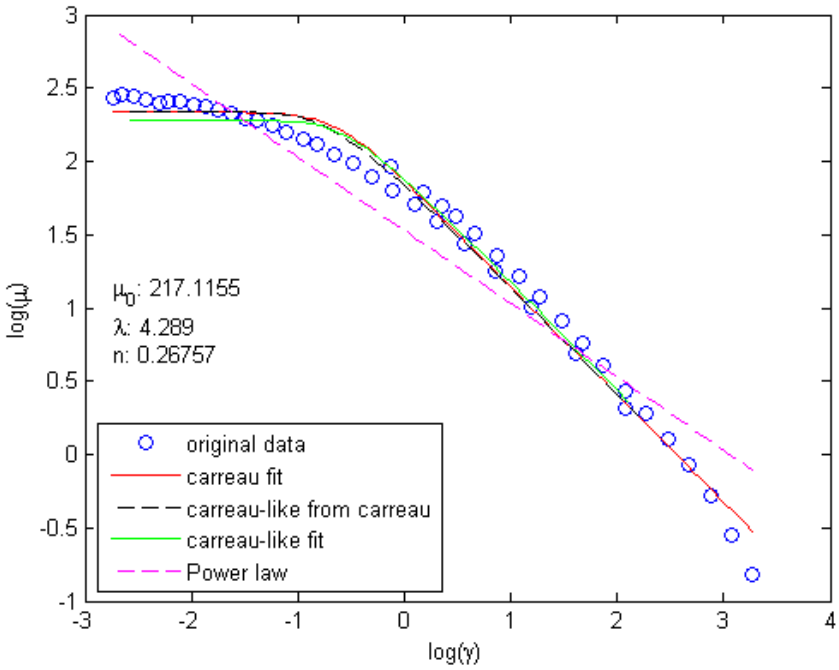

Figure 21: Viscosity vs. shear rate for a typical gel on log-log scale

A typical result for a hydrogel's viscosity vs. shear rate is plotted on the log-log scale in Figure 21. The yields stress is determined from stress relaxation and is

subtracted from the raw stress, negative stress and other anomalous data are removed from the low shear region. This stress is then divided by the shear rate to yield viscosity. The data indicates a Carreau or Carreau-like fluid is the most suitable model because zero stress viscosity is clearly visible at low shear regions. In the linear region, the fluid acts according to the Power Law model, since a straight line in log-log plot indicates a power relation.

There are three ways of fitting a Carreau model to the data. By a Carreau-fit, a Carreau-like fit, or a Carreau-like model from Carreau-fit. Carreau and Carreau-like are different models that incorporate the same rheological properties. The important distinction is while in the Carreau model stress and viscosity is a function of shear rate, in a Carreau-like model the relation is reversed. Carreau-like parameters can be converted from Carreau parameters[85], the difference between the two methods are not only in the final model used but also in the way model is fitted. Linear fits that minimize the sum of residuals are in different units for the two models, one is minimizing the stress while the other is minimizing the shear rate. In the example above, all three models gave approximately the same result, however this is not always the case. The data fitted with the Power Law model is also plotted with a dashed line. The model has the worst fit because it cannot factor in the zero shear viscosity behavior.

3.3.5 Rheology of Gel Aging

Gels are expected to have a long shelf life, even under high temperature storage conditions in areas without refrigeration. A gel past expiration have chemical and mechanical changes that make the product unsuitable for application. Accelerated aging is one way of determining the expiration of a product with a shortened time frame for testing. This can be achieved by subjecting the gel to a high temperature of around 40 °C, with samples tested monthly. Typically, the physical property is measured by viscosity at a predefined shear rate of 1 sec^{-1}, this value can be observed to decrease over time as the long polymer structure of the gel breaks down. It is of interest to test how aging of a gel influences its properties in drug delivery, more specifically the spreading of such gel after application. Since the gel is not a simple Newtonian fluid, a single viscosity measurement is insufficient to characterize the fluid. A more comprehensive rheological experiment can be conducted on the gel for a range of shear rates. This is shown in Figure 22 for a fresh gel and a gel that has been aged for 12 months.

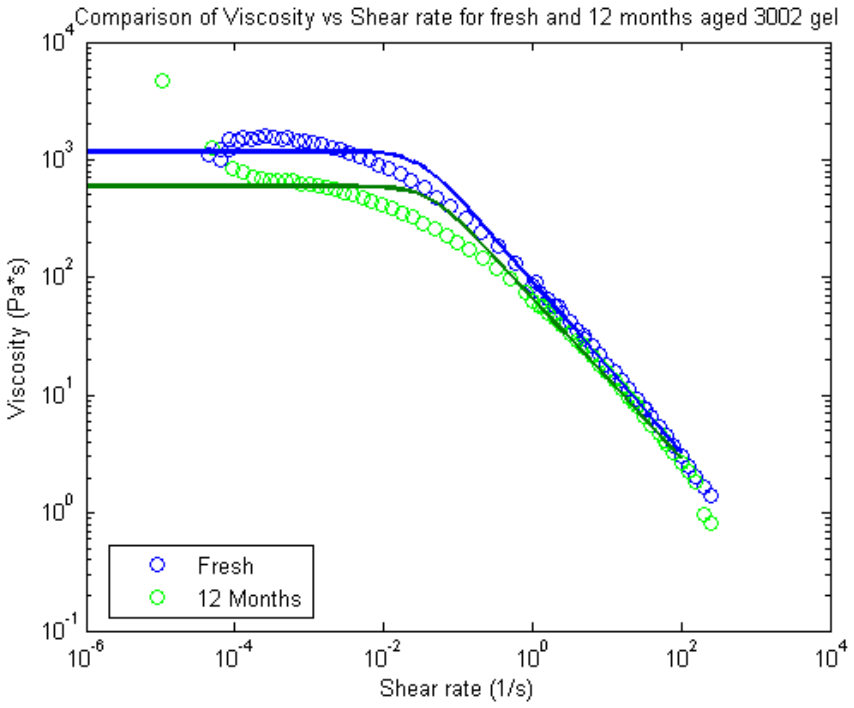

Figure 22: Rheology of a fresh and 12 months aged 3002 gel

The plot shows at 12 months the viscosity for an aged gel is lower than that of a fresh gel, which is more prominent in the low shear rate regions. If only the viscosity at 1 inverse second is measured, which means the behavior at low shear rates cannot be observed. Two Carreau-like fits are overlaid, with only very small differences in viscosity at higher shear rates. Spreading comparison of the two gels with volume of 2 mL and 4 mL is in Figure 23. The aged gel spread faster than the fresh gel, this effect is more pronounced for a high volume gel. Due to faster spreading, the aged gel is observed to have leaked at around 100 minutes, while the fresh gel leaks at around 3 hours. This difference will affect drug delivery as well as user preference.

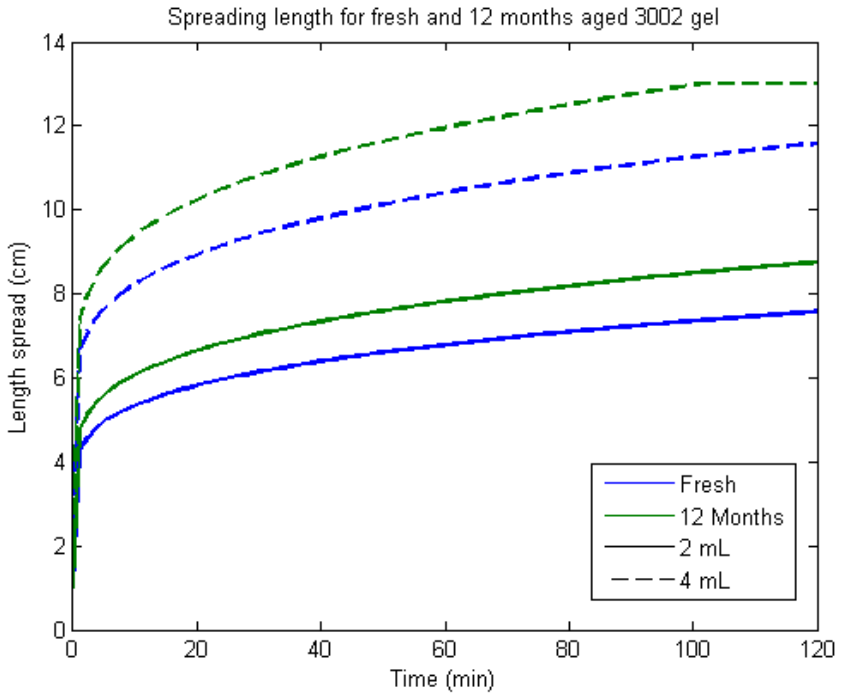

Figure 23: Gel spreading for fresh and aged gel at 2 mL and 4 mL

3.3.6 Comparison with Compliant Wall Model

This chapter focused on flow in a channel squeezed by a rigid wall. Another formulation of squeezing flow for a Carreau-like fluid was developed by Szeri et al [85, 87, 88] for a compliant wall. In the compliant wall model the force applied by the wall is proportional to the local gel height, so the height of the gel is now a function of position and time instead of uniform. In addition, instead of a finite boundary for the leading edge of a gel, this formalism has gel height defined as non-zero in the entire one dimensional infinite domain. As an initial condition, the gel is assumed to follow a functional shape, in this case a Gaussian distribution. The spreading of the gel can be visualized by the function of height at each time point (Figure 24). The gel spreads the

fastest initially, like the rigid wall model. The first time point is in blue, the height is flattened immediately to the next time point in turquoise. Due to the fact the leading edge of the gel for a compliant wall model is hard to define, there is not a single way to compare with the rigid wall model. One way to define the leading edge is to treat the height distribution as a statistical probability distribution function and then use four times the standard deviation[85] as the extent of spreading.

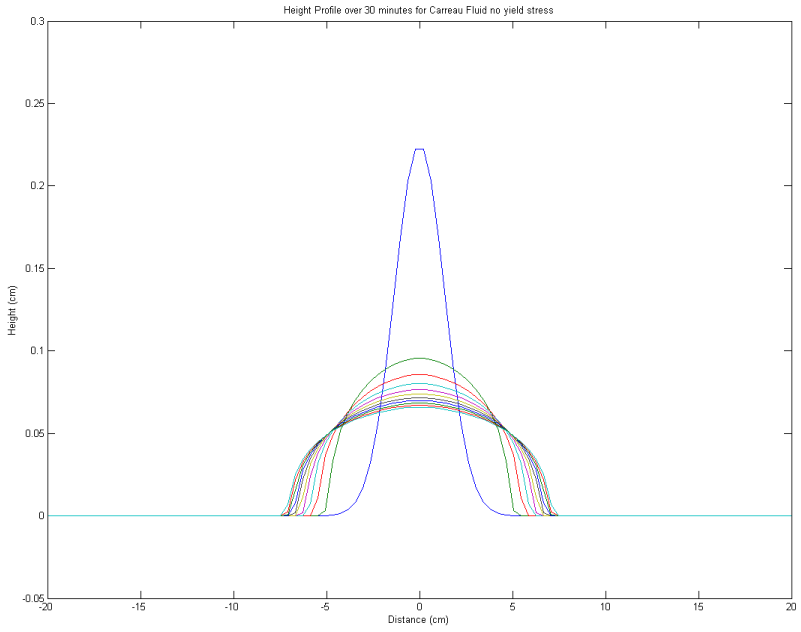

Figure 24: Height profiles at different times for the compliant wall model

Comparison between the extent of spreading for the compliant and rigid wall models is plotted in Figure 25. Three test gels with different rheological properties are used at 3 mL. The compliant wall model is expected to spread less, because a compliant wall can better distribute the stress throughout the gel, decreasing the maximum shear

stress on the gel. For gels DG 1 and DG 3, the ratio of area coated is around 0.7, meaning a compliant wall coated less than rigid wall, and for the gel DG 2 the ratio is slightly more than 1. The gel DG 2 is a bolus gel with height yield stress and viscosity at all shear rates, the difference in coated area can be attributed to the way yield stress is handled between the two models. Overall the ratio between two models is close to unity after the first few minutes of spreading.

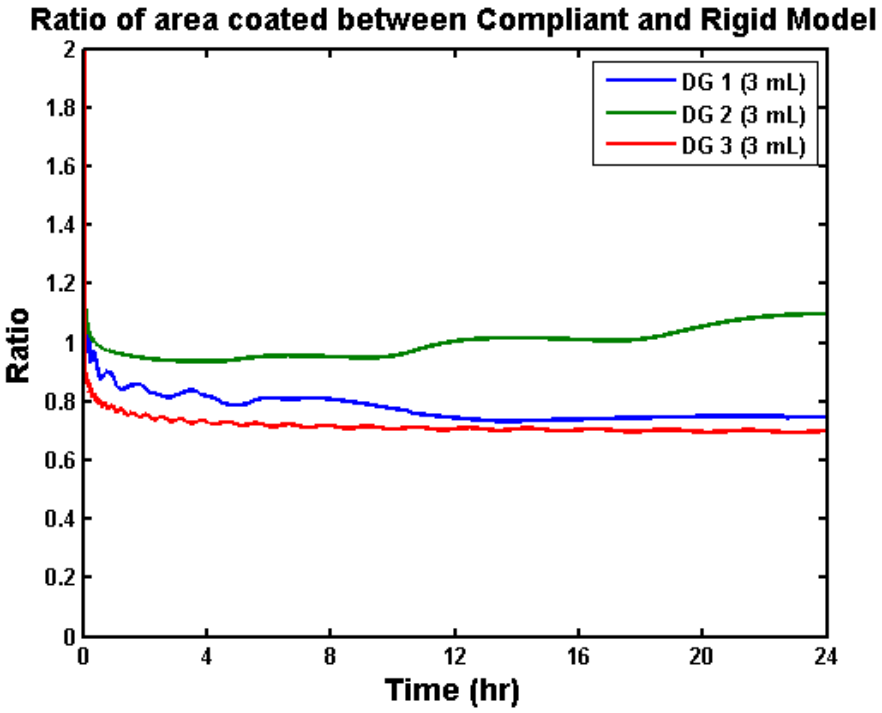

Figure 25: Area coated ratio between compliant and rigid wall model

3.4 Discussion

Gel spreading in the vaginal canal is modeled here in a rectangular geometry. This model is a more realistic adaptation of an earlier model of spreading under infinite plate geometry. The spreading model takes gel rheology and volume as an input and

can output the time dependence of spreading area and spreading length. This information can help design gels that can deliver more drugs by fast coating initially, and also slow spreading after completely coating the entire vaginal canal in order to minimize leakage. Gel leakage can affect user preference and adherence to the product, which studies have shown to be a major factor in gel effectiveness.

Three models of gel rheology are explored, from the simplest to the most complex they are a Power Law fluid, a Herschel-Bulkley fluid, and a Carreau-like fluid with yield stress. Each new model builds on the previous one by each adding an additional parameter. A Power Law fluid has two parameters, the flow consistency index and flow behavior index. The Herschel-Bulkley model adds a yield stress to the two parameters from Power Law model. And the Carreau-like fluid adds a zero shear viscosity. The solution to each model is progressively harder to solve computationally.

The first model is of a Power Law fluid, which can be thought of as a more advanced version of a Newtonian fluid that has an additional parameter that changes viscosity as a function of shear rate. The solution for a Power Law fluid is an explicit relation for the height of the gel as a function of time and can also be easily converted to coated area or spreading length by knowing the volume of the gel and channel width. There are a lot of similarities between this channel flow problem and radial flow of a Power Law fluid being squeezed by two infinite plates. The basic form of the two equations is the same, with the difference being the two constants in the equation.

Comparing flow for the two models, the channel flow is able to spread faster and create a larger coated area. This difference arises because stress is more evenly distributed in the cylindrical model while in a canal the constraints forces higher stress at the leading edge of the channel.

The second model, for a Herschel-Bulkley fluid is essentially a Power Law model with yields stress. A yield stress is the theoretical limit for which fluid would not flow if applied stress is less than the yield stress. Solution to the flow problem is an ordinary differential equation for height based on the current height and the rheological parameters. Notably time is not a dependent variable. This independence means the problem is time invariant and does not have any memory effects, which is consistent with physical theory. The solution to this problem can be checked by setting the yield stress to zero, which would reduce to the Power Law model, and indeed the solution agrees with this prediction.

The last and most advanced model is the Carreau-like model, which adds a zero shear viscosity to the Herschel-Bulkley model. Zero shear viscosity is sometimes observed in complex fluids such as hydrogels. It characterizes a limiting viscosity as shear rate approaches zero, contrary to the Power Law and H-B models where the theoretical viscosity as shear rate decreases is infinite. The solution to this problem is an integral equation at each time point, where given the current height, the wall velocity has to satisfy the integral of pressure gradient yielding the total applied force.

Numerically this solution is similar to an ordinary differential equation except at each time step the solution to the integral equation has to be solved by another numerical method. The Carreau-like method asymptotically approaches the Herschel-Bulkley model when the zero shear viscosity approaches infinity. This observation can be tested by setting the zero shear viscosity to an unrealistically high value, which yields the same result as a Herschel-Bulkley fluid.

Use of rheological models depends on rheological parameters measured experimentally. Obtaining these measurements is not trivial. It involves finding the yields stress by stress relaxation experiment, and then using this value as a baseline in measuring the stress strain behavior of the gel over a range of shear rates. Transient thermal effects can be ignored, since the gel will heat up to body temperature within a few seconds after application due to high thermal diffusivity. The final step is fitting the model to rheological data. Three different methods of fitting a Carreau model are explored, and the results show all of them gave good fits to the rheological data.

Rheology is important in determining the shelf life of a gel. And in the reverse case, gel rheology can be used to find the age of an unknown gel. An accelerated aging experiment was performed with a sample gel and the result showed that an aged gel will experience lower viscosity and faster spreading compared to a fresh gel. Faster spreading in general improves drug delivery. However, faster spreading could be worse

for adherence due to potential gel leakage. Spreading computations show that the aged gel spreads only slightly faster, and leaks earlier than a fresh gel.

Comparison can be made between the rigid wall spreading model and another model developed in UC Berkeley for a compliant wall. The result is very similar when both models use the same rheological parameters, gel volume, and channel width. The ratio of spreading as a function of time for the two models varies from 0.7 to 1.1; this difference is most likely due to infinite vs. finite domain spreading and the difference between how stress is distributed. Similarity between the two models is encouraging.

3.5 Conclusion

A rheological model of the spreading of a gel is adapted to a rectangular geometry for the vaginal environment. The result is a more accurate representation of gel spreading compared to the previous models. Three different constitutive models of rheology are created and provide solutions of varying complexity from an explicit solution to an ordinary differential equation to an integral equation. Methods for fitting rheological measurements to experimental data are also explored with applications in gel aging. The model of a rigid wall is compared to a compliant wall model which yielded comparable results.

4. Combining Gel Spreading and Drug Transport

4.1 Introduction

Chapter 2 and Chapter 3 are both useful in understanding drug transport from a vaginal gel to mucosal tissue. However, neither model is complete. In the first model of Chapter 2, gel is assumed to have perfectly coated the entire vaginal canal. This is only true for a low viscosity gel after initial gel insertion. In the second model of Chapter 3, a detailed model of gel flow has been developed, but the model does not include drug delivery. A logical follow up then is to combine the models of drug delivery and gel flow to form a combined model of both behaviors[26]. In this model, spreading for the gel is first computed from methods in Chapter 3. Since drug spreading occurs independently of drug transport, this step can be decoupled from the drug transport process. A second step is to use gel spreading as an input and then calculate drug transport into the vaginal tissue. The method from Chapter 2 can be used and adapted to this new model. The key difference being while the previous case is a perfect coating model in one dimension, spreading coupled with drug transport is fundamentally a two-dimensional problem in the direction of gel spreading and tissue depth. This model assumes the concentration in the third width dimension is symmetrical and homogeneous.

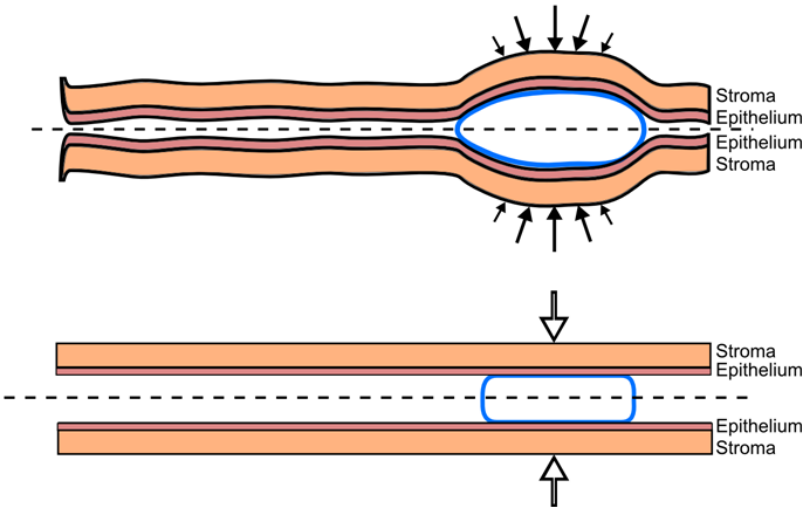

Figure 26: Geometry of gel spreading and drug transport. Top is an exaggerated picture of the model and the bottom is a rectilinear approximation

The spreading problem and the rectilinear approximation are shown in Figure 26. A gel is inserted in an initial position along the canal, the left opening is the introitus, and the right end is towards the fornix (not shown). Due to the small height of the gel compared with the width, spreading can be approximated as rectilinear in the bottom of Figure 26. Pressure of the flow is vented under atmospheric boundary conditions at the introitus to the left. The presence of the introitus and fornix in this model allow the gel to leak if it spreads past the introitus, and the gel will stop flowing at the fornix. The epithelial and stromal layers are also indicated on the figure. Force applied by the compliant vaginal wall exerts pressure proportional to the applied gel volume, but in this model a simplification is made where the applied force is assumed to be the total force of the rigid wall.

4.2 Materials and Methods

4.2.1 Geometry of the Model

Drug delivery in the vaginal mucosa by a gel derives from two interacting mass transport processes, gel flow due to the squeezing by the walls of the canal and drug diffusion from the gel into the tissue. Gel flow is independent of drug transport, thus it can be computed first and the results used as input to the solution of diffusive drug transport into the tissue.

This model introduces more physically significant characteristics of the human vaginal canal, which is an improvement over gel spreading introduced in Chapter 3. The base model of spreading is still a rectangular coordinate system with squeezing by two rigid walls. But instead of spreading under an infinite canal, here the canal is finite with opening on one end (introitus) and another closed end (fornix). Gel is typically inserted as a bolus by a piston-type applicator. The bolus is assumed to be approximately rectangular due to a narrow height of the gel, which is also the initial condition of the canal. Initial gel placement influences its flow over time due to: gel may spread to an extent that is outside of the introitus and begins to leak and/or the innermost edge of the gel may flow up to the wall of the fornix and cease to move. In this analysis, like in Chapter 2 the Cartesian coordinate system is used with the y axis at the centerline of the gel and the canal, which is symmetrical between the top and the bottom. The volume of microbicide gels ranges from 2 to 5 mL, with a 5 mL gel showing significant leakage.

In this analysis gel of 2 and 4 mL are picked as representative of both high and low volume.

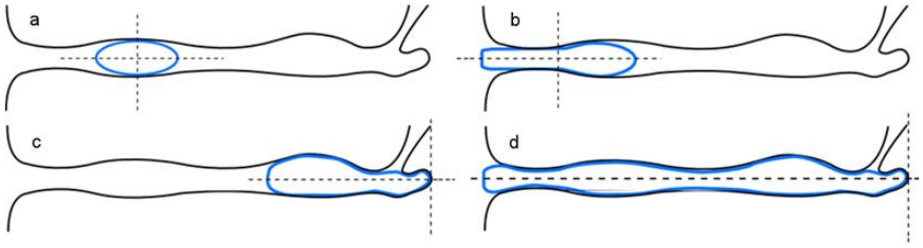

Figure 27: Four different cases of gel flow dependent on the initial position of inserted gel, where it can either leak and/or flow in one direction only

Depending on the initial gel placement and flow there are four different configurations that can be applied to the symmetrical gel flow model in Chapter 3 (Figure 27). These differ in relation to whether or not the distal edge of the gel and the proximal edge reach either boundary during the course of flow. If the distal edge reaches the introitus the gel will leak, this is modeled as a reduction in gel volume. If the proximal edge reaches the inner boundary at the fornix, gel flow will be unidirectional towards the introitus, in terms of the model a unidirectional flow is just half of the bidirectional flow from Chapter 3. Depending on the parameters of the problem, the overall flow during the time course of interest might be a sequence and combination of one or more cases.

4.2.2 Rheology of Test Gels

In this analysis, the rheological behavior of the gels is characterized as Carreau-like fluid with yield stress. This is the most advanced and accurate model of rheological

behavior, in fact other rheological models can be considered a subset of Carreau-life fluid. The primary benefit of this model over simpler models such as Power Law is that it can accurately account for low shear strain behavior, which plays a major role in governing the flow rate.

Three test gels are used in this model. They were created with properties that bracket a range of potential candidate gels, with a range of rheological properties. The gels are made from hydroxyethylcellulose with glycerol, methyl paraben, propyl paraben, and phosphate buffer to maintain pH. Gel rheological properties (Table 4) were measured at body temperature (37°C) using a constant stress protocol on a TA Instruments model AR 1500ex rheometer (using a 4° cone and 20 cm plate configuration). Yield stress is measured using residual stress as a surrogate by stress relaxation experiments in a Brookfield 5HB DV-III Ultra rheometer with a CPE-40 cone[70]. The gel was initially stressed at 10 sec^{-1} for 5 min, and then relaxed for 14 min, during which time stress was measured to determine the limiting value.

Table 4: Rheological parameters of three test gels

Gel	**Yield Stress** τ_0 (dynes/cm^2)	**Zero Shear Viscosity** m_0 (Poise)	**Flow Consistency** m (dyne/cm^2 x s^n)	**Shear Thinning Index** n
DG-01	20	3820	1300	0.261
DG-02	380	2070	1960	0.219
DG-03	0	175	153	0.344

4.2.3 Governing Equations for Drug Transport

Drug transport from gel into the vaginal mucosa is characterized in this model by a two-dimensional unsteady convection-diffusion mass transport process. The vaginal mucosa consists of two histologically different layers, the epithelium and the stroma (Figure 26). This model is similar to the model in Chapter 2 with four different compartments for gel, epithelium, stroma and the blood. Unlike the earlier model, the epithelium and the stroma compartments for the tissue are now two dimensional, while the gel and the blood compartments are assumed to be homogenous. This is due to the fact diffusion coefficient of the drug in gel is several orders of magnitude higher than the diffusion coefficient in the tissue compartments. The transport from gel spreading is also much higher than diffusion, in essence a fast spreading gel is well mixed by convective transport. The Péclet number (Figure 28) of gel spreading compared with diffusion for Tenofovir is at least one order of magnitude higher than unity over a period of 24 hours. In Chapter 2 gel concentration was found to be nearly uniform with depth, and a similar assumption can be made here.

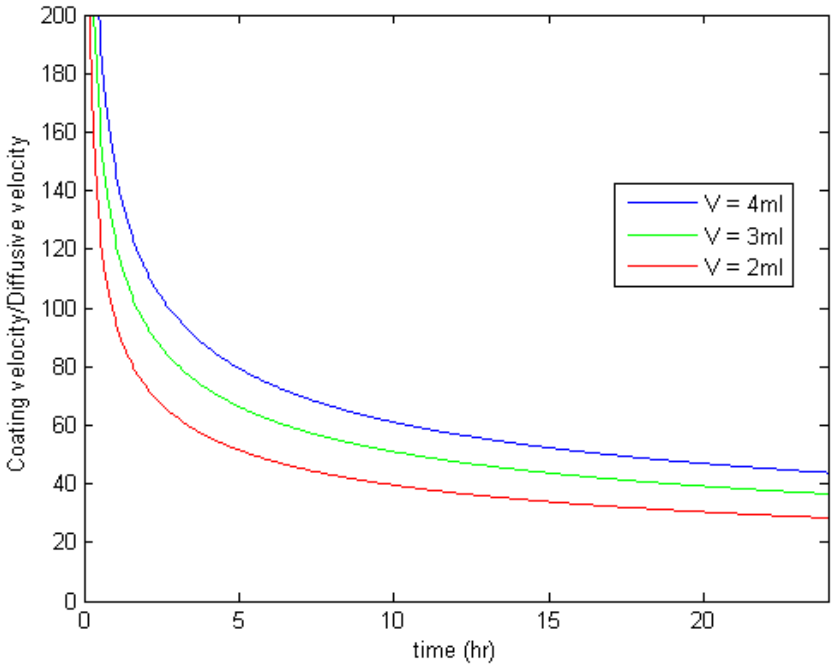

Figure 28: Péclet number of gel spreading and diffusion

Tenofovir diphosphate production is included in the epithelial and stromal compartments, which contain cells that Tenofovir enter and become phosphorylated. The stroma contains HIV infectible host cells that are believed to be a primary source of HIV transmission. Thus TFV-DP concentration in the stroma is the key output of this model.

$$\frac{dC_G}{dt} = D_E \frac{4w}{V_G} \int_{x=0}^{L} \left. \frac{\partial C_E}{\partial y} \right|_{y=0} dx - k_D C_G \qquad \text{(a)}$$

$$\frac{\partial C_E}{\partial t} = D_E \left(\frac{\partial^2 C_E}{\partial x^2} + \frac{\partial^2 C_E}{\partial y^2} \right) - k_{on} \left\{ C_E \phi_E - \frac{C_{DP}}{r} \right\} + k_{off} C_{DP} \qquad \text{(b)}$$

$$\frac{\partial C_S}{\partial t} = D_S\left(\frac{\partial^2 C_S}{\partial x^2} + \frac{\partial^2 C_S}{\partial y^2}\right) - k_B C_S - k_{on}\left\{C_S \phi_S - \frac{C_{DP}}{r}\right\} + k_{off} C_{DP} \quad \text{(c)}$$

$$V_B \frac{dC_B}{dt} = \int_0^{h_s}\int_0^{d} k_B C_S \, dxdy - k_L C_B \quad \text{(d)}$$

$$\frac{\partial C_{DP}}{\partial t} = k_{on}\left\{C_{TFV}\phi - \frac{C_{DP}}{r}\right\} - k_{off} C_{DP} \quad \text{(e)}$$

Equation 44

The conservation of mass equations for Tenofovir and Tenofovir diphosphate are in Equation 44. The concentrations are defined in terms of per unit volume of material. For example Tenofovir diphosphate concentrations are per volume of tissue even though these metabolites are only found in host cells. In the first Equation 44a gives concentration C_G in the gel compartment as a function of time. The variable D_E is the diffusion coefficient in the epithelium and C_E is the concentration in the epithelium. The variable w is the width of the canal, L is the distance from the center to the edge of the gel, and V_G is the gel volume. Together the integral gives the mass transport in epithelium from the gel. The epithelial transport terms are used because it is much slower than the transport in the gel and thus is the rate limiting step. Drug concentration in gel is also reduced due to imbibing of ambient vaginal fluid, this is modeled as a first order process with rate constant k_D [25]. Drug transport in epithelium (Equation 44b) is a 2-dimensional unsteady diffusion process. The concentration is C_E with diffusion coefficient D_E. The last two terms of the equation are the creation and elimination rate

for Tenofovir diphosphate, where k_{on} is the formation rate of TFV-DP, k_{off} is the elimination rate of TFV-DP, ϕ_E is the volume fraction of cells in the epithelium, and r is the fraction of TFV converted to TFV-DP within the cells. Drug transport in stroma (Equation 44c) is also a 2-dimensional unsteady diffusion process with a first order loss term for the uptake of drug into vasculature with rate constant k_B, assuming blood vessels are assumed to be distributed relatively uniformly throughout the stromal layer. Where the concentration is C_S, diffusion coefficient is D_S, and the TFV-DP production mechanism is similar to the one in the epithelium except with a different host cell volume fraction ϕ_S. In the blood compartment (Equation 44d), the mass balance of concentration C_B is governed by the input from the stroma divided by V_B (the volume of the blood compartment) and loss due to metabolism by the body with first order rate constant k_L. The time rate of change for TFV-DP (Equation 44e) has two components on the right hand side of the equation. The first is the rate of formation k_{on} multiplied by the difference between the current level of TFV-DP and the saturation level based on the local Tenofovir concentration C_{TFV} either in the epithelium or the stroma, the proportion of host cells ϕ, and the fraction r of TFV that can be converted to TFV-DP. This term is inside Macaulay brackets $\{\}$ (defined such that the expression inside the brackets is zero when it has a negative value, because the TFV-DP formation rate must be nonnegative).

The second component is the rate of elimination, or conversion from TFV-DP to TFV governed by the rate constant k_{off}.

4.2.4 Boundary and Initial Conditions

Boundary and initial conditions for the system of equations are in Equation 45.

$$C_G = \Phi_G C_E \ @\left(y = 0, 0 \le x \ge L\right) \quad \text{(a)}$$

$$\frac{\partial C_E}{\partial y} = 0 \ @(y = 0, x > L) \quad \text{(b)}$$

$$C_E = \Phi_E C_S, D_E \frac{\partial C_E}{\partial y} = D_S \frac{\partial C_S}{\partial y} @\left(y = h_E\right) \quad \text{(c)}$$

$$\frac{\partial C_S}{\partial y} = 0 \ @\left(y = h_E + h_s\right) \quad \text{(d)}$$

$$\frac{\partial C_E}{\partial x} = 0 \ @ \left(x = 0 \text{and} x = d\right) \quad \text{(e)}$$

$$\frac{\partial C_S}{\partial x} = 0 \ @ \left(x = 0 \text{and} x = d\right) \quad \text{(f)}$$

$$C_G\left(t_0\right) = C_0 \quad \text{(g)}$$

$$C_E\left(t_0\right) = 0 \quad \text{(h)}$$

$$C_S\left(t_0\right) = 0 \quad \text{(i)}$$

$$C_B\left(t_0\right) = 0 \quad \text{(j)}$$

$$C_{DP}\left(t_0\right) = 0 \quad \text{(k)}$$

Equation 45

The coordinate system here is different from gel spreading computations, since the gel spreading has a movable origin depending on whether the gel has leaked or has reached in the fornix. Area of the epithelium under the gel is a concentration boundary with a partition coefficient Φ_G (Equation 45a), and the area not under the gel is a no flux boundary (Equation 45b). The boundary between the epithelium and stroma is a continuous boundary with a partition coefficient Φ_E (Equation 45c). The boundary at the left, right, and bottom of the tissue is assumed to be no flux (Equation 45d, Equation 45e, Equation 45f). Initially when the gel is inserted at time t_0 it has concentration C_0 (Equation 45g), while all other compartments have zero concentrations initially (Equation 45h - Equation 45k).

4.2.5 Parameters in the Model

The parameters in the model are in Table 5. Many are the same as the previous analysis of a perfect coating in Chapter 2. The epithelial and stromal layers have thicknesses of 200 μm and 2.8 mm respectively[71]. The model contains values for the length d and the width w of the vaginal canal, which vary among women[72]. The model is based on ranges of human vaginal morphometric data, with three different representative sizes as “average”, “small”, and “large”. The small and large sizes is used to contrast spreading and leakage by the three test gels, while the average sized vagina is used for mass transport and concentration distribution. The three rate constants for gel dilution, drug transport from stroma to the blood, and drug loss from the blood

stream are discussed earlier in Chapter 2. These parameters are obtained by fitting the model to human Tenofovir PK data. Diffusion coefficients in tissue are determined via confocal Raman spectroscopy, the value for epithelium and stroma are 7 x 10^{-8} and 4 x 10^{-7} cm^2/sec respectively[14]. Partition coefficient is 0.75 for the gel epithelium interface and 1 for the epithelium stroma interface. These were derived from initial experimental measurements of Tenofovir transport in specimens of fresh porcine vaginal tissue also using confocal Raman spectroscopy[14]. The kinetic parameters for TFV-DP, k_{on} and k_{off}, were estimated based on PK studies of TFV-DP formation[37]. The value of V_B, volume of distribution in the blood compartment is 75 L[47].

Table 5: Parameters in gel spreading and drug transport model

Parameter	**Symbol**	**Value**	**Reference**
Diffusion Coefficient in Epithelium (cm^2/s)	D_E	7 x 10^{-8}	[14]
Diffusion Coefficient in Stroma (cm^2/s)	D_S	4 x 10^{-7}	[14]
Gel/Epithelium Partition Coefficient	Φ_G	0.75	[14]
Epithelium/Stroma Partition Coefficient	Φ_E	1	[14]
Epithelial Thickness (cm)	h_E	0.02	[71]
Stromal Thickness (cm)	h_S	0.28	[71]
Rate Constant due to Dilution in Gel (hr^{-1})	k_D	1.22	[25]
Rate Constant for Stroma Blood Transport (hr^{-1})	k_B	0.119	[25]

Rate Constant for Loss in Blood (hr^{-1})	k_L	1.41	[25]
Rate of Formation for TFV-DP (hr^{-1})	k_{on}	0.693	[37]
Rate of Elimination for TFV-DP (hr^{-1})	k_{off}	0.00413	[37]
Volume Fraction of Cells in Epithelium, Stroma	ϕ_E, ϕ_S	0.95, 0.1	[26]
Proportion of TFV-DP Converted from TFV	r	0.1	[26]
Initial Concentration in Gel (ng/mL)	C_0	10^7	[78]
Volume of Distribution for Blood (L)	V_B	75	[47]
Length of Small, Average, and Large Vagina (cm)	d	12, 13, 15	[72]
Width of Small, Average, and Large Vagina (cm)	w	3, 3.35, 3.5	[72]
Surface Area of Small, Average, and Large Vagina (cm^2)	A	72, 87, 105	[72]

4.3 Results

4.3.1 Spreading in Large and Small Vagina

The first results are for spreading of the three test gels. The gels were designed with different compositions leading to different rheological behaviors. DG1 is a gel that most closely resembles vaginal gels that were used in the past, DG2 is a "bolus" gel that has a high yield stress and viscosity, and DG3 is the least viscous gel that has no yield

stress. Gel spreading is simulated for two morphometrically relevant vaginal sizes termed “small” and “large”. The small sized vagina has dimensions with length 12 cm and width 3 cm (area of 72 square centimeters) and the large sized vagina has dimensions with length 15 cm and width 3.5 cm (area of 105 square centimeters). The results are plotted in Figure 29 for a small vagina and Figure 30 for a large vagina. Different line styles on each plot indicate both the fraction of area coated (solid) and gel volume leaked (dashed). Line colors are for three different volumes, and the triangles are for different gel insertion points (either in the middle of the vagina or at the fornix).

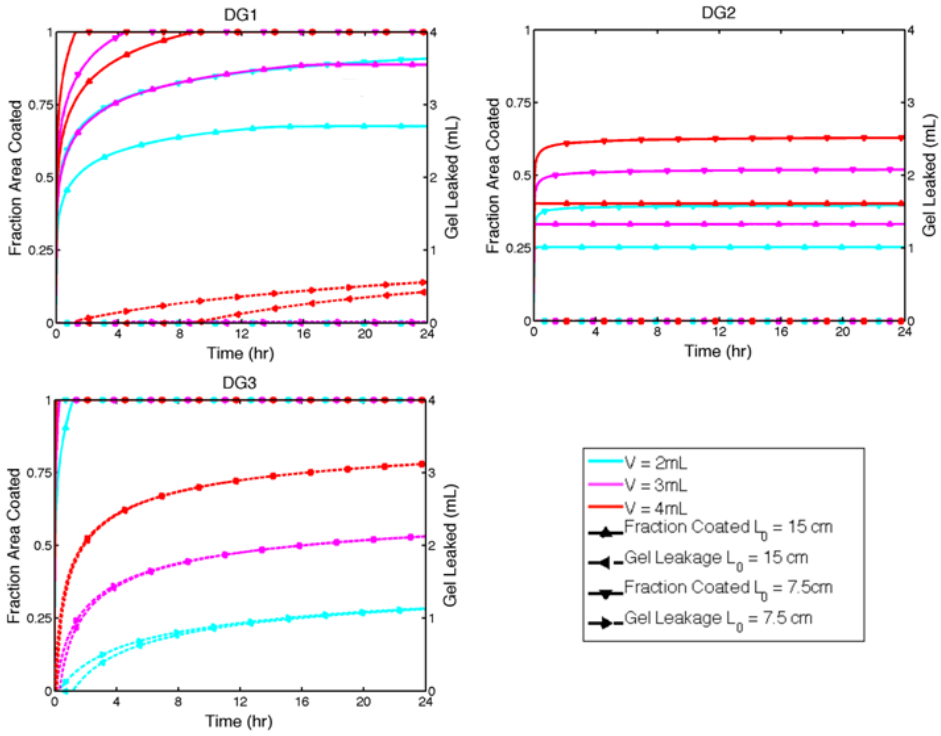

Figure 29: Fraction of area coated and volume leaked for a large sized vagina

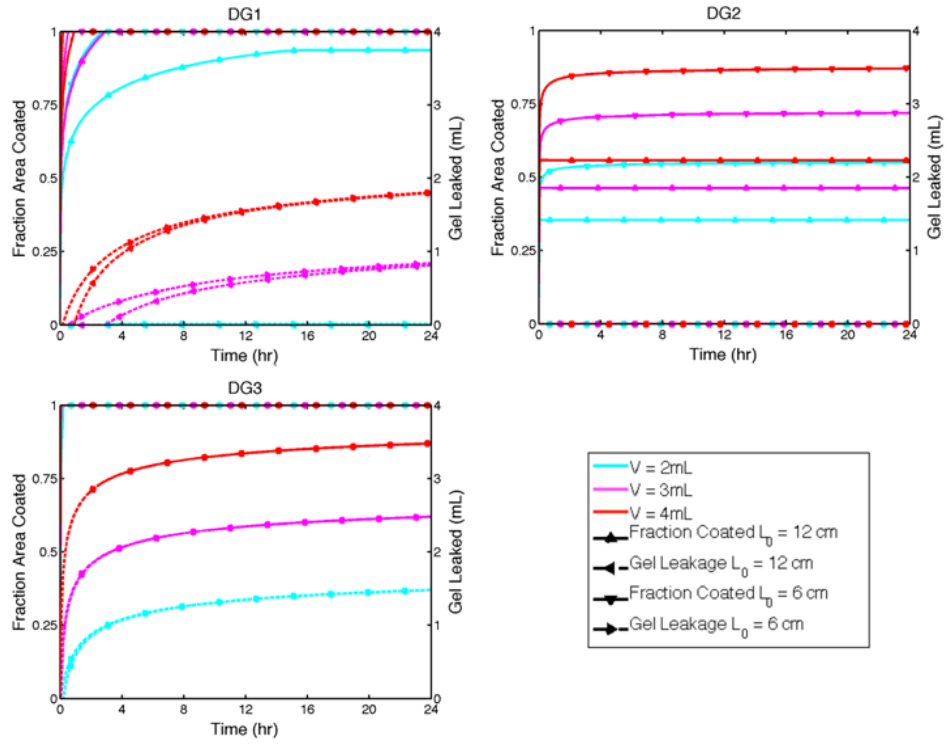

Figure 30: Fraction of area coated and volume leaked for a small sized vagina

For each gel, the volume, vaginal size, and gel placement affect both the fractional area coated and the volume of gel leaked. In DG1, for a large vaginal size only the 4 mL gel leaks, and for a small vaginal size both the 3 mL and 4 mL leaked. The coating area for 4 mL gel is complete for both sizes, but with a 3 mL gel complete coating is dependent on initial gel placement. When placed near the fornix, this gel does not coat completely while it does when placed near the middle of the canal. A 2 mL DG1 gel does not coat completely in the large vagina but coats better when placed near the middle. The other two gels, DG2 and DG3 are at the opposite ends of the spectrum. DG2 with a high yield stress does not leak with all volumes and vaginal sizes. Coated area reaches a

steady state within 2 hours after initial insertion, and stays constant throughout the rest of the 24 hour period. A higher volume and small vaginal size both produce better coated area. DG3 on the other hand leaks within the first hour in all cases, but coats completely within that time frame. Higher initial volume causes more gel leakage.

4.3.2 Heat Map of Concentration Distribution

Drug transport from a spreading gel into the mucosal tissue is characterized by two-dimensional concentration values over time. Heat map of the concentration distribution can be plotted to visualize, here for 3 mL of DG1 gel, inserted at the inner end of an average sized vaginal canal (Figure 31). The concentration for TFV and TFV-DP are plotted at times of 1 hour, 2 hours, 4 hours, and 24 hours post initial gel application. The x axis is the direction of gel spreading with the end of the vagina at 13 cm, the y axis is depth into the tissue up to a maximum value of 0.3 cm.

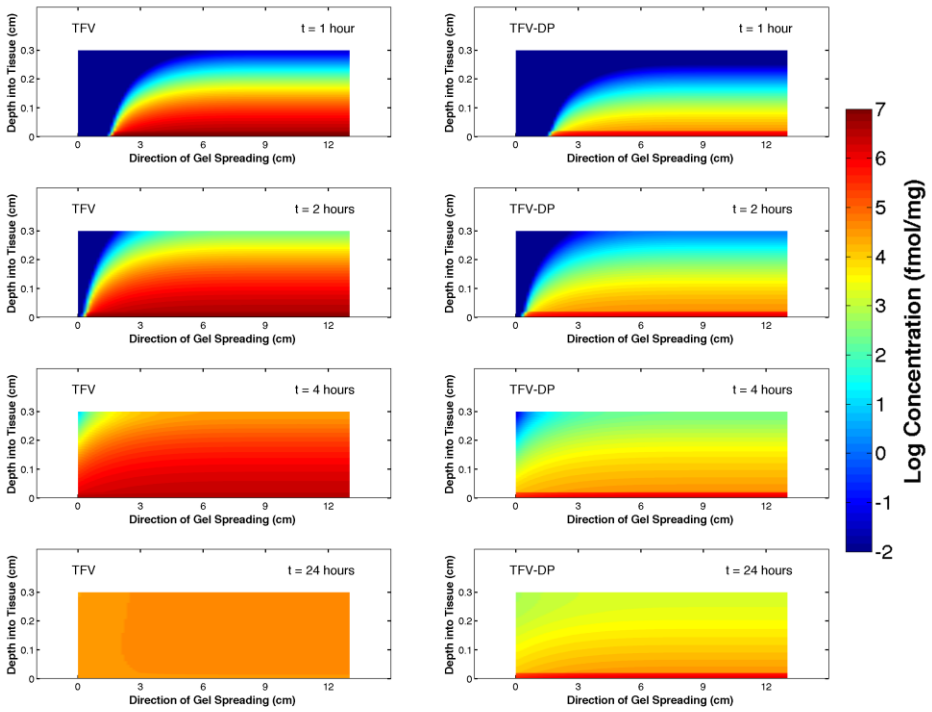

Figure 31: Concentration distribution for TFV and TFV-DP on the log scale

Concentration distribution of TFV in the x direction matches closely with the extent of gel spreading. The leading edge of the gel is effectively the leading edge of the TFV concentration profile. Peak concentrations in tissue diminish over time, due to gel spreading and leakage, and as drug diffuses down into the tissue it is being cleared in the stroma. At times up to 4 hours, the maximum concentration in the tissue is about 10^7 fmol/mg throughout most of the stroma. At 24 hours the tissue has concentration between 10^4 fmol/mg and 10^5 fmol/mg. The longitudinal concentration distribution of TFV-DP also corresponds with gel spreading. Concentration (per unit tissue volume) is higher in the epithelium than stroma due to higher concentration of cells. Overall, TFV-DP concentration distribution follows that of the TFV for relatively short times.

However, for longer times (>8 hours) TFV-DP concentration approaches a relative steady state due to its slow clearance rate.

4.3.3 Volume-averaged Concentration in Multiple Compartments vs. Time

Volume averaged concentration vs. time of drug concentration in each compartment (gel, epithelium, stroma, and blood) yield plots analogous to measurements of drug concentrations in experimental pharmacokinetic studies [78]. Figure 32 and Figure 33 are plots for concentration of TFV and TFV-DP for gels DG1 (at 3mL), DG2 (at 4mL), and DG3 (at 2 mL). The volumes are chosen for each gel that gave optimal performance in terms of coating and leakage in the spreading computations from earlier. In these computations the dimensions in the vaginal is an average sized with length of 13 cm and width of 3.35 cm, providing a total surface area of approximately 100 square centimeters. For these gels the total mass of drug loading is conserved across volumes, as an alternative computation can be made for which drug concentration is conserved. The initial drug concentration is thus inversely proportional to gel volume. Total drug loading is set at 40 mg, which is the mass of Tenofovir corresponding to a 1% gel at 4 mL volume used in previous clinical trials[46, 93].

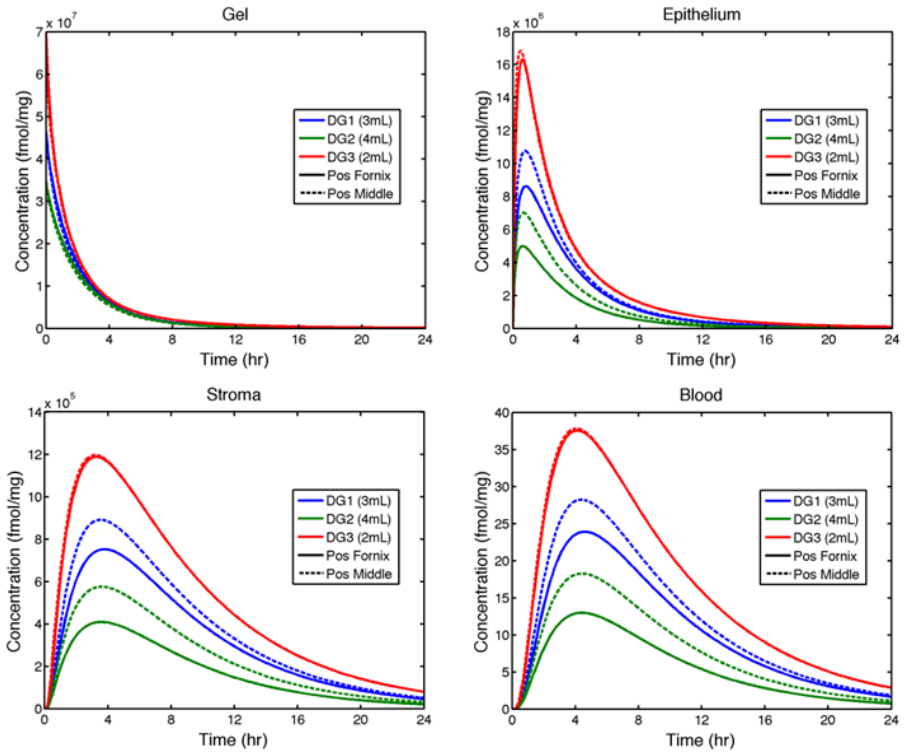

Figure 32: Volume averaged TFV concentration in gel, epithelium, and blood

Insertion of gels into the fornix gives lower TFV concentrations in the epithelium and stroma than insertion to the middle of the canal. Stromal AUC values are about 15%, 30% and 1 % lower for gels DG1, DG2, and DG3. The average stromal concentrations of TFV-DP follow the same pattern for all three gels. They rise to a quasi-steady state value in about 6 hours for all gels, and then remain nearly constant beyond the interval of computation (due to the slow decay rate for TFV-DP). Peak values of TFV-DP concentrations are higher for gel insertion to the middle of the canal, by about 15%, 40%, and 0.5% for gels DG1, DG2, and DG3, respectively. Thus results for gel DG3 (the lowest viscosity, relatively "runny" gel) are insensitive to the site of insertion, because it coats

the entire length of the canal so rapidly. Overall, results in Figure 33 indicate that the rank ordering of effective drug delivery performance (TFV-DP concentrations in stroma) for the gels is DG3 (2mL) > DG1 (3mL) > DG2 (4mL).

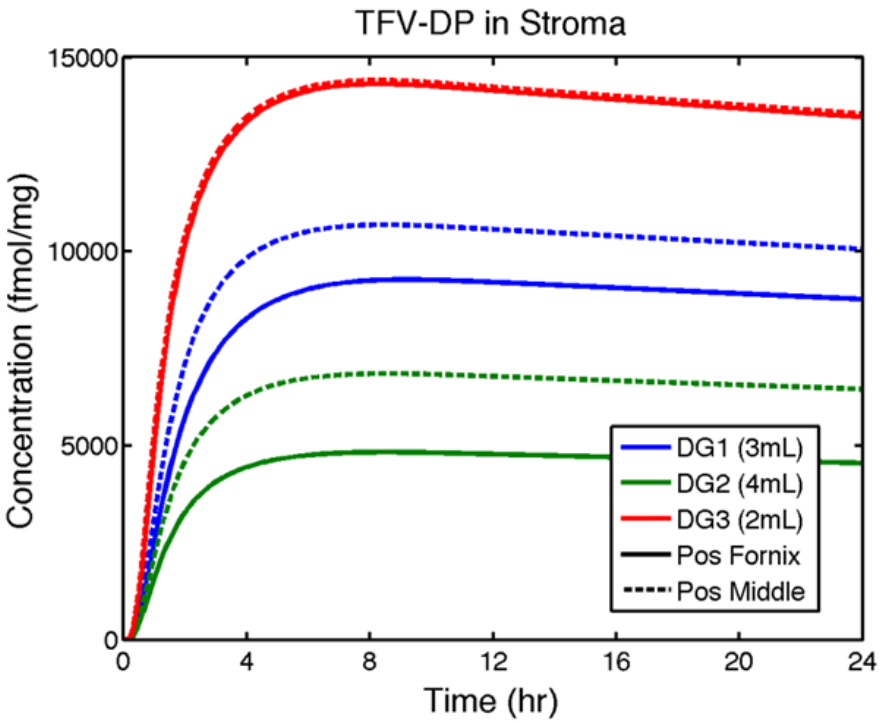

Figure 33: Volume averaged concentrations of TFV-DP in stroma

4.3.4 Percent of Stroma Protected with TFV-DP

Pharmacodynamic potency of Tenofovir is manifested through concentration of Tenofovir diphosphate in HIV infectible host cells. Many studies have investigated the relationship between Tenofovir concentrations in tissue and the infectibility of that tissue. The EC_{50} value for Tenofovir has a range of 1 log[47]. However, very few studies have focused upon the relationship between concentrations of Tenofovir diphosphate and HIV infectibility. The problem is compounded by the fact that different HIV-

infectible cell types produce different intracellular TFV-DP concentrations and they have inherently different TFV-DP dose response. The analysis here uses the upper limit of experimentally determined EC_{50} for Tenofovir and increases this hypothetical value by up to 2 logs. The fraction of the total volume of the stromal layer that achieves a concentration of TFV-DP higher than the reference value is termed "Percent Protected", this is a key measure that relates to the prophylactic effectiveness against HIV. It is an objective, mechanistically derived measure that can be related to characteristics of the gel, drug, vaginal environment, etc. The lower bound value for Tenofovir EC_{50} is taken as 0.5 μM of Tenofovir. The TFV-DP concentrations in human vaginal biopsies after dosing with the 1% TFV gel are approximately two logs lower than the measured TFV concentrations. Hence the lower bound for EC_{50} of TFV-DP is chosen as 0.005 μM (5 fmol/mg). Figure 34 illustrate the application of this computation to gels DG1, DG2, and DG3, varying gel volume and Tenofovir loading. This exercise provides insight into practical decisions that developers must make, once a gel composition has been decided, about what volume to apply and whether variations in loaded drug concentrations (compatible with safety, stability, and solubility requirements) are needed. For each gel, a reference condition of coated area within one hour is picked. This area needs to be as close to the size of the canal as possible for each gel volume. Because DG2 coats slowly the reference volume is increased from 4 mL to 5 mL. Then two computations are made for each gel at the reduced volume, first with the same concentration and second by

picking concentration that maintained the total drug loading. These computations are performed for an average sized vaginal canal of 13 cm long by 3.35 cm wide with the gel inserted into the fornix.

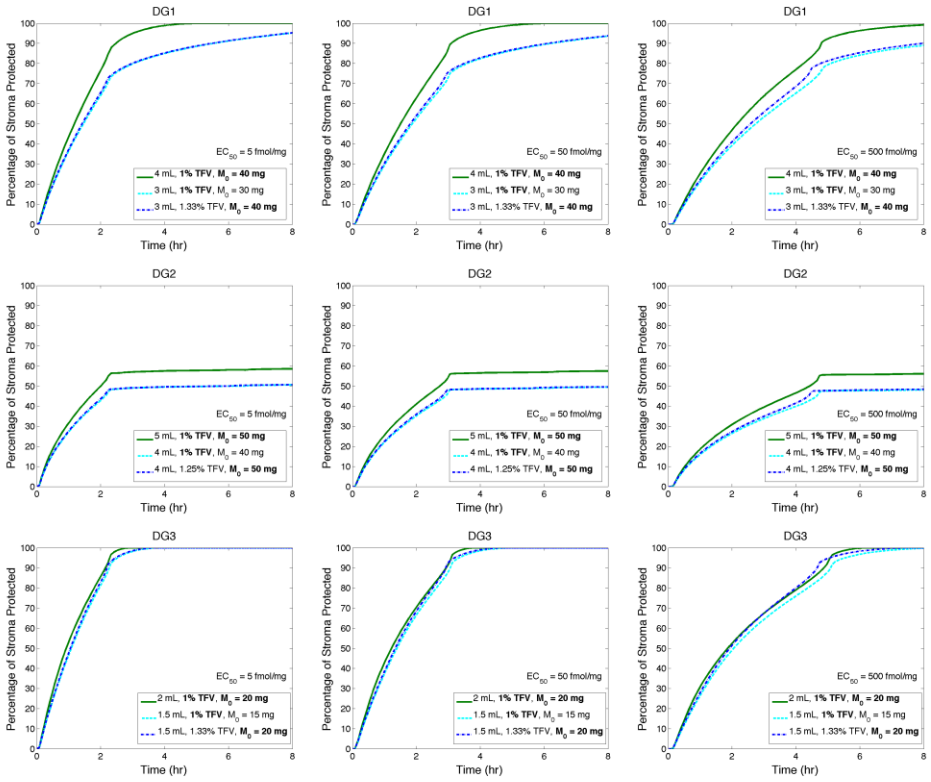

Figure 34: Percent Protected of the stroma. Rows are gels DG1, DG2, and DG3. The columns are different EC_{50} values of 5, 50, and 500 fmol/mg

From Figure 34, Percent Protected value rises sharply in the first 2 to 4 hours, after which the curve bends over and approaches a maximum value over a range of times, from almost instantaneous (DG2) to several hours (DG1). Thus protection increases initially at a fast pace, during an interval in which at least 90% of its maximum value is reached. This peak value is sustained at near steady state because of the slow clearance rate of TFV-DP from cells. Although there are some variations in duration of

the half-life for TFV-DP amongst different cell types, the rates are all on time scales much greater than 24 hours[3, 54]. The Percent Protected measure can also be characterized by the time needed to reach the bend on each curve (t_{bend}) and the peak value of Percent Protected (PP_{max}). For all gels higher gel volume achieves the highest Percent Protected most rapidly. Reducing volume and conserving either TFV concentration or the total mass produces indistinguishable result from each other. So gel volume, not the TFV concentration is the dominant factor in Percent Protected. However, quantitative differences across volumes and drug loading are negligible for DG3. This gel, which has a low viscosity, achieves peak values of Percent Protected the fastest out of all three gels even though the mass of drug in it is the lowest. This is because the gel spreads so rapidly, creating a thin coating layer over the entire canal. Higher volume (4 mL) for DG1 loaded at 1 % TFV achieves 100% protection, but it is slower than DG3. Reducing its volume to 3 mL also reduces the peak protection to about 90%. This results from the competition between increased TFV delivery due to increased coating, and the loss of TFV due to gel leakage plus clearance of TFV in the stromal layer. DG2, the very high viscosity gel, never achieves more than 60% protected because it only coats a fraction of the total length of the vaginal canal. For all gels, the effect of increasing the threshold EC_{50} value for protection is the increased time interval for which the steep rise Percent Protected occurs (t_{bend} increases). However, this 2 log

variation of EC_{50} has little effect on the maximum value of achieved percent protection (PP_{max}).

4.3.5 Plots of Combined Percent Protected and Gel Coating

In the earlier sections spreading and Percent Protected were both plotted as a function of time, but in separate plots. Plots of gel spreading contain information about the drug delivery and leakage of prototype gels, while Percent Protected is the best measure of drug effectiveness. The information from both plots is easier to absorb if they can be combined. The following uses both axis of a traditional plot as well as the color of the graph to convey information from both spreading and Percent Protected.

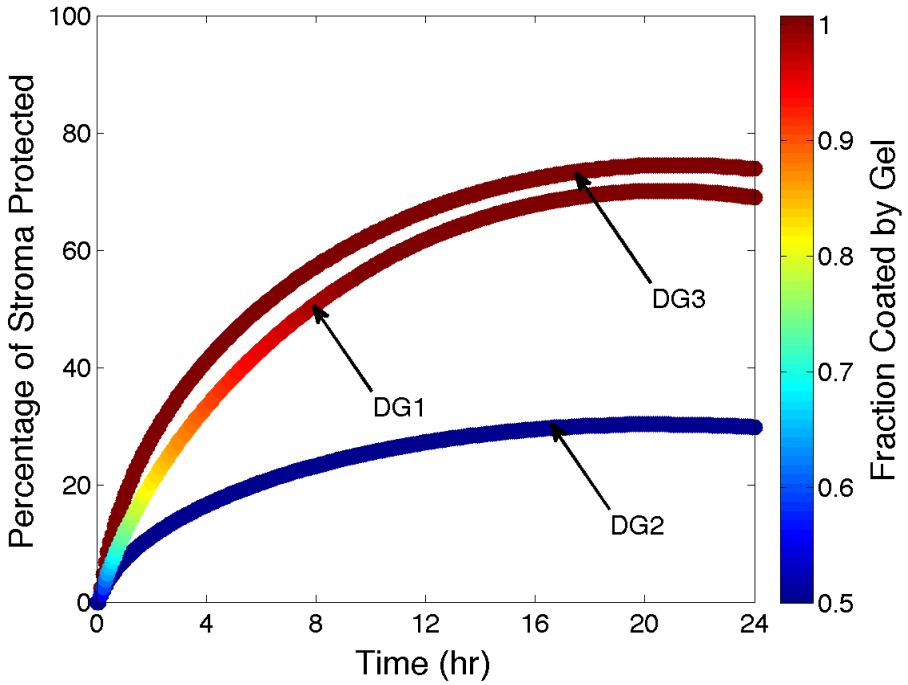

Figure 35: Percent Protected and fraction coated for three test gels

Figure 35 shows performance comparisons across the 3 gels. The y-axis indicates percent of stromal tissue protected against HIV infection as a function of time after initial gel insertion. Both DG1 and DG3 gels show the greatest amount of protection, with DG3 being slightly higher, while DG2 is much lower. The colors of the lines are for the fraction of the vaginal canal surface coated by gel over time. Coating reduces bare surfaces directly exposed to semen and virus. DG2 is the most viscous and coats about half of the canal over 24 hours, DG3 coats the entire canal in less than 1 hour, and DG1 gradually coats the entire canal in 8 hours. DG3 provides the best coating, which also means it will leak out of the vagina soon after application. DG1 offers both good protection and better gel retention within the canal. A less leaky gel improves user acceptability, and is a key to increasing user adherence for gels. Plots such as these can also yield the optimal volume for each gel if they are plotted as separate lines.

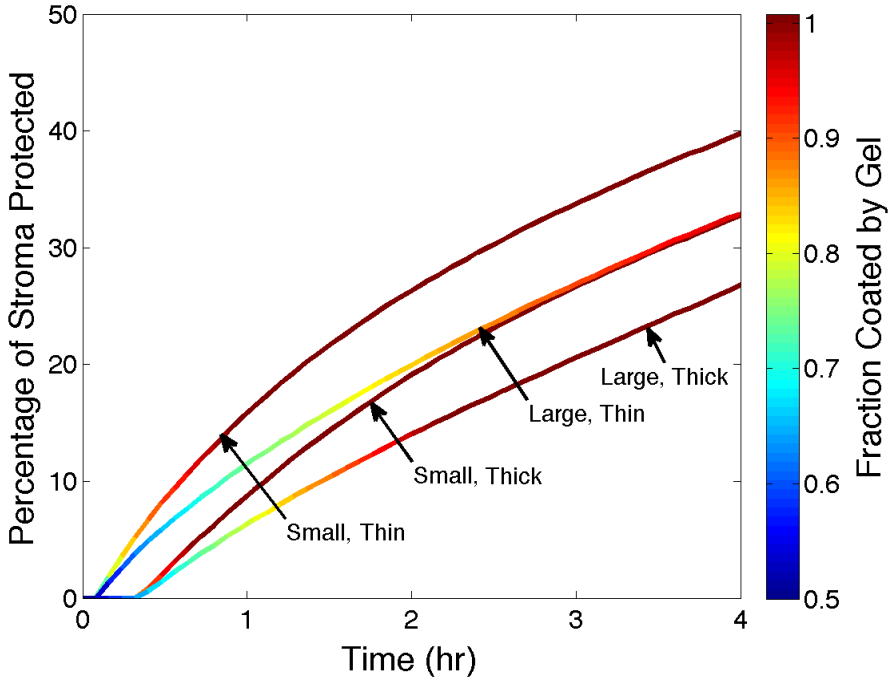

Figure 36: Percent Protected and fraction coated for different vaginal dimensions and epithelial thicknesses

In Figure 36, Percent Protected and fractional gel coating are plotted for varying biological conditions of either small or large vaginal canal and a thick or thin epithelium (depending on the phase of the menstrual cycle). The gel coats much faster in a small vagina compared to a large one, with both small cases coating the entire length of the canal in less than one hour. The large canal with thick epithelium coats in 2 hours, while the large and thin canal did not coat completely by 4 hours. The difference between thick and thin epithelium is due to the varying level of vaginal fluid production in the menstrual cycle: a thicker epithelium is associated with a higher level of vaginal fluid. A thicker epithelium also impede drug transport to the stroma, the Percent Protected of a

thick epithelium is around 7% lower than for a thin epithelium. Coincidently, the small/thick and large/thin conditions gave similar level of protection after 2 hours.

4.3.6 Sensitivity of Model Parameters

Predictions made by models are dependent on the fidelity of the values of parameters in them. Deterministic vaginal drug distribution modeling, as all PK modeling embodies a great many parameters that characterizes properties of the drugs, their vehicles, their dosage regimens, the host environments, etc. There is uncertainty in the value of parameters in the model and this contributes to the overall uncertainty in the predictions, as well as those inaccuracies in the model itself. As a reference, experimental data on drug concentrations in vaginal microbicide PK and efficacy studies are beset with variability, the origins of which are not fully understood. Empirical population based PK modeling for microbicide gels and intravaginal rings has begun analyses which quantify the uncertainty in clinical trial data[92, 96]. One use of such modeling is to define ranges of expected values of drug concentrations sampled as specified times after gel insertion. This could be used to assess whether or not gel was applied as instructed and reported by users[96], and could also guide selection of best times after product insertion to obtain samples in those studies.

In this simple example, deterministic modeling is used to address variability in human PK data, several parameters are perturbed that results from natural biological variability in gel users: the dimensions of the vaginal canal, the thickness of the

epithelial layer, the volume of gel inserted, the location along the vaginal canal which gel is inserted, the volume of vaginal fluid production, and the exact interval between gel insertion and time of biopsy measurement. First for each parameter an upper and a lower bound is determined independently of the variation of other parameters: (1) vaginal size was taken as large or small based on human morphometric data (L = 15 cm, W = 3.5 cm, or L = 12 cm, W = 3 cm), (2) epithelial thickness of 200 μm or 300 μm, (3) gel volume of 4 mL or 3 mL, (4) site of gel insertion was to the inner fornix or midway along the vaginal canal, (5) vaginal fluid dilution rate of gel was increased by a factor of two, and (6) interval between gel insertion and time of measurement with an off set of 30 minutes. The simulation is not a full statistical analysis of how the distribution of uncertainty in each parameter impacted model predictions. Rather, it considers 64 separate combinations of parameter values based on using the upper and lower bounds of each. The output of each model is the C_{max} value for Tenofovir in a biopsy, and the concentration of Tenofovir diphosphate in the stroma at 4 hours after gel application. The 64 values of each output can give a simple first order log-linear statistical model that incorporates all 6 parameters.

$$C = b_0 b_1^{x_1} b_2^{x_2} \ldots b_6^{x_6}$$

Equation 46

In Equation 46, C is the output concentration, the x_i's are parameters from 1 to 6, and the b_i's are coefficients determined from the fitting to the model. The value of b_0

is the approximate baseline concentration when all parameters are at the baseline value ($x_i = 0$). If any parameter is not at baseline, then $x_i = 1$ and the corresponding b_i has an independent multiplicative effect on the value of C. The equation is log linear, and by taking the natural log on both sides in Equation 47, each parameter x_i is linear.

$$\ln(C) = \ln(b_0) + \ln(b_1)x_1 + \ln(b_2)x_2 + \ldots + \ln(b_6)x_6$$

Equation 47

A linear regression can then be performed on the 64 data points each with a corresponding set of parameters indicating whether they are at the baseline or comparison value. R^2 values for predictions of the deterministic simulation concentration by their statistical models were 0.972 and 0.990, respectively, for TFV in biopsy and TFV-DP in stroma. Results of this model to simulated experimental measurements of TFV and TFV-DP concentrations are given in Table 6.

Table 6: Effects of the 6 parameters on log-linear model for coefficient variation. Unit for concentration is fmol/mg. Values are multiplicative factor for any variable that is part of the Comparison column, the baseline factor is 1

	Baseline	**Comparison**	**Biopsy TFV**	**Stromal TFV-DP**
Baseline Value	-	-	7.84 (7.58, 8.11) x 10^5	6.80 (6.63, 6.97) x 10^3
Vaginal Size	Small	Large	0.77(0.75, 0.79)	0.77(0.76, 0.78)
Gel Volume	3 mL	4 mL	1.18(1.15, 1.21)	1.17(1.15, 1.19)
Place of Insertion	Middle	Fornix	0.86(0.84, 0.88)	0.85(0.84, 0.87)
Epithelial	200 μm	300 μm	0.92(0.90, 0.95)	0.66(0.65, 0.68)

Thickness				
Gel Dilution	Half	Original	0.65(0.64, 0.67)	0.65(0.64, 0.67)
Time	t-30 min	t	1.09(1.06, 1.11)	1.04(1.02, 1.06)

Results in Table 6 show that gel dilution and vaginal size are the parameters that have the most effect on TFV concentrations in simulated biopsy. That is, larger vaginal size reduces concentration by 23%, and increasing dilution effects cause a 35% decrease. For TFV-DP concentrations in stroma, the thickness of the stroma is as important as gel dilution, a 50% increase in thickness reduces concentration by 34%. In future follow up, second order log linear models can be created to account more fully for interactions between pairs of parameters.

4.4 Discussion

The model used here expanded on previous computations in gel spreading and drug transport by combining both a two-dimensional model of drug distribution in the lumen and mucosa of the vaginal canal. Additionally, this model incorporates the mechanisms of Tenofovir diphosphate formation, which is the key metabolite in preventing viral replication in host cells. Furthermore, the first pharmacodynamics parameter for protection against HIV is introduced. This parameter, termed Percent Protected, converts the concentration distribution of TFV-DP PK to a measure derived

from experimental EC_{50} values that can inform the effectiveness of each particular dose over time.

Gel rheology and the spreading model from Chapter 3 are applied to three candidate test gels in morphologically accurate sizes of the vaginal canal. The three test gels exhibit vastly different rheological properties and can be classified as a normal spreading gel (DG1), a bolus gel that does not spread (DG2), and a leaky gel which spreads the fastest (DG3). Plots of spreading and gel leakage show the tradeoff between fast spreading gels and the amount of gel leakage. This information can be used to find the optimal volume to use for each test gel as well as pick the best gel that both spread well and has minimal leakage. Vaginal size is also an important factor especially for a leaky gel in a relatively small vagina, where leakage is much more significant.

The fundamental output of this model is concentration distribution over two spatial dimensions and time. This information can be best visualized as a movie with each frame being the heat map of concentration at specific times. Snapshots at set times of the heat map can also be plotted to show concentration levels. These plots can inform how both gel spreading and diffusion affect the concentration levels in tissue. In a normal spreading gel, the leading edge of the gel is effectively the leading edge of the highest concentration in tissue. The rate limiting step for such a gel is the diffusion coefficient in epithelium and stroma. For a gel that coats the entire canal, the lowest concentrations are found at the depth of the stroma. Plots of TFV-DP show a similar

trend. Due to the slow decay rate of TFV-DP, the concentration distribution is essentially the same as the distribution of the maximum concentration for Tenofovir in the stroma. The epithelium has the highest levels of TFV-DP because a higher volume fraction of cells are found there. The half-life of TFV-DP is very long, on the order of multiple days, which is why the heat plot does not show a visible decrease in concentration at 24 hours.

Another way of visualizing the data is to average the concentration in each compartment and plot it over time. This can then be compared with classic PK measures of average concentration as well as to the earlier one-dimensional model in Chapter 2. The concentration levels are different depending on the test gel used with DG3 being the highest and DG2 the lowest. Despite the fact DG3 leaks significantly it is still able to deliver the most drugs due to both faster rate of spreading and a higher initial concentration (because the optimal volume for DG3 is the smallest when conserving total drug mass, the concentration is higher for a smaller volume). Average concentration of TFV-DP show a similar trend with DG3 being the best. The drop off in concentration over time is nearly flat due to long TFV-DP half-life.

Pharmacokinetic model of drug delivery predicts Tenofovir distribution over time and space. This information can be used to with experimental EC_{50} value to give the first pharmacodynamics parameter for the model called Percent Protected. This value represents time dependent protection against HIV. The percentage is the fraction of vulnerable stromal tissue that has TFV-DP levels higher than a threshold. This threshold

can be approximated experimentally by the EC_{50} value, and here a two log factor of safety is added in the computations. The result showed which vehicle, including gel formulation, volume, and drug concentration, offers the best protection against HIV and when. The gel DG3, despite leakage, offers the best protection at the shortest amount of time. The gel is able to achieve 100% protection after 6 hours for the worst case and 2 hours for the best case depending on the threshold concentration.

Microbicide gels not only need to deliver enough drugs to vulnerable areas of the body but also need to be easy to use. This two part problem can be summarized by two parameters, Percent Protected as a measure of drug efficacy and gel spreading/leakage as a measure of user acceptability. These two factors can be combined in a single plot as a function of time by plotting one variable on the y axis and the other variable represented by the color axis. These plots show how variations in gel design and biological factors influence drug delivery and spreading of Tenofovir gels. An ideal microbicide candidate should be able to achieve a high degree of protection in a short amount of time in addition to fast spreading but with only a small amount of leakage.

Sensitivity analysis on the key parameters in the model can show which contributes the most to variations in observed Tenofovir PK. This analysis used a log linear model fitted to variations in model parameters. The result indicates that gel dilution and vaginal size contribute the most to variability. Secondary factors such as gel volume, place of insertion, and time of biopsy sample have lesser effect. Varying

epithelial thickness has a small effect on TFV levels in the biopsy but has a much greater effect on TFV-DP concentration in the stroma. This is due to epithelium being part of the biopsy, so a larger size will not inhibit transport into the tissue, but a thicker epithelium will inhibit the transport to the stroma. This underscores a bigger point on inferences from biopsy samples on the protective effect of the drug, where in certain cases a direct correlation cannot be drawn between biopsy measurements and TFV-DP concentration in the stroma.

4.5 Conclusion

Combining gel spreading and drug transport is the logical next step after developing the two models independently. In addition, the kinetics of TFV-DP formation are included in this model for a better representation of the pharmacokinetically active ingredient in HIV prevention. TFV-DP PK can be used to form the first measure of PD in this model as Percent Protected of the stroma. This measure informs how variations in the model from both the delivery vehicle and the biological environment influence the delivery of the drug. The threshold concentration is inferred from experiments on the EC_{50} value of Tenofovir and applied to the model with additional factors of safety. Model predictions can be compared to previous one dimensional model of drug transport and to experimental data which gave good agreement. Parameter sensitivity computations for the model showed vaginal size and rate of dilution are the most important factors in TFV biopsy and TFV-DP levels in the

stroma. In addition, epithelial thickness is important for stromal TFV-DP concentration only.

5. Model of Intravaginal Rings

5.1 Introduction

Intravaginal rings[50, 66, 82] offer an alternative to gels for use as microbicide delivery vehicles. Compared with gels, rings can be placed in the vagina for up to a number of weeks at a time. This increased convenience could lead to greater adherence to microbicide use, which has been a problem plaguing the gel dosage form[2, 58]. In addition, using a ring would not lead to adverse reactions such as leakage[26], and this could increase adherence of the microbicide product.

Key features of a microbicide ring include its physical dimensions and its release rate of drugs. A ring is supposed to deliver drug for an extended period of time, and thus the design of the rings will require much higher drug mass compared with that for gels. Two different release mechanisms have been proposed for a ring, matrix and reservoir release rates[16, 66, 83]. The matrix ring contains a homogenized material that is infused with candidate API; the drug is released via diffusion out of this matrix. The release rate can be computed using simple diffusion theory, and release rate decreases as the amount of drug in the matrix is consumed. The reservoir ring on the other hand is a more advanced design with a core material containing drug and a sleeve outside surrounding it which controls release rate. In this design the drug is theoretically able to maintain an almost constant flux of drug over the life of the ring. This is the preferred

design for microbicide IVRs. Consequently, the reservoir ring design will be used in this model.

A number of drugs have been proposed for use in microbicide rings. These include Dapivirine[57], Maraviroc[24], and Tenofovir[43]. There have been two recent Phase III trials of Dapivirine rings. The first, called ASPIRE, recently showed effectiveness especially with high user adherence[4]. Initial statistical analysis of another trial called IPM 027 (The Ring Study) is currently being completed[20]. An additional trial with a Tenofovir ring is being conducted by CONRAD[90]. Dapivirine and Maraviroc are relatively hydrophobic, which means they are well suited for use in the design of a ring, where the solubility mismatch between the ring material and the fluid environment can lead to a higher level of drug loading into the ring. On the other hand a hydrophobic drug might encounter problems in transport through the aqueous vaginal luminal fluids. Tenofovir is a well known drug, which has been used in a number of phase III trials with a microbicide gel[44, 46, 59]. Overall, these trials show efficacy against HIV infection, provided a sufficient level of adherence is achieved. The relatively hydrophilic nature of Tenofovir can also aid its transport through fluids in the lumen. The model here will focus primarily on Tenofovir. The previous work on vaginal gels delivering Tenofovir can be adapted to inform the model here of a ring in the vaginal environment.

This analysis will build upon experience gained previously by Geonnotti and Katz for a model of a Dapivirine ring[28]. The Tenofovir ring differs from the Dapivirine in drug release rate, diffusion coefficient in the tissue, transport rate to the blood, and the partition coefficient of drug between fluid and tissue. Both the drug release rate and partition coefficient effectively scale the concentration in tissue and the blood. The diffusion coefficient and transport rate to the blood give the primary time scales for drug transport. If those two parameters are comparable for two drugs, then the time and space dependent concentration profiles should be similar.

Several key questions will be addressed in the modeling here. The model will help researchers to answer the question of how vaginal fluid and blood concentrations relate to the concentration in the stroma. This is important, because there is much more variability in concentration measurements in biopsies than in experimentally sampling blood or vaginal fluid concentrations, especially for blood. Other questions relate to whether the drug release rate from the ring is sufficient for protection against HIV, and the length of time needed to achieve this value after ring insertion. In addition to the steady state behavior of the ring, an important transient problem involves effects of temporary ring removal prior to sex.

5.2 Materials and Methods

5.2.1 Geometry of the Model

Ring deployment in the vaginal environment is a three dimensional problem. Unlike the spreading gel problem, where there are no significant variations in the width dimension, the ring itself is not uniform in any of the three dimensions. Thus a simple reduction cannot be performed to limit the number of primary physical dimensions in the problem. Modeling the ring problem in three dimensions presents a challenge due to the mismatch in length scales. The length and width of the vaginal canal are on the order of centimeters, while the dimension into the depth of the tissue is only a few millimeters. This means that the grid size will have to be on the length scale of the tissue depth, but when this is applied to the longer width and length direction the number of grid points becomes extremely large. The time step used in computing diffusion problems scales with the square of the spatial dimension. Thus the large number of grid points makes this problem very challenging computationally.

In order to reduce the complexity of the computation, the three dimensional problem is reduced here to two dimensions. One way of achieving this is to formulate and solve the projections of the three dimensional problem in different planes. Results from those projections can be carefully combined to objectively draw inferences about the full three-dimensional problem. From symmetry, the plane at the centerline should have no out of plane contributions to drug transport. There are three planes of

symmetry each corresponding to the axis of the Cartesian coordinate system. But due to the fact that the characteristic dimension is the direction of flow, this axis cannot be eliminated. This leaves two orthogonal projections for the problem (Figure 37). The first projection is along the sagittal plane of the body dividing the body down the middle, and the second along the coronal plane of the body which cuts the ring through its major plane. The sagittal plane model computes drug distribution along the length of the canal and in the tissue, while the coronal plane model is able to show concentration variations in the width direction. Taken together, these two projections give information that provides a good estimate of the full three-dimensional concentration distribution.

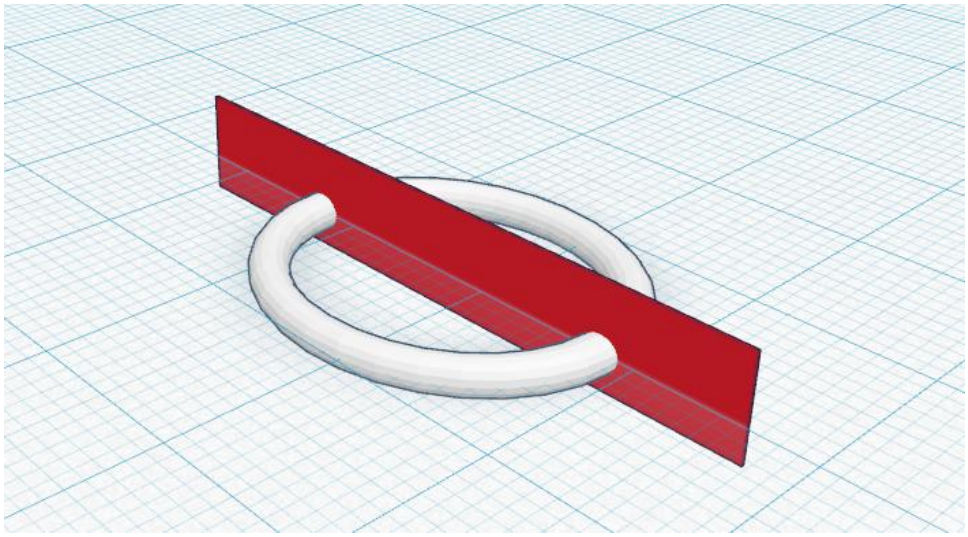

Figure 37: Two different projection of the ring model to 2D. The sagittal plane is represented by red and coronal plane is the blue grid.

Due to the complex geometry of the problem, a finite difference method cannot be easily applied with non-rectangular boundaries. A finite element analysis is more appropriate for this problem. Solution to this problem is obtained with COMSOL

Multiphysics software, in which physical processes like fluid flow can be coupled with transport equations in the form a diffusion-convection problem. The meshgrids generated for the two projections are in Figure 38 for the sagittal plane projection and Figure 39 for the coronal plane projection. Note here that due to symmetry, the out of plane and into the plane sides of the coronal plane projection are equal. Thus, the problem being solved here is half of the full geometry.

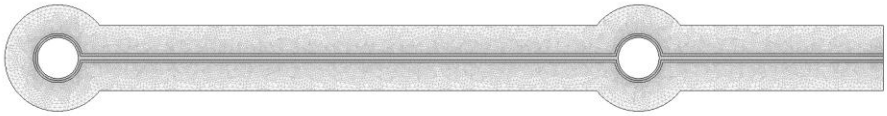

Figure 38: Two-dimensional geometry of the ring cut in the sagittal plane. The plot shows the meshgrid used in the computation. The right hand side is the introitus; the mid plane is vaginal fluid; and the two circles are cross-sectional cuts of the IVR.

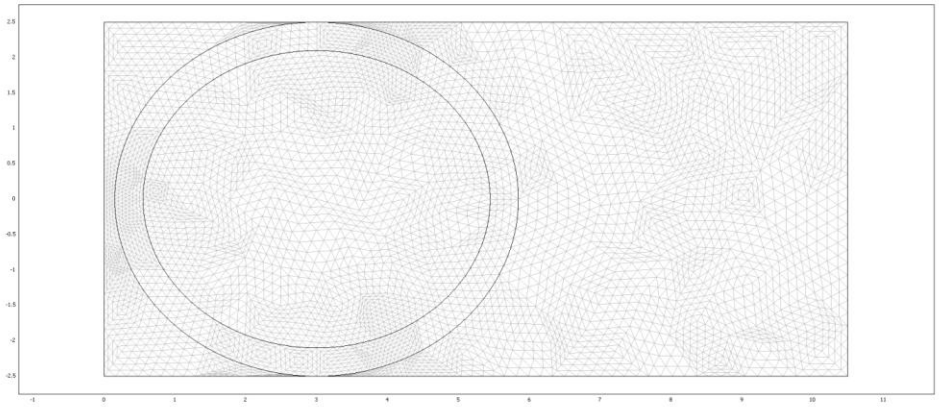

Figure 39: Two-dimensional geometry of the ring cut in the coronal plane. The plot shows the meshgrid used in the computation. The right hand side is the introitus;

the ring is shown on the left; and depth into the tissue is the direction perpendicular to the image plane.

5.2.2 Governing Equations and Boundary Conditions

5.2.2.1 Fluid Mechanics Model

Common to both projection models is the fluid layer. Ambient vaginal fluid has a typical volume of approximately 1 mL[69], with a constant rate of production of around 6 mL/day from the tissue[69]. The geometry of the lumen is rectangular in the collapsed state with one end near the fornix being closed and one end open at the introitus. The flow is driven by constant uniform production of vaginal fluid by the tissue. Thus fluid can leak through the introitus out of the vaginal canal.

$$\rho\frac{\partial u}{\partial t} - \nabla\cdot\eta\left(\nabla u + (\nabla u)^T\right) + \rho(u\cdot\nabla)u + \nabla p = F \quad \text{(a)}$$

$$\nabla\cdot u = 0 \quad \text{(b)}$$

Equation 48

The governing equations are the standard Navier-Stokes equation (Equation 48a) and the continuity equation (Equation 48b) for an incompressible fluid. The boundary conditions are no flux at the fornix, constant velocity at the tissue (derived from fluid production rates), and zero pressure at the introitus. The solution to this fluid flow is a velocity field which can be inserted into the drug mass transport equation for the two projection models.

5.2.2.2 Sagittal Plane Model

The sagittal plane projection model is the closest to the previous gel models, containing a fluid layer as well as the epithelium and stroma. The analyses here extends that for a Dapivirine ring model by Geonnotti and Katz[28]. The new model builds on the previous analysis with differentiated epithelial and stromal layers, and including our lab's latest measurements of Tenofovir diffusion coefficients in the epithelium and stroma[14]. In addition the fluid mechanics in this model is computed simultaneously with the transport problem and the stroma now has a transport term that accounts for uptake into the blood stream[25].

$$\frac{\partial C_f}{\partial t} = D_f \nabla^2 C_f - \nabla \cdot \left(v C_f \right) \quad \text{(a)}$$

$$\frac{\partial C_e}{\partial t} = D_e \nabla^2 C_e \quad \text{(b)}$$

$$\frac{\partial C_s}{\partial t} = D_s \nabla^2 C_s - k_b C_s \quad \text{(c)}$$

Equation 49

Drug mass conservation equations for this model are given in Equation 49. The three compartments are the fluid (Equation 49a), epithelium (Equation 49b), and stroma (Equation 49c). The fluid compartment equation has a convective term based on vaginal fluid velocity (computed separately). The stroma contains a first order kinetic term for the transport of the drug out from stroma and into the vasculature. There are numerous internal and external boundary conditions for the problem. All external boundaries are

no flux, with the exception of the introitus, where the flux is governed by the convective transport. Internal boundary conditions are continuous with a drug partition coefficient between compartments. The partitioning cannot be explicitly defined in COMSOL. However, this can be remedied by defining the flux between two compartments as the difference between concentrations modified by the partition coefficient times an arbitrary large number (Equation 50). The boundary between the ring and the fluid is a flux condition computed from the release rate of the ring divided by its surface area. Initial condition of this problem is zero concentration everywhere.

$$flux = M\left(c_1\Phi - c_2\right)$$

Equation 50

5.2.2.3 Coronal Plane Model

The coronal plane model is much simpler than the sagittal plane model in that it only contains a single compartment, the vaginal fluid. Flow is once again computed from the previous fluid mechanics computations. Transport from the fluid to tissue presents a unique challenge to model since the tissue compartment is not an explicit part of the problem. The transport to the tissue can be estimated by another first order reaction term, the magnitude of which can be calculated from mass transport of a gel from Chapter 2.

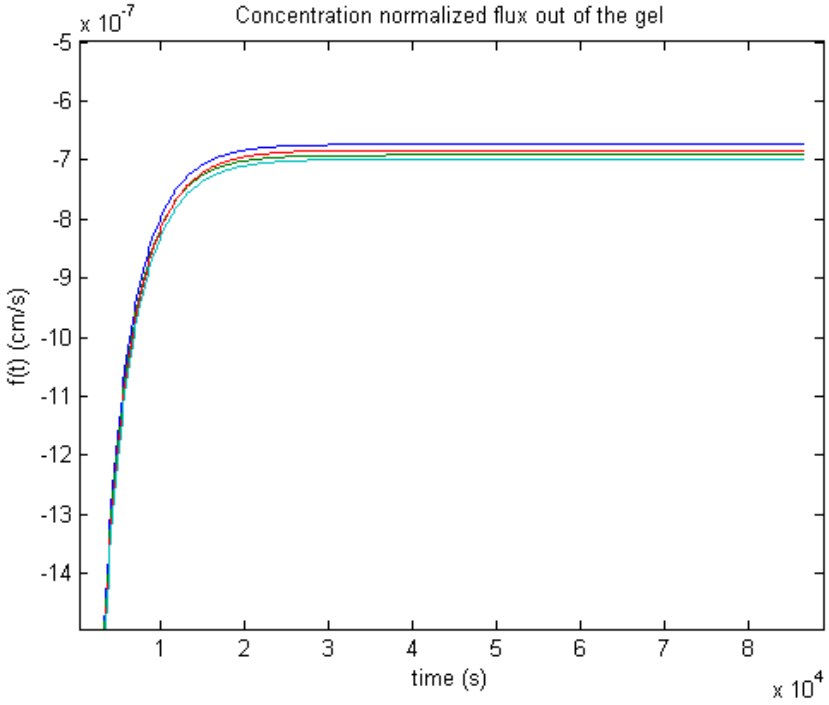

Figure 40: Gel concentration normalized flux of delivery by a vaginal gel in one dimension (Chapter 2).

The rationale for a first order reaction term is motivated by normalized drug flux into the tissue vs. gel concentration computed from the one dimensional problem of Chapter 2 (Figure 40). This parameter is nearly constant 4 hours post gel dosing, and the constant here can be used to calculate the kinetic rate of drug transport into the tissue. The first order dependence of flux on concentration is not surprising given that all terms in the governing mass transport equations have linear dependences on concentration. This effect can motivate further analysis on the dependence of tissue concentration profiles upon the applied concentration at the tissue surface by gels, rings or other dosage forms. Despite the unclear input term in this problem, a variation of linear time-

invariant theory[18] could be adapted from one dimensional tissue transport to give a better estimate of concentration profile in the tissue for the coronal plane model.

$$\frac{\partial C_f}{\partial t} = D_f \nabla^2 C_f - \nabla \cdot \left(v C_f \right) - k_t C_f$$

Equation 51

Conservation of mass for drug transport in the coronal plane model is given in Equation 51. Transport in the single fluid compartment is based on diffusion and convection with mass transfer to the tissue. Boundary conditions are no flux on the top, bottom, and left (fornix), with a mass flux boundary derived from convective transport on the right (introitus). In addition, the areas containing the ring have a mass creation term that is equal to the total ring flux divided by surface area over two, noting that the model is actually in the half plane of the transport. This is akin to the gel transport problem where top and bottom halves are symmetrical.

5.2.3 Parameters in the Model

Parameters used in the model are listed in Table 7. Vaginal geometry, diffusion coefficients, and kinetic rates are adapted from previous models of vaginal Tenofovir transport by a gel[25]. The dimensions of ring are common to current designs, with a diameter of about 5 centimeters (typical upper bound for the width of the vagina canal) and a cross-sectional diameter of 4 to 5.5 mm. The rate of vaginal fluid production varies greatly in women from 3 to 11 mL/day with a median rate of 6 mL/day[69]. The release rate of Tenofovir from a ring is approximately 10 mg/day *in vitro*[43].

Table 7: Parameters in the Tenofovir ring model

Parameter	Symbol	Value	Reference
IVR Dimensions (cm)	$a \times b$	5.7x5.0	[8]
IVR Cross-sectional Diameter (cm)	D	0.4	[77]
Vaginal Length (cm)	L	10.5	[72]
Vaginal Width (cm)	w	5	[72]
Epithelial Thickness (μm)	h_e	200	[71]
Stromal Thickness (μm)	h_s	2800	[71]
Vaginal Fluid Thickness (cm)	h_f	0.01	[69]
Vaginal Fluid Production (mL/day)	q	6	[69]
Diffusion Coefficient in Fluid (cm^2/s)	D_f	$6x10^{-6}$	[25]
Diffusion Coefficient in Epithelium (cm^2/s)	D_e	$7x10^{-8}$	[14]
Diffusion Coefficient in Stroma (cm^2/s)	D_s	$4x10^{-7}$	[14]
Partition Coefficient between Fluid/Epithelium	Φ_1	0.75	[14]
Partition Coefficient between Epithelium/Stroma	Φ_2	1	[14]
Rate Constant for Stroma Blood Transport (s^{-1})	k_B	$4.17x10^{-5}$	[25]
Tenofovir IVR Flux (mg/day)	J	10	[43]

5.3 Results

5.3.1 Heat Plot of Concentration in Sagittal Plane Model

The fundamental output of this model is concentration over space and time. Akin to the model of gel spreading and drug delivery, all information from the model cannot be shown easily in two dimensional graphs. Likewise, the best way to visualize the concentration distribution is to plot a heat map of concentration at select times. A heat map of concentration for the sagittal plane projection model is given in Figure 41 on the log scale.

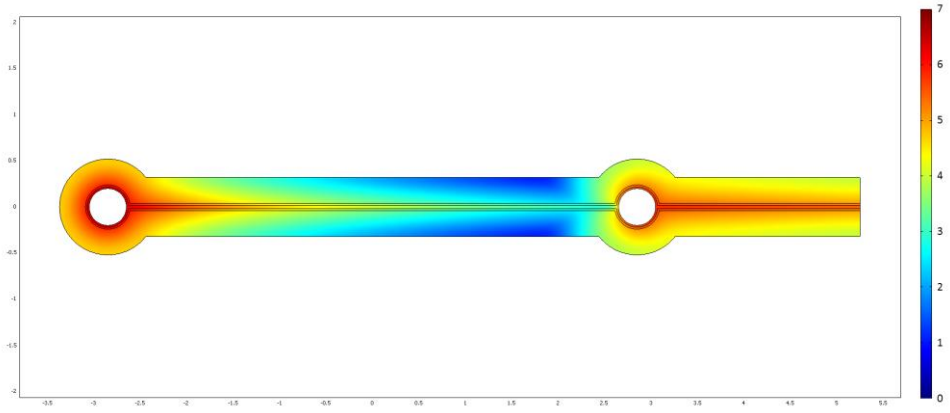

Figure 41: Heat map of concentration on the log scale (log fmol/mg) for the sagittal plane projection model 1 day post ring insertion.

Here the colors represent the log of Tenofovir concentration 24 hours after ring insertion. The concentration value ranges from under 10 fmol/mg to 10^7 fmol/mg. The highest concentrations are achieved around and downstream (extreme right of the plot) from the ring. The lowest concentrations (deep blue) are found deep into the tissue

before the lower segment of the ring. Concentrations above 10^3 fmol/mg are found in most of the tissue.

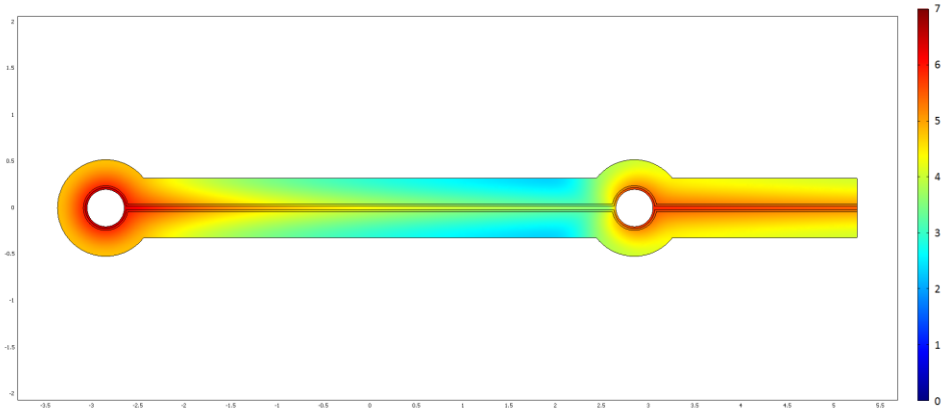

Figure 42: Heat map of concentration on the log scale (log fmol/mg) for the sagittal plane projection model at steady state.

Intravaginal rings are designed to be used for up to one month. After computing the transient concentration changes in the model, a steady state concentration is found approximately 5 days post ring insertion. The steady state concentration on the log scale is plotted in Figure 42. This concentration distribution profile is similar to the 1 day case. One major difference is that minimum concentration levels are now significantly higher. Previously the low was on the order of 10 fmol/mg, at steady state. This region now has concentrations up to 10^3 fmol/mg. Fluid concentrations are also higher than the 1 day case, with levels of at least 10^6 fmol/mg along the entire canal.

5.3.2 Heat Plot of Concentration in Coronal Plane Model

A heat map of fluid concentration in the coronal plane model is plotted in Figure 43. The concentration here is on the linear scale because of the relatively small changes in concentration over the entire fluid region as compared with the sagittal plane model. Under steady state conditions the highest concentrations are found in the region near the middle of the ring towards the fornix. The fluid velocity upstream is lower, so more drug can be found there. The other high region of drug concentration is on the edges of the ring. Because of ring geometry the edges create the highest area per line in the direction of flow. Lowest fluid concentrations are found upstream of the ring on the left corners and in the middle downstream of the ring. Steady state values are plotted here due to the fact the tissue is not included in this model. Importantly, inferences about tissue concentrations can be drawn from the steady state concentration values in the lumen because the base model of tissue transport is linear with applied concentration.

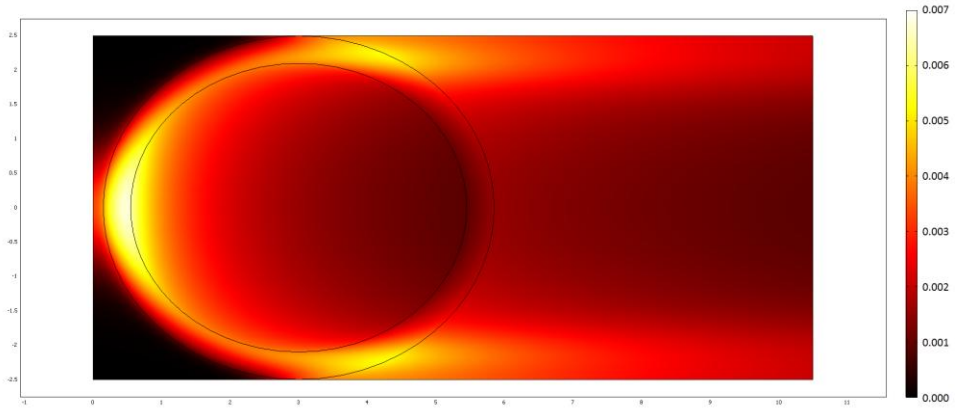

Figure 43: Heat map of concentration on the linear scale (fmol/mg) for the coronal plane projection model at steady state.

5.3.3 Average Concentration in each Compartment

Average concentrations in each compartment vs. time for the sagittal plane projection (Figure 42) and the previous gel model are plotted in Figure 44. This projection model is used as an approximation for the overall three-dimensional volume. The sagittal plane projection is at the centerline of coronal plane model (Figure 43), and shifts of this line gave similar levels of total concentration since the source ring section is about the same. This means the sagittal plane should be a good approximation for the entire vaginal canal. The gel model contains three compartments, gel, epithelium, and stroma, with Tenofovir diphosphate present in the epithelium and stroma. An additional compartment, the biopsy, is simply a weighted average of the entire tissue. Since the stroma is approximately 14 times thicker than the epithelium, a simulated biopsy concentration is very close to the stromal concentration. This is in contrast to the

gel, where transient concentration in the epithelium is much higher than the stroma, so the biopsy scales more with epithelial concentration. Concentration of Tenofovir in the epithelium and stroma peaks at around 2 hours and decays over the course of the day, while TFV-DP reaches the maximum around the same time but does not decay as rapidly due to its long intracellular half-life. In the ring model, the vaginal fluid is a counterpart compartment to the gel. Concentration there rises rapidly within the first hour and then levels off. The epithelium and the stroma compartments follow a similar pattern; concentrations at 24 hours are both higher than those in the gel model. Average concentrations for the ring vehicle reach a steady state approximately 3 days post initial insertion. These concentration levels are comparable to dosing by a gel. Maximum concentrations in the gel in general are about a log higher than for the ring.

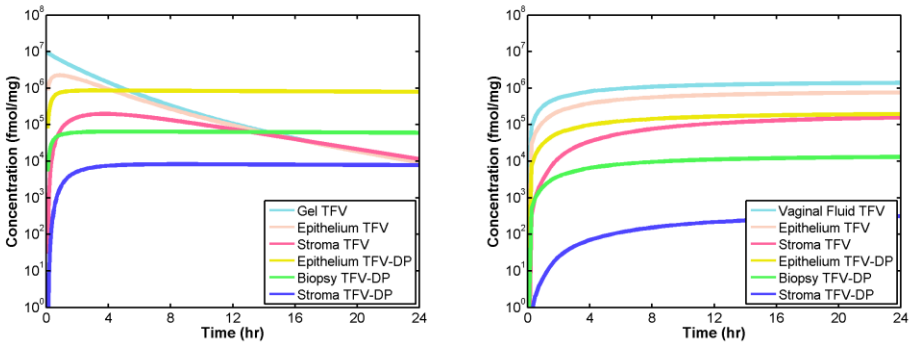

Figure 44: Comparison between average concentration in each compartment for the gel (left) and the ring (right).

5.3.4 Percent Protected after Ring Insertion and Removal

Percent Protected (PP), defined as the percentage of stromal tissue volume in which concentration is above a reference EC_{50} concentration against HIV, is plotted in

Figure 45 for the sagittal plane projection model. The EC_{50} is generally measured in vitro as a cutoff concentration for which a drug is expected to be effective. The EC_{50} value of 500 fmol/mg (left) is the highest level previously used in the study of a Tenofovir gel; here, the 5000 fmol/mg (right) is also used as a contrasting case which the Percent Protected level does not reach 100%. The three lines are the PP of a ring after initial insertion, after removal post steady state, and as a comparison to the PP level of a gel after insertion.

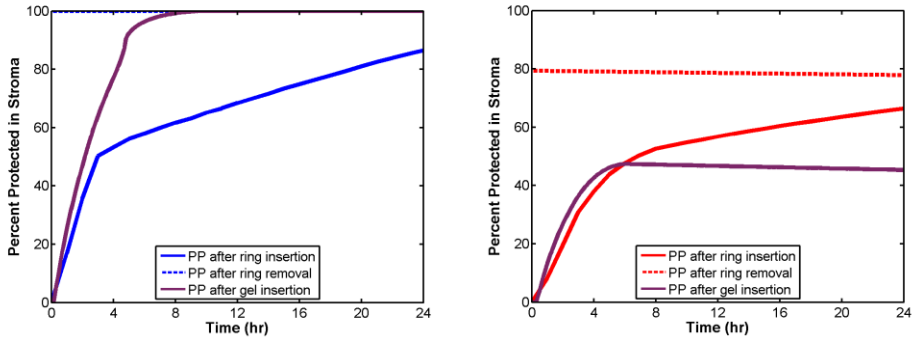

Figure 45: Percent Protected plot after initial ring insertion, after ring removal, and after initial gel insertion for EC_{50} of 500 fmol/mg (left) and 5000 fmol/mg (right).

In the 500 fmol/mg case both the ring and gel can reach 100% Percent Protected. However the gel reaches the level after 8 hours with the ring taking longer than 24 hours. Post ring removal, the PP value stay at 100% over 24 hours. The rise of PP after ring insertion can be seen in two distinct phases, the first rapid phase lasting around 4 hours, and a slower rise from there until steady state. The first phase is likely due to the lateral concentration gradient as it follows the movement due to vaginal fluid flow. The second phase happens after the drug has filled the entire lumen, after which transport is

a slower process by diffusion vertically into the tissue. The plot for an EC_{50} of 5000 fmol/mg shows the gel concentration plateauing at 47% PP after 6 hours. At this point the gel is mostly depleted, transport of Tenofovir is much slower and the plateau is maintained by the long half-life of TFV-DP. Percent Protected of the ring is a bit higher at 79% in steady state. It decreases very slowly after ring removal, and time to steady state after initial insertion is also longer than 24 hours.

5.3.5 Percent Protected with Parameter Variations

Percent Protected is computed for a variety of cases of drug release rate and vaginal fluid production. Results at steady state are given in Table 8 for EC_{50} values of 5000 fmol/mg on the left and 500 fmol/mg on the right. Release rate of the drug is varied from 5 mg/day to 20 mg/day with 10 mg/day being the standard condition in prior computations. Vaginal fluid production rates are 0 mL/day, 3 mL/day, 6 mL/day, and 12 mL/day, with 6 mL/day being the standard condition. An additional condition for a thicker epithelium is included for a vaginal production rate of 12 mL/day. This corresponds to the proliferative phase of the menstrual cycle in which the epithelium becomes thicker and vaginal fluid production is increased. The results show that on the low end for a 5 mg drug release and no fluid production, the Percent Protected values are 48.9% and 65.5% for the two levels of EC_{50}. On the high end Percent Protected is 100% with a 20 mg release and 12 mL fluid production rate for both EC_{50} values. A thicker epithelium increases Percent Protected slightly if it is not already at 100%. This

unintuitive effect is due to the fact that the most vulnerable area of the tissue is downstream from the ring. Thus a slower transport will actually increase concentration at the critical region while only having a small effect on transport in the region already containing high concentration.

Table 8: Percent of stroma protected with varying drug release rate per day (row) and vaginal fluid production per day (column), the last column has a thicker epithelium(*). Values are for EC_{50} of 5000 fmol/mg (left) and 500 fmol/mg (right) at steady state. Bolded cell is the baseline condition.

	0 mL	3 mL	6 mL	12 mL	*12 mL
5 mg	48.9%/65.5%	61.4%/79.0%	69.9%/98.2%	86.0%/100%	90.1%/100%
10 mg	53.9%/70.5%	66.0%/86.0%	**79.4%/100%**	95.7%/100%	98.8%/100%
20 mg	58.9%/75.5%	71.2%/92.8%	88.9%/100%	100%/100%	100%/100%

5.4 Discussion

Delivery of Tenofovir by a vaginal ring is modeled here by a classic diffusion convection mass transport process. Two different projections of the three dimensional problem are presented. The first is down the centerline showing transport within vaginal fluid as well as into the tissue. The second is entirely within the vaginal fluid, with local concentration proportional to that of the tissue.

The highest concentration in the tissue is found very close to the ring near the fornix. This region has the lowest convective velocity due to being furthest from the introitus. The lowest concentration levels are found up stream of the ring, where the

drug has to travel against the direction of flow before entering the tissue. However when averaged across the width of the canal concentration near the top of the ring is higher than that near the introitus. This agrees with a pharmacokinetic study of the Tenofovir ring in sheep [43], in which the proximal fluid concentration was about half a log higher than the distal fluid. The ratio of maximum to minimum concentration levels in the vaginal fluid is approximately three logs. To minimize the area with the lowest concentration, a vaginal ring will need to be inserted as close to the fornix as possible, since the tissue upstream of the ring will have the least protection. This suggests that if the shape of a vaginal ring were rectangular or more angular, it would minimize the area of tissue that receives the least amount of drug. However, those geometric possibilities may not be realistic for a ring to be acceptable to users.

Average concentrations in all compartments rise rapidly within the first few hours and gradually level off over the course of the first day. Steady state concentration is reached at approximately the 5 day mark. Tissue closest to the epithelial surface reaches its maximum very rapidly, and over the course of a few days the concentration gradient gradually rises to cover the deeper areas of the tissue. Average concentration in a simulated biopsy is 10^5 fmol/mg with 10 mg/day drug release and 6 mL/day vaginal fluid production. This compares to values in biopsies in a pig-tailed macaques study[64] at 10^5 ng/mL using a ring formulated to release about twice as much drug as the human equivalent. Converting the previous two numbers to units of ng/mL a human equivalent

release rate can be obtained by multiplying 0.3 to the first number and 0.5 to the second, with the resulting difference of less than a log. Maximum average concentration of a ring is about 1 log lower in all compartments than a Tenofovir gel. However, the concentration level for a ring can be sustained for a much longer time. Tenofovir diphosphate concentrations in both models level off then decay gradually due to its long half-life.

Despite lower average maximum concentration in the ring model compared to the gel model, percent of the stroma protected by Tenofovir at steady state is the same or higher for the ring. At a lower threshold of 500 fmol/mg the gel reaches 100% protection at around 8 hours, while for the ring it takes more than 24 hours. For the higher 5000 fmol/mg threshold the ring offers a higher degree of protection after 6 hours compared to the gel. Maximum protection is 79% for the ring and 47% for the gel. A gel is a better choice if protection is needed within a few hours. However, if a ring is used consistently it offers a higher level of protection for an extended period. Ring removal is less detrimental if the EC_{50} threshold is 500 fmol/mg, where the Percent Protected is 99% after 4 hours. However, at a higher threshold of 5000 fmol/mg the Percent Protected drop off immediately post removal. This suggests a short ring removal time is important for maintaining a high degree of protection throughout the tissue, while removal up to a few hours is acceptable if the requisite protective concentration is lower.

Different effects on Percent Protected are explored with varying drug release and vaginal fluid production rates. Percent Protected values are higher with increased drug release and vaginal fluid production. Variations in vaginal fluid production are more important, going from 0 mL to 12 mL per day, during which the Percent Protected increases around 30% for EC_{50} value of 5000 fmol/mg and 500 fmol/mg. Quadrupling drug release rate from 5 mg to 20 mg per day only increase Percent Protected by about 10%. This result shows the importance of vaginal fluid convection in transport for this problem, where doubling fluid production rate is approximately twice as effective as doubling drug flux in protecting the stroma. In the proliferative phase of the menstrual cycle both epithelial thickness and fluid production rate are increased, with the two factors both contributing to better drug delivery in the most vulnerable region of the tissue along the vaginal canal.

5.5 Conclusion

The model here for drug distribution for a Tenofovir ring shows its potential for effective drug delivery and prevention of HIV. Convection in the lumen from vaginal fluid production is the dominant factor in drug transport. Intravaginal rings need to be placed near the fornix in order to minimize area of tissue with low drug concentration. Data on ring migration after placement from this location (e.g. using MRI) would be very helpful in better understanding the potential for ring effectiveness. Average concentration in tissue is expected to be about one log lower than that for a single dose

of vaginal gel, but that concentration level is sustained over the time duration of ring residence. The protective effect of the vehicle as measured by the Percent Protected for stroma after multiple days for the ring is higher than that for the gel. Temporary removal of the ring does not significantly decrease protection even after a few days, however the time needed to reestablish maximum protection will need to be taken into account.

6. Model of Rectal Enemas

6.1 Introduction

Infection by HIV virions due to receptive anal intercourse is a global pandemic, and the need to mitigate it is substantial. Different microbicide product types have been intended for application to the vaginal and rectal canals. Gels were the original dosage form first designed for the vagina and then later for the rectum[21]. Recently an enema has been proposed as a rectal microbicide delivery vehicle[39]. Potential advantages of this enema dosage form include user behavior and adherence, where cleansing enemas are often already used by people prior to receptive anal intercourse (RAI). In addition, the low viscosity of the enema fluid can aid spreading and delivery of drug across a large surface area, and compared with gels enema fluid can be applied at a much higher volume thus potentially delivering significantly more drug. Many factors must be taken into account in design of a microbicide enema product. These include achieving target pharmacokinetics (PK) for the active pharmaceutical ingredient (API). That PK depends on drug and enema properties (volume and drug loading) in relation to the timing of application and the properties of the rectal canal. Both computational as well as experimental preclinical studies can contribute to this design process. Deterministic computational compartmental PK models have been developed for vaginal microbicide gel and intravaginal rings[26]. These are now being used in gel design. In particular, they are providing valuable information about the interactions between gel properties

and applied volume in governing PK. For example, a goal in such modeling has been to determine if reduced gel volumes, which might be more preferable to users, can achieve satisfactory PK. Another goal is to obtain information about the time interval from gel insertion to achievement of protective drug mucosal drug concentrations, the degree of such protection, and its duration.

The analysis here is the application of vaginal PK model in the rectal environment for a microbicide enema, applying it to the drug Tenofovir, which is the lead API for the project. In contrast to the stratified squamous epithelium of the vagina, the rectal mucosa contains a single layer of columnar epithelial cells above the lamina propria (stroma) and it lines the surface down to the crypts in the tissue. The difference in rectal and vaginal mucosal structure is the primary factor taken into account for the model here. In this model, enema distribution along the canal for which the drug is being delivered is a assumed to be fast and complete, like the first model of vaginal Tenofovir delivery by a gel[25]. This is a reasonable assumption for the initial model since the enema fluid has a very low viscosity; a follow up problem will tackle the extent of enema distribution. Factors that can be varied in this problem include the geometry of the crypts, expulsion time of the fluid, and effects of enema tonicity. The notion is that hypotonic enema fluid might promote advective fluid transport into the tissue which could aid drug transport[56] , which is adapted to the model here. Another possible effect of tonicity is the size of crypt opening. The existence of closed crypts is based on

observations with a hypertonic enema[53]. Although at the extreme case a smaller crypt opening might not close off completely, it might be small enough that small air pocket could be trapped in the opening, preventing contact with the enema fluid and thus effectively closing off the crypt. The model here considers the effects of this possible phenomenon on drug transport, recognizing that it is a hypothetical example with some physiological motivation.

6.2 Materials and Methods

6.2.1 Geometry of the Model

The geometry and morphology of the lower colorectal canal vary with location, and exhibit both macroscopic and microscopic features[68, 86]. On the macroscopic scale rectal folds create creases and canyons on the mucosal surface. On the microscopic scale, there are rectal crypts and smaller crevices. The large folds are found in the relatively short anal canal, which is about 2 to 5 cm long, ending in the anal verge[67]. This region contains a stratified squamous epithelium (Figure 46, right). The rectum, which is much longer than the anus, possesses crypts (Figure 46 left and Figure 47) on the surface with a thin columnar epithelium. This is the area upon which will be focused, noting that the thinner columnar epithelium is much more vulnerable to infection. Rectal crypts are the most anatomically significant surface feature on the length scale of drug transport. These are about 40 – 120 μm in diameter and about 1 mm in depth. As seen in Figure 47, they are spaced about 150 μm apart. The characteristic length for transport into the mucosal

tissue is only about one millimeter, i.e. the thickness of the mucosa. Larger features such as curvature of the surface and of the large folds can be neglected (i.e. approximated as flat) due to the small characteristic transport length.

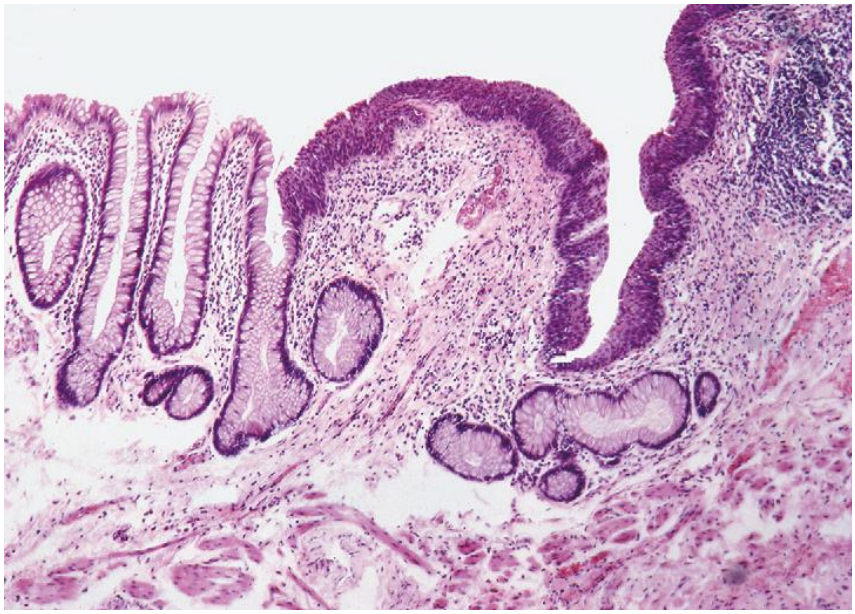

Figure 46: Microscopic image of the anorectal junction[68]. Rectal crypts with simple columnar epithelium are visible on the left. Stratified squamous epithelium is on the right.

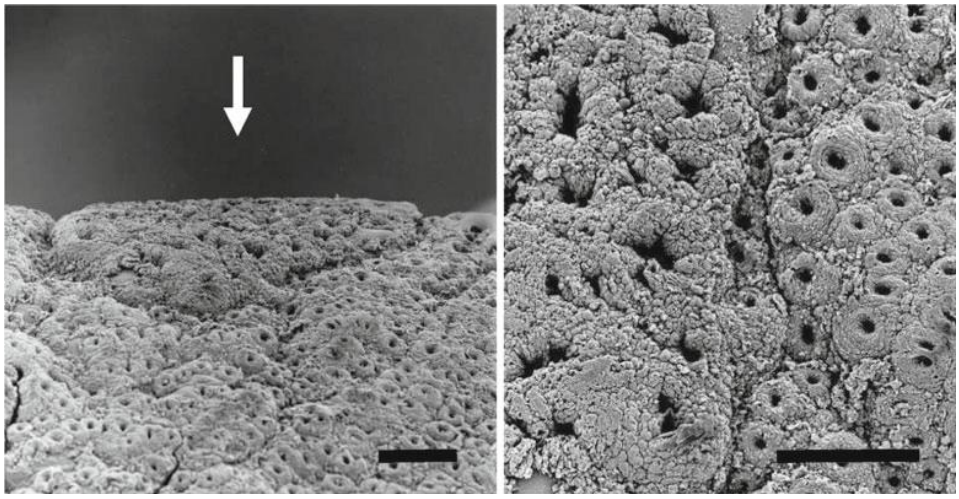

Figure 47: SEM of rectal crypts in the upper anal canal[86]. In the upper zone, there are domed structures (arrow) that contain many large crypts. Bars are 300 μm.

The geometry of the crypt is represented as a circular cylinder down into the tissue (Figure 48). The overall geometry consists of a mosaic of crypts, which can have varying sizes (Figure 47). The characteristic length for each crypt are its radius, the thickness of its epithelial layer, the separation distance between adjacent crypts, and the depth of the crypt down into the mucosal tissue. The enema fluid fills the canal into which the crypt inserts, and the enema fluid covers the mucosal surface and the crypt opening. Two cases are considered: "open" and "closed" crypts, as described above. For the former, there is direct contact and drug exchange between the enema fluid and the fluid within the crypt. The core analysis here focuses upon drug transport into a single crypt and hence into its mucosa. Total drug transport is then the summation over all the crypts. This geometry lends itself to uses of a cylindrical coordinate system within each crypt (Figure 48) with origin at the top of the crypt ($z = 0$). Transport is axisymmetric,

and depends only upon the radial and longitudinal dimensions r and z. There are thus 4 length scales for the overall drug transport problem: r_c, r_e and r_s are the radial dimensions for the crypt, epithelium, and stroma respectively; and h_e and h_s are the thicknesses of the epithelium and stroma within the tissue (r_e and h_e should be equal).

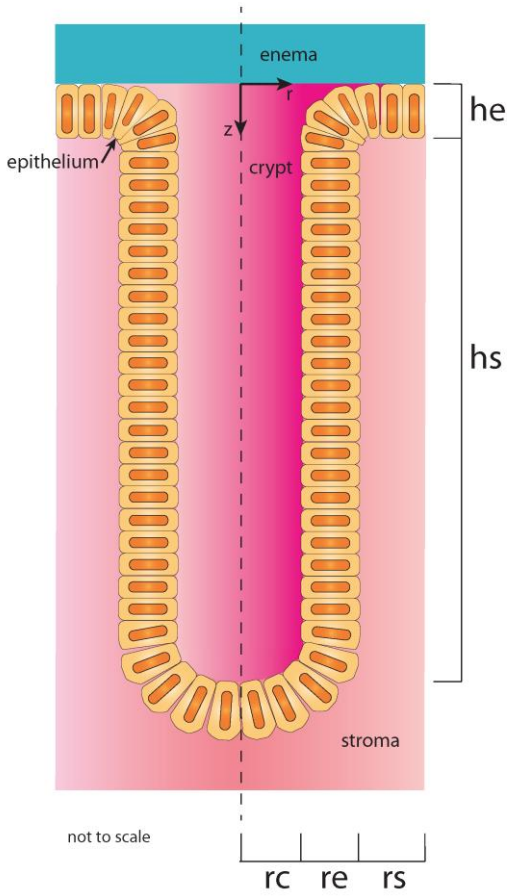

Figure 48: Drawing of the crypt geometry in this model, showing the cylindrical coordinate system used for computations. The enema fluid fills the canal above the crypt.

6.2.2 Governing Equations

There are five compartments overall in the model: the enema fluid within the lumen, the interior of a crypt, epithelium, stroma, and the bloodstream. The luminal enema fluid compartment is taken as a reservoir (constant, uniform concentration) since the mass of drug transported from it to the crypt is a small fraction of mass in the fluid. The governing equations of conservation of mass for Tenofovir and Tenofovir diphosphate have been adapted from the previous work on drug delivery by a vaginal gel[25, 26]. The key difference is use of cylindrical coordinate system vs. a rectangular coordinate system, which is adapted to the different mucosal structure. Advective transport terms within the crypt and tissue are introduced to account for possibly varying degrees of water uptake by the rectum[10].

$$\frac{\partial C_{TFV}}{\partial t} = D_f \nabla^2 C_{TFV} - v_c \cdot \nabla C_{TFV} \quad \text{(a)}$$

$$\frac{\partial C_{TFV}}{\partial t} = D_e \nabla^2 C_{TFV} - v_t \cdot \nabla C_{TFV} - k_{on}\left\{C\phi_e - \frac{C_{DP}}{n}\right\} + k_{off} C_{DP} \quad \text{(b)}$$

$$\frac{\partial C_{TFV}}{\partial t} = D_s \nabla^2 C_{TFV} - v_t \cdot \nabla C_{TFV} - k_b C_{TFV} - k_{on}\left\{C\phi_s - \frac{C_{DP}}{n}\right\} + k_{off} C_{DP} \quad \text{(c)}$$

$$\frac{\partial C_{DP}}{\partial t} = k_{on}\left\{C_{TFV}\phi - \frac{C_{DP}}{n}\right\} - k_{off} C_{DP} \quad \text{(d)}$$

Equation 52

The governing conservation of mass equations for Tenofovir and Tenofovir diphosphate are given in Equation 52. The first equation, Equation 52a, is the transport

of TFV within the crypt fluid. Here C_{TFV} is the concentration of Tenofovir, D_f is the diffusion coefficient in the fluid, v_c is the advective velocity down the crypt, t is time, r is the radial dimension, and z is the depth dimension down into the tissue. Equation 52b gives the transport of TFV in the epithelium, where D_e is the diffusion coefficient, v_t is the advective velocity in the tissue, and C_{DP} is the local Tenofovir diphosphate concentration. The last two terms account for TFV-DP production and loss kinetics, the first is formation of TFV-DP with a rate constant k_{on} and the second term is the elimination of TFV-DP with rate constant k_{off}. The curly brackets are Macaulay brackets (Where the expression becomes zero when it is negative inside bracket. This ensures that the formation rate is always nonnegative). Inside the Macaulay bracket ϕ_e is the volume fraction of cells in the epithelium, due to the close packing of cells its value is close to one. n is the ratio of TFV-DP to TFV inside each cell at steady state. The third equation, Equation 52c, is conservation of mass for TFV in the stroma. This equation is almost identical to that for the epithelium, with subscript s denoting the stroma, and the addition of a term for loss of Tenofovir to the bloodstream with rate k_b. The assumption is that the capillaries are uniformly distributed in the stroma, so that the uptake of each drug molecule by the blood is proportional to the local concentration, this leads to a first order kinetic term[25]. Finally, Equation 52d is conservation of mass for TFV-DP in the epithelium or the stroma compartment. Here ϕ is the volume fraction of cells specific to

each compartment. The advective velocities in both the crypt and tissue are dependent on position and net volumetric advective flow to the rectum.

6.2.3 Boundary and Initial Conditions

The time-dependent boundary conditions at the top of the crypt surface are given by Equation 53a and Equation 53b. When the time is less than the enema application, t_e, the boundary condition for TFV concentration at the surface is given by enema concentration C_0 multiplied by the partition coefficient between the fluid and the epithelium Φ_{fe}. For a closed crypt, the boundary condition at the top surface of the crypt is no flux, both during enema retention and after expulsion. At the interface between the crypt fluid and epithelium, there are two boundary conditions: one is on TFV concentration, with partition coefficient Φ_{fe} (Equation 53c), and the other is continuous TFV flux (Equation 53d). Analogous boundary conditions occur at the interface between the epithelium and the stroma, here with partition coefficient Φ_{es} (Equation 53e), and also continuous flux conditions (Equation 53f and Equation 53g). The boundary condition in the radial direction at the outer margin between the stroma of adjacent crypt is assumed to be no flux due to symmetry (Equation 53h), and the boundary condition at the bottom of the crypt tissue is also no flux (Equation 53i). Initial condition of the problem is zero concentration everywhere (Equation 53j), and the applied enema is assumed to be a reservoir with constant concentration.

$$C\left(z=0, t \le t_e\right) = \Phi_{fe} C_0 \quad \text{(a)}$$

$$\frac{\partial C}{\partial z}\left(z=0, t > t_e\right) = 0 \quad \text{(b)}$$

$$C_f\left(r=r_c\right) = \Phi_{fe} C_e\left(r=r_c\right) \quad \text{(c)}$$

$$D_f \frac{\partial C_f}{\partial r}\left(r=r_c\right) = D_e \frac{\partial C_e}{\partial r}\left(r=r_c\right) \quad \text{(d)}$$

$$C_e\left(r=r_c+r_e, z=h_e\right) = \Phi_{es} C_s\left(r=r_c+r_e, z=h_e\right) \quad \text{(e)}$$

$$D_e \frac{\partial C_e}{\partial r}\left(r=r_c+r_e\right) = D_s \frac{\partial C_s}{\partial r}\left(r=r_c+r_e\right) \quad \text{(f)}$$

$$D_e \frac{\partial C_e}{\partial z}\left(z=h_e\right) = D_s \frac{\partial C_s}{\partial z}\left(z=h_e\right) \quad \text{(g)}$$

$$\frac{\partial C}{\partial r}\left(r=r_c+r_e+r_s\right) = 0 \quad \text{(h)}$$

$$\frac{\partial C}{\partial z}\left(z=h_e+h_s\right) = 0 \quad \text{(i)}$$

$$C\left(t=0\right) = 0 \quad \text{(j)}$$

Equation 53

6.2.4 Parameters in the Model

Parameters used in the enema model are given in Table 9. The crypts may be filled with mucus, which should have similar diffusion coefficient for Tenofovir that was measured previous for a vaginal gel since both have comparable hydration. Other parameters are adapted from the previous analysis of a vaginal gel[26]. Concentration of the enema is $1x10^7$ ng/mL (a 1% solution), this is the typical concentration used for a

water based solution just below the solubility limit of Tenofovir in water. The diffusion coefficient for epithelium is $1x10^{-7}$ cm^2/s and for the stroma is $4x10^{-7}$ cm^2/s. Due to hydrophilic nature of Tenofovir, the partition coefficient of the drug is 0.75 between the fluid and epithelium, and is unity at the interface between epithelium and stroma. The crypt is assumed to have two possible sizes – large or small (Figure 47). The large crypt has a radius of 60 μm, and a stromal separation of 45 μm to the next crypt. The small crypt has a radius of 20 μm with the same stromal separation distance. Epithelial and stromal thicknesses are estimated from histological images, which are 15 μm and 1000 μm respectively. The total retention time of enema is taken to be 5, 10, or 20 minutes. The rate constant for transport of TFV to blood is the same value as obtained in the prior analysis for vaginal gel[25]. It is not yet possible to directly measure advective fluid velocities as discussed above. In the model here an upper bound for advective velocity in the tissue is based upon measurements of net fluid absorption by the rectum[10]. The maximum velocity can be estimated by dividing the highest rate of water uptake by the total surface area of the rectum. This total velocity is then fed into a model of water uptake in the tissue, where each volumetric area in the stroma can be assumed to absorb the same amount of fluid coming from the nearest source either at the tissue surface or the sides of the crypt. This velocity field is used to find the velocity profile in the crypt by mass balance. Parameters related to TFV-DP formation kinetics include the volume fraction of cells in the epithelium and stroma, rate of formation and elimination of TFV-

DP, as well as the steady state ratio of TFV-DP to TFV. These rates were estimated from pharmacokinetic studies of diphosphate formation[37].

Table 9: Parameters in the enema model

Parameter	Symbol	Value	Reference
Enema concentration (ng/mL)	C_0	$1x10^7$	[56]
Diffusion coefficient in fluid (cm^2/s)	D_f	$6x10^{-6}$	[25]
Diffusion coefficient in epithelium (cm^2/s)	D_e	$1x10^{-7}$	[14]
Diffusion coefficient in stroma (cm^2/s)	D_s	$4x10^{-7}$	[14]
Partition coefficient of fluid/epithelium	Φ_{fe}	0.75	[14]
Partition coefficient of epithelium/stroma	Φ_{es}	1	[14]
Radius of crypt: large/small (μm)	r_c	60, 20	[86]
Stromal radii: large/small (μm)	r_s	45, 20	[86]
Epithelial thickness (μm)	r_e, h_e	15	[68]
Stromal thickness (μm)	h_s	1000	[68]
Time of enema application (min)	t_e	5, 10, 20	
Rate constant of transport to blood (hr^{-1})	k_b	0.119	[25]
Advective velocity in crypt	v_c	computed	
Advective velocity to tissue (μm/s, max)	v_t	0.52 μm/s	[10]

Volume fraction of cells in epithelium	φ_e	0.95	[26]
Volume fraction of cells in stroma	φ_s	0.1	[26]
Rate of formation of TFV-DP (hr^{-1})	k_{on}	0.693	[37]
Rate of elimination of TFV-DP (hr^{-1})	k_{off}	0.00413	[37]
Equilibrium ratio of TFV-DP to TFV	n	0.1	[26]

6.2.5 Numerical Solution of Governing Equations

Numerical solution of the system of differential equations in Equation 52, subject to boundary and initial conditions in Equation 53, was obtained by the finite difference method. The physical space was first discretized in the radial and depth direction with 5 micron spacing. Spatial derivatives were computed using the central difference method. The result was a system of coupled ordinary differential equations at each time point. Which was then solved using Matlab's[60] Runge-Kutta 4,5 method. Compared to the two-dimensional vaginal gel problem in a rectangular coordinate system, special attention was needed to adapt to the two-dimensional enema problem in cylindrical coordinates. Second derivatives involving the radial distance were taken at half step between each point, and volume integrals for calculating spatial average concentrations were evaluated in cylindrical coordinates.

6.3 Results

6.3.1 Heat Map of Typical Solution

The fundamental solutions to this model are the concentration distribution of Tenofovir and Tenofovir diphosphate as a function of position in the crypt fluid and the mucosa as well as time post initial application. Due to axial symmetry of the model (Figure 48), the spatial dependence is in two dimensions for the radius from center of the crypt and the depth into the mucosa. The heat map or concentration distribution at particular time is plotted in Figure 49 for TFV at 5 minutes after dosing in a small crypt. The crypt fluid is "open", i.e. contiguous with the fluid in the enema. The colors correspond to concentration values from 0 ng/mL (blue) to 10^9 ng/mL (maroon). Due to higher TFV diffusion coefficient in the crypt fluid, the concentration there is much higher than the surrounding tissue. The highest concentration in the tissue is found in the epithelium near the surface in contact with the enema. To preserve aspect ratio of this plot, only the top 20% of the crypt is shown. The lower 80% of the tissue and crypt contains much lower TFV levels than the top.

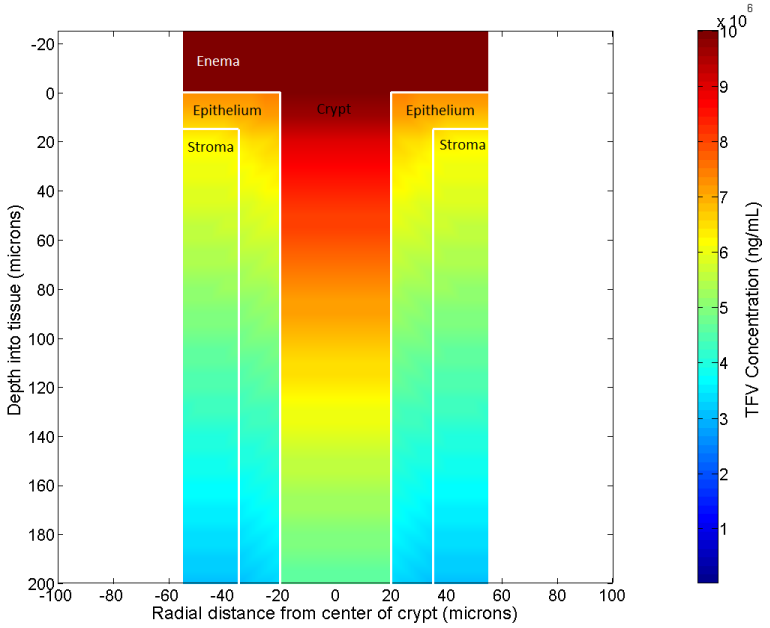

Figure 49: Heat map of Tenofovir concentration distribution in the upper part of a crypt and mucosal tissue at 5 minutes post dosing. The crypt has a small size and is open to enema fluid.

6.3.2 Effects of Variable Enema Retention Time

Enema retention time is clearly a critical factor in drug delivery, here the contrast is made with varying retention times of 5, 10, and 20 minutes. Complete enema expulsion is assumed at the end of the retention time. Results for times up to two hours post enema application are given in Figure 50. For contrast, the results for TFV concentration in the complete coating vaginal model[25] are also included. The purpose was to illustrate consequences of different luminal and mucosal structures of the vagina and rectum, and sustained retention time of the gel. The subplots in Figure 50 are fluid

in the crypt (or gel for the vaginal model), epithelium, stroma, and Tenofovir diphosphate in the stroma. The crypt can be either open or closed.

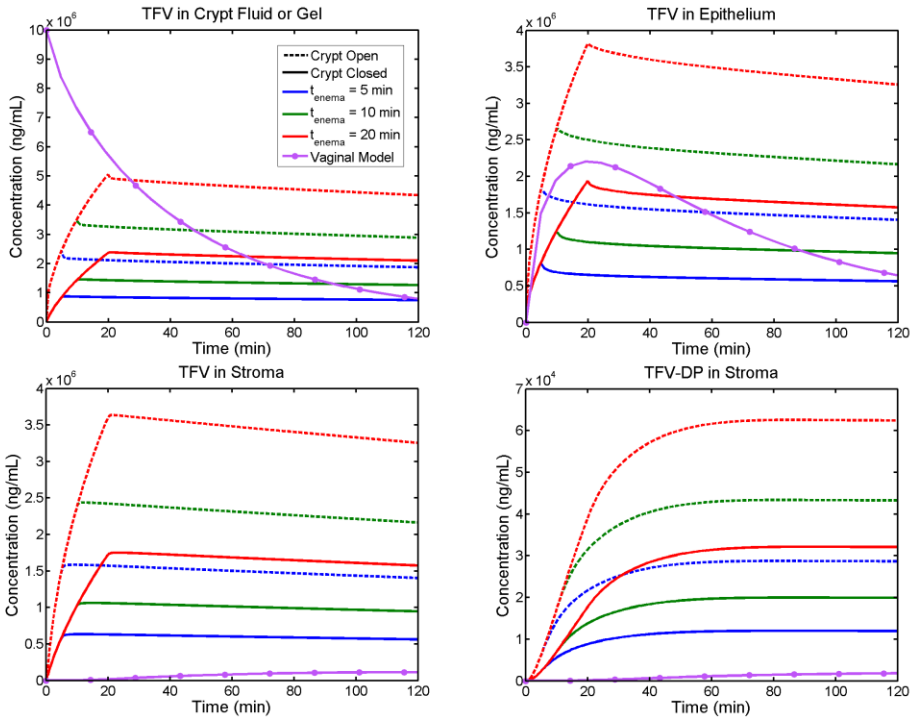

Figure 50: Volume-averaged TFV and TFV-DP concentrations in different compartments for an enema applied for 5, 10, or 20 minutes and with an open/closed small crypt size, contrast with results for vaginal model.

Average concentration in the vaginal gel is initially at 10^7 ng/mL (the same as the enema), and the concentration in the crypt is initially 0. By around the half hour mark, the concentration in the gel has decreased due to leakage and dilution to a similar level as the crypt. Since enema retention is only minutes long, TFV concentrations in the crypt fluid and mucosal tissue begin to level off immediately after enema expulsion. Concentration for an open crypt is higher than those for a closed crypt, with the difference increasing with longer enema retention time. In the epithelium, vaginal

concentration follows a similar rise compared with the crypt open case. The peak concentration is at 20 minutes post dose, with a much faster drop off compared to the rectal case. Most of the drug is contained in the upper epithelium. Both stromal TFV and TFV-DP concentrations are much higher in the rectal case than the vaginal one. This is primarily due to the thinner epithelium of the rectum.

6.3.3 Effects of Crypt Size

Results for a large versus small crypt are shown in Figure 51. Their respective sizes are in Table 9. Enema application time is 5 minutes with either open or closed crypt.

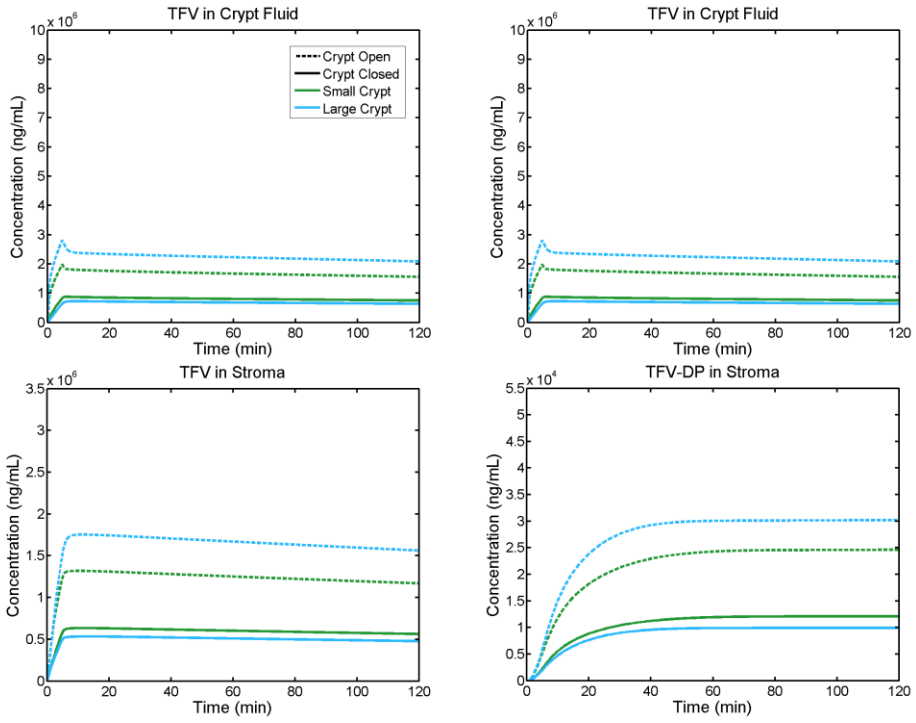

Figure 51: Average TFV concentrations in different compartments for small or large crypts, which are open or closed. Enema retention time is 5 minutes.

If the crypt is closed, the difference between a large and a small crypt is minimal. This is because with a closed crypt, the primary mode of transport is through the epithelium at the surface, which has the same thickness for both crypt sizes. If the crypt is open, then the difference is much more pronounced, with a large crypt having higher TFV concentrations in the crypt fluid, epithelium and stroma, and higher stromal TFV-DP. The difference is approximately 50% for Tenofovir in the tissue and approximately 25% for TFV-DP. Here, the concentration is actually lower for a large crypt for the closed case. This is possible due to a larger crypt leaching more Tenofovir from tissue surrounding the crypt.

6.3.4 Effects of Advective Fluid Flow

Figure 52 gives results for effects of the maximum advective velocity, one half of the maximum, and no advection. With a closed crypt, advection in the crypt is zero, and only a small convective force exists on the surface of the epithelium. This effect is too small to be detected and all crypt closed cases are merged into a single line. Advective flow is possible with enemas of different tonicity which then drives the rectum's natural tendency to absorb extra fluid.

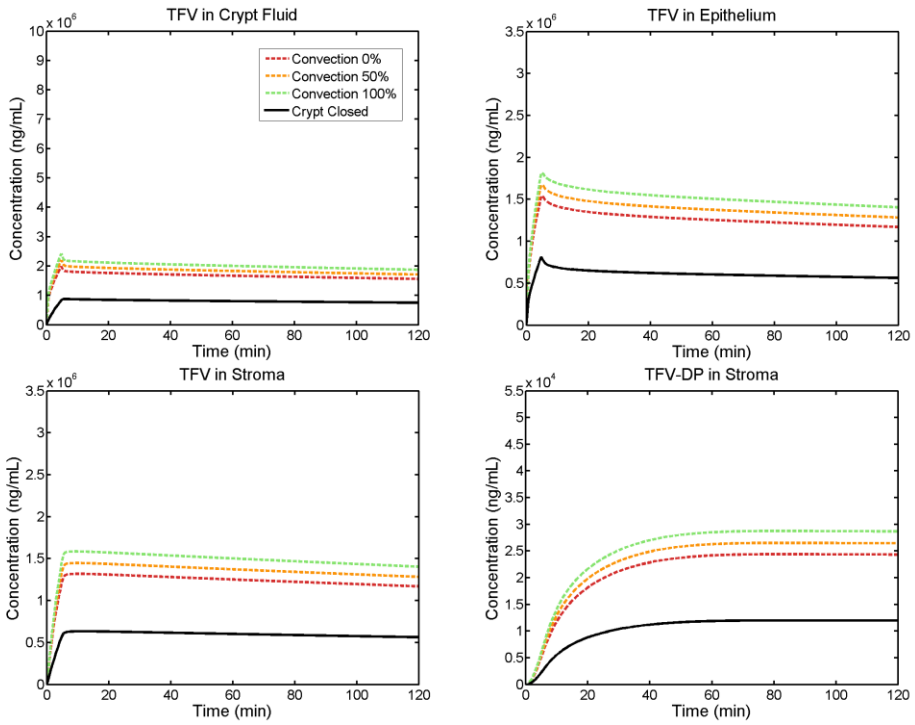

Figure 52: Average concentration in compartments with varying advective flow. Enema retention time is 5 minutes.

Overall the effect of advective flow appears to be relatively small for drug transport within the crypt and adjacent mucosal tissue. For the open crypt the difference in concentration between 0% and 100% maximum advective velocity is less than 20%. Once again the open versus closed crypt status is a much more important factor in drug transport.

6.3.5 Concentration Profiles as a Function of Depth

It is of interest to compute the local stromal drug concentration as a function of depth and time after enema insertion. This profile provides biophysical insight to the non-uniformity of TFV concentration distribution within the stroma, and consequently

to that of TFV-DP. For the vaginal PK model, accounting for this non-uniformity was important with respect to the uncertainties in interpretation of concentrations in biopsies. Figure 53 plots TFV concentration vs. depth down into the tissue at different times.

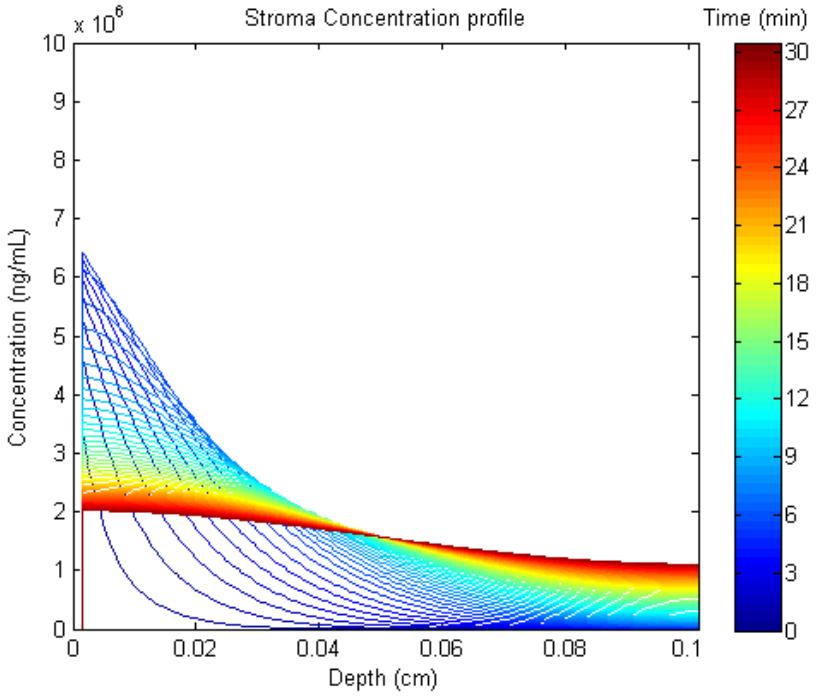

Figure 53: TFV concentration profile versus depth of the stroma after 5 minutes of enema retention for a small crypt.

Here the concentration in the stroma at each depth is averaged (in the radial direction for each compartment at each depth) for a particular time point (color axis, with blue for short and red for longer time points). The aspect ratio of the depth to the width varies from 8 to 18 depending on the size of the crypt. Because the radial stromal dimension is small compared to the longitudinal size of the crypt downwards, the

concentration variation in the former is small compared to that of the latter. The plot shows an initial high concentration near the surface of the tissue that gradually flattens out to the bottom of the crypt. A noticeable increase in concentration at the bottom of the tissue occurs around the 12 minute mark.

6.3.6 TFV-DP Concentration in Stromal Host Cells

This modeling approach was previously used to create summary interpretations of TFV-DP concentrations in vaginal stromal host cells with respect to target values that are deemed prophylactic against HIV[26]. A similar analysis can be conducted here using a target prophylactic TFV-DP concentration of 500 fmol/mg from EC_{50} measurements[47]. The Percent Protected measure, which is the fraction of entire stromal volume in which local TFV-DP concentration equals or exceed this target value is computed here as a function of time after enema application. This spatial average TFV-DP concentration is proportional to the average concentration per host cell. Assuming uniform distribution of host cells, the Percent Protected based volume average concentration is thus equal to the Percent Protected based upon an average host cell concentration. The time dependence of Percent Protected after enema application is illustrated in Figure 54.

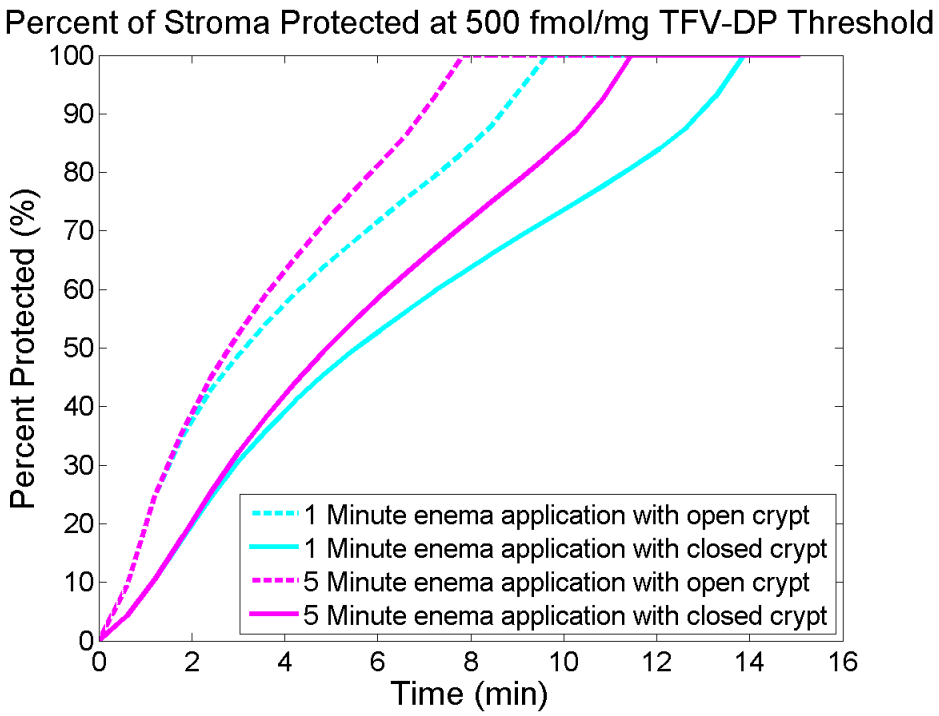

Figure 54: Percent of stroma volume protected after 1 minute and 5 minutes of enema retention for a small sized crypt.

Here 100% Percent Protected of stroma is achieved with either 1 minute or 5 minutes of enema application. The time to 100% protection is longer for 1 minute vs. 5 minutes, and is also longer if the rectal crypt is closed.

6.3.7 Simulated TFV and TFV-DP Concentrations in Biopsies

The detailed spatial-temporal mapping of concentrations of TFV and TFV-DP output by this model can be translated to computations of their values in rectal biopsies. This involves taking a volume average of concentrations in geometric domain that simulates the tissue taken in a biopsy. Since the diameter of a crypt is about 40 – 120 μm and diameter of the biopsy in a human is about two orders of magnitude larger, a single

biopsy will sample many crypts. Thus, the concentration measured in a single crypt and in the tissue between it can approximate the concentration in the entire biopsy assuming small variation between crypts. The depth of the rectal biopsy in a human is about 3 mm, this defines the depth of the volume in the simulation of a biopsy. However, in the computations the depth only goes down to about 1 mm, but since the drug is concentrated near the surface, TFV and TFV-DP in the tissue lower than 1 mm is negligible when compared to the upper levels. Thus increasing the biopsy depth is effectively diluting the concentration of the drug by a constant proportion. This is illustrated in Figure 55 and Figure 56 for TFV and TFV-DP with simulated biopsies.

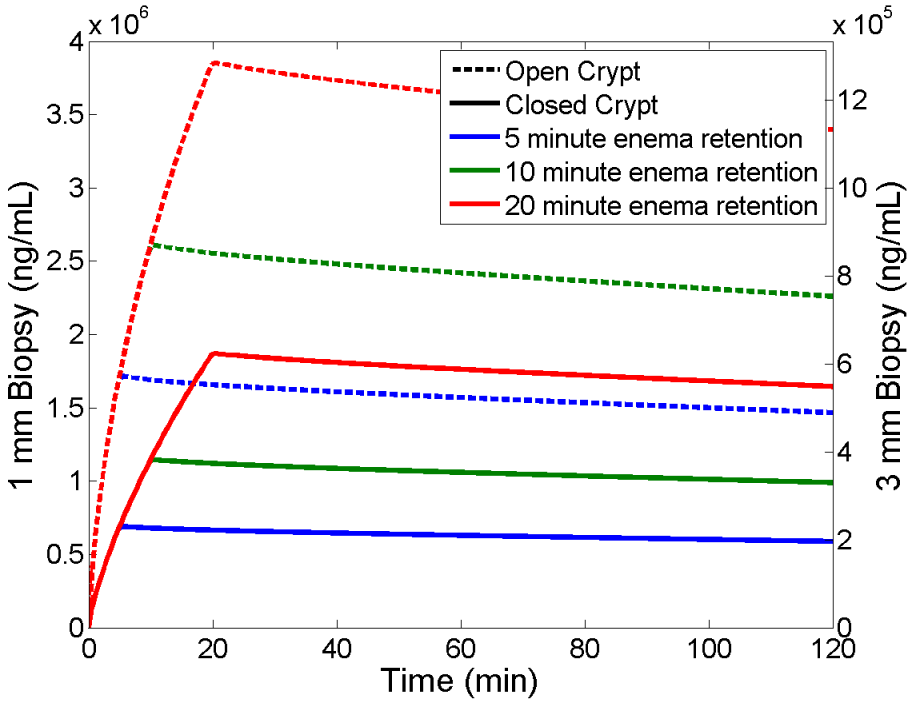

Figure 55: Results for TFV concentrations in a simulated biopsy. Enema retention and crypt openness are varied. Biopsy is either 1 mm or 3 mm.

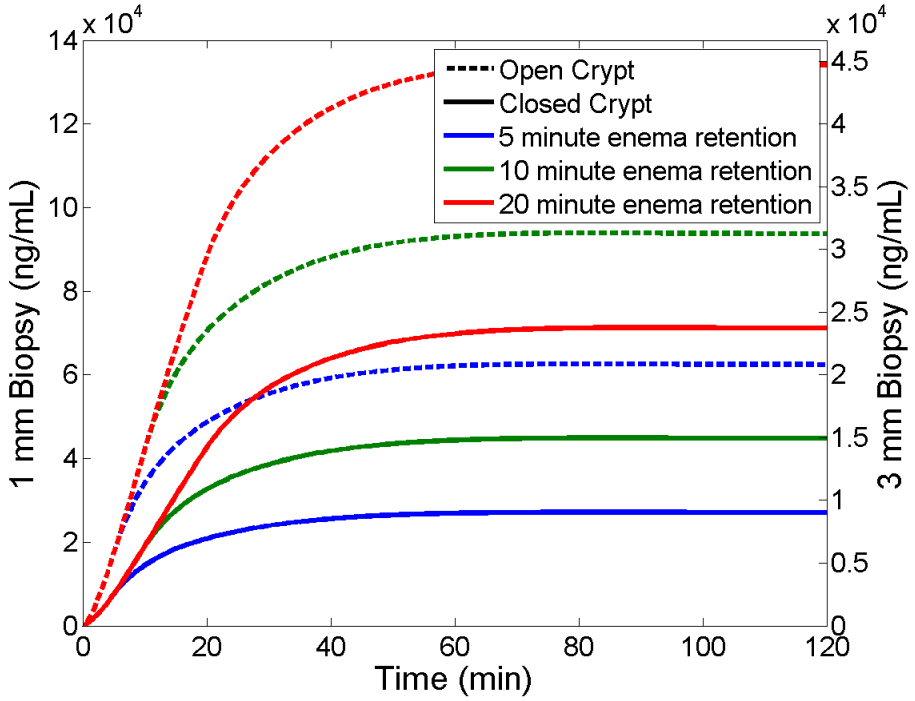

Figure 56: Results for TFV-DP concentrations in a simulated biopsy. Enema retention and crypt openness are varied. Biopsy is either 1 mm or 3 mm.

The plots above varies enema application time as well as crypt openness, both are significant factors in measured biopsy concentrations. The shapes of these curves are qualitatively similar to those for TFV and TFV-DP concentrations in the stroma because the time scale of TFV rise is similar for all cases, so the proportionality of TFV-DP is preserved. The only noticeable difference is a longer rate of decay for TFV-DP as expected from a long intracellular half-life.

6.4 Discussion

There is less research conducted for rectal microbicides than for vaginal formulations. Mechanistic modeling of drug delivery in the rectal environment can aid

the design and research efforts of a rectal enema. This work can relate enema vehicle design, biological factors, and typical use to the delivery of Tenofovir in the target environment. Furthermore, the model is able to predict tissue biopsy or blood measurements in human or animal trials.

This model builds on previous work done for the delivery of Tenofovir by a vaginal gel[25], and a subsequent analysis[26] incorporating two-dimensional transport in the tissue as well as TFV-DP kinetics. In this model, the distribution of enema fluid is assumed to be extremely fast due to low viscosity of the applied fluid. This suggests an almost instantaneous distribution of the enema that partitions the rectum to areas that are in contact with the delivery vehicle and areas that are bare. The analysis here will focus on the area of the rectum that is in contact. Rectal crypts are structures in the rectum that is on the same length scale as drug transport. Computations can be made for a single crypt and applied to other crypts with similar properties. Different crypt properties, including size and whether it is open or closed can be used in calculating the effect on drug transport.

Similar to previous analysis on the vaginal gel, the concentration distribution is expected to show a very steep gradient into the tissue. However, the distribution in the rectum (Figure 49) is not as steep as the vaginal model, shown here on a linear scale instead of a log scale typically needed for the vaginal model. This is primarily due to the presence of the crypt or, more precisely, the crypt fluid which can aid the transport of

drug down into the tissue as a result of having a much higher diffusion coefficient compared to the surrounding tissue. Biopsy results are more dependent on the highest concentration level of the tissue, which is found in the upper stroma and epithelium.

The four main factors varied here for delivery of drug into the tissue are the duration of enema retention, crypt size, magnitude of convective flow into the tissue, and whether the crypts are open or closed. The first plot shows the contrast in enema applied time with both open and closed crypts. An open crypt is able to deliver about twice as much drug as a closed crypt. Despite the fact that the crypt opening is only about a quarter of the total surface area, a large diffusion coefficient in the crypt fluid can greatly enhance transport. Increasing the retention time of the applied enema also increases the drug delivery. This change is consistent in all compartments. Both the epithelial and stromal compartments have similar concentrations and time profiles in the enema model. This is in contrast to the vaginal model plotted in violet, where the concentration in epithelium is much higher than that of the stroma. The rectal epithelium is very thin, and wraps around the crypt all the way down to the end of the stromal layer. This geometry allows fast transport and similar concentration values between the two layers, and the deep epithelium gave rise to a similar depth profile between the layers as well. As expected, the TFV-DP concentration follows the rise of TFV in stroma initially but decays at a much slower rate.

The two other factors in the model are crypt size and advective velocity in the crypt. Both are a much smaller factor in drug delivery when compared to enema application time and whether the crypt is open or closed. Having a large crypt increases transport by less than 50%, but only for the crypt open case while the difference is almost negligible for a closed crypt. Advective velocity is driven by the rectum's natural tendency to absorb fluids. This effect could be tuned with different tonicity of applied enema. However the overall change in drug delivery is small, with the difference in concentration between no advective flow and maximum flow of only around 20%.

Concentration profiles for each time point as a function of depth shows more clearly the longitudinal distribution of Tenofovir. In contrast to the vaginal model, the concentration gradient into the tissue is very steep initially but gradually flattens over a time period of 30 minutes. This is primarily due to the enhanced transport properties of the rectal crypt, where the drug can be distributed fairly rapidly down into the depth of the crypt. In addition the rectal epithelium and stroma are both much thinner than their vagina counterparts, further enhancing transport.

The measure of Percent Protected of stroma, first introduced in the earlier vaginal gel model is also applied here. Due to enhanced drug transport properties of the rectum, particularly with crypt fluids and a thin mucosa, Tenofovir diphosphate concentration is able to reach a prophylactic level much faster than in the vagina. Even with rectal enema retention time of only 1 minute, the Percent Protected level is still able

to reach 100% although in the extreme case, i.e. with a closed crypt, it takes over 14 minutes to reach such a point. A longer enema application time and open crypts will both decrease this critical time point. This is promising, since long enema retention time is unrealistic and potentially could cause a reduction in adherence. Furthermore a wait time of around 15 minutes to reach 100% is much better than the vaginal gel model in which it is a few hours. However, this observation does not account for transport of the virus which presumably is slower in the vaginal case as well.

Plots of simulated biopsy values both for TFV and TFV-DP show how variations in time and other factors could influence measured concentration. Typically a biopsy is around 3 mm thick, but since this model only considers a mucosa that is 1 mm thick, any extra thickness will contain no drug. In essence thicker biopsies dilute measured concentration linearly as a function of the total thickness. Thus in order to get a more accurate representation of the actual mucosal concentration, a biopsy will need to account for the depth at which it is taken in addition to the averaged concentration value. The measured biopsy concentration for a 1 mm case is actually higher than the concentration in the stroma. This is due to the biopsy's inclusion of crypts, which have a higher amount of drug than the rest of the tissue. The plots can also be used to find an optimal time to take biopsies. Concentration increases steadily until around the 20 minutes for TFV and 60 minutes for TFV-DP, after which the concentration levels off to a plateau. Taking the biopsy around the plateau will most likely decrease sensitivity of

measured concentration in time. This is preferable because it can decrease variability in an already highly variable measure.

6.5 Conclusion

Rectal enemas are emerging as a viable addition to existing microbicide delivery vehicles. Modeling of drug distribution after application of the enema is important in determining its effectiveness as well as factors that could impact the delivery of a pharmacologically active amount of drug to infectible cells in the body. Results of the model showed good protection in local tissue against HIV infection under areas in contact with the enema. Compared with vaginal delivery, a rectal enema has a few key advantages. In the rectum, a thinner epithelium and mucosal tissue allow rapid penetration of the drug. Physiological features such as the fluid filled rectal crypt and the tendency of the rectum to absorb fluid enhance drug delivery. Furthermore, a high volume of applied enema will allow a larger area of the rectum to be coated. Results from a biopsy measurement are also simulated here, where the most important factor in measurement variability is the biopsy thickness.

7. Conclusions

7.1 Summary

This work focused on the development of mathematical models for drug delivery by anti-HIV microbicides, first in the vaginal environment by a gel, then expanded to delivery by a vaginal ring, and finally extended into the delivery by a rectal enema. The goal is to accurately compute distribution of microbicides over time and space in the body in order to infer the level of protection against HIV and to aid microbicide research by predicting relevant experimental pharmacokinetic measures such as biopsy and blood concentrations. Results can help in development of microbicide products by identifying important factors that govern PK and that can be controlled in product design. Results also address how variability in PK derives from variability in biological and biophysical factors, and this can help explain the empirically defined population variability in clinical trials.

The first model is of a Tenofovir delivering gel in the vaginal environment. The basic assumption is perfect coating of the gel over the epithelial surfaces along the canal soon after initial insertion. A simple one-dimensional model of drug distribution in the mucosa can be created using transport theory with diffusion and reaction kinetics. The model has yielded surprisingly good agreement with existing clinical data on biopsy and blood concentrations after single and multiple doses. Variability in the model, including effects on measured biopsy and blood values, is also explored. Epithelial

thickness and sampled biopsy thickness are two important factors that influence the measured drug concentrations in biopsies. In particular, the biopsy thickness could be controlled or at least measured experimentally, but it is rarely if ever reported in the literature. Epithelial thickness in women varies by about 50% during the menstrual cycle. Model results show that a thicker epithelium delays the unset of maximum concentration and lowers the value in the stroma as well as decrease the proportion of drug in the stroma to the total tissue biopsy.

Distributions of vaginal gels in the lumen are next explored in a fluid dynamic analysis of the spreading problem. This is an extension of previous work in our lab on gel rheology and spreading. Here improvement is made in three key areas. First, while the original model focused on spreading in an infinite plate or with radial symmetry, this new model considers spreading in a constrained channel with lateral symmetry. Second, simpler rheological models such as Power Law and Herschel-Bulkley models for the gel are replaced with more advanced models, i.e. Carreau-like fluid and Carreau-like fluid with a yield stress. Third, a more anatomically accurate model of the vaginal canal is created as a finite channel that has a closed and an open end representing the fornix and introitus, respectively. This model thus analyzes gel spreading and also accounts for, and quantifies, gel leakage from the introitus. The solution to the most complex model of a Carreau-like fluid with yield stress is an integral equation that is related to the Reynolds equation of the problem. Resulting computations can be used to

find the coated area as a function of time, including gel leakage which influences user adherence to indicated gel use. These results can and are input next to modeling of drug mass transport from a spreading gel. Because this model contains a comprehensive 3 or 4 (including a yield stress) parameter constitutive model for the gel, the role of gel rheology in spreading is thus delineated. This can help not just in optimizing gel rheology during gel design, but in interpreting changes in gel rheology during aging as an additional measure of gel stability..

Gel spreading is next combined with drug mass transport to create a more comprehensive model of drug delivery. This is applied to the microbicide Tenofovir. In this model, the mucosal tissue contains separate layers for the epithelium and stroma (which contains most of the host cells that HIV can infect). Tenofovir concentration distribution in two dimensions vs. time is computed. In addition to Tenofovir, the kinetics Tenofovir phosphorylation to its antiviral (reverse transcriptase inhibiting) form Tenofovir diphosphate, TDV-DP, are included. This new model thus incorporates the role of gel spreading into the transport of drug molecules from the gel into and through the tissue. The interacting roles of gel rheology and volume are delineated. The results improve upon our earlier ones in identifying and describing the roles of gel and vaginal factors on drug transport and protection against HIV. Predicted concentration distributions of TFV-DP are interpreted with respect to experimentally determined EC_{50} value to give a new, objective pharmacodynamic measure of protection, the percentage

of total stromal volume (or, equivalently, of cells in the stroma) the achieves the target EC_{50} concentrations. This new measure, termed Percent Protected, provides a much better indicator of drug efficacy than volume-averaged concentration values that have been used previously. Sensitivity analysis of the parameters in the model is also implemented to determine the most important factors for drug delivery.

The model of mucosal drug delivery by a vaginal gel can be extended to delivery by a vaginal ring. While a gel is formulated for daily or episodic use, a ring is expected to function for a month or more. Here, the problem approaches steady state conditions for both fluid flow and drug transport. Computations are made for two different projections of the problem, the sagittal plane model which includes two cross-sections of the ring in vaginal fluid and tissue, and a coronal plane model which is in the fluid layer with a flat ring and a simulated tissue boundary. The results indicate vaginal fluid production is a key parameter that governs drug transport, and ring placement in the lumen also strongly affects protection in tissue since drug transport upstream of the ring is extremely limited. Temporary removal of a ring for under a few hours does not drop the Percent Protected in the stroma significantly. This would be beneficial for users who want to remove the ring prior to sex.

Models of transport in the vaginal mucosa can be adapted to the rectal environment for an enema containing microbicides. Key differences between the two mucosal tissues are the structures and thicknesses of the epithelial and stromal layers

and the presence of crypts in the rectal mucosa. Compared to vaginal gel delivery, Tenofovir delivery by an enema achieves a higher concentration in the tissue shortly after each dose. Key parameters in transport are the time of enema retention and whether the crypts are open or closed. The model assumes perfect coating of enema fluid over the tissue, with the exact target area or volume of the enema currently not included in the analysis. Percent Protected measure of the stroma showed promising results; 100% can be achieved much more rapidly after enema vs. vaginal gel applications. This protection is not instantaneous, needing around 15 minutes post enema application. This contrasts with the wait time for delivery to the vaginal mucosa, which is on the order of hours.

This dissertation analyzed the distribution and transport of microbicides, in particular Tenofovir, for use as pre-exposure prophylaxis against HIV. Models in the vaginal environment for a gel and ring gave good agreement with existing clinical data. Rectal microbicide application is also explored with a model of a Tenofovir enema. The end result is a set of predictions that can aid the design of microbicide delivery systems by informing about the most salient parameters in drug delivery. Other variables such as the dosage regimen, biological variability, and usage differences are also taken into account. This will enable better interpretation of clinical results and the formulation of improved microbicide products.

7.2 Future Directions

Interpretation of the results in these models cannot be made in absolute terms, even though the model output include detailed value of concentration and other derived measures. This is because intrinsically biological variability is usually on the order of multiple logs, but these are not completely accounted for in the current model. Of course, future improvements in the model could potentially decrease variability, but it cannot be expected to eliminate significantly more than the current method. The two other ways of interpreting the results are the qualitative measures and relative comparison. Qualitative measures include the shape of each curve and their approximate magnitude. This information can give a general sense of the concentration or drug efficacy in each computation. Relative comparison by altering different parameters can give a sense of the contribution of each to the model. A relative measure is preferable to an absolute measure because it is able to cancel out some of the hidden variability in the problem.

All three models from vaginal gel to vaginal ring to rectal enema can be expanded to include more accurate parameters and more comprehensive features. The vaginal gel model is perhaps the most complete, with the addition of a compliant wall model and laterally inhomogeneous mucosa as possible extensions to the problem. Compliant wall is a more accurate representation of the force exerted by the vaginal canal. Laterally inhomogeneous mucosa could potentially account for microscopic

variations in the vaginal mucosa including rugae folds and locally varying thickness of epithelium and stroma. In the ring model, a more comprehensive coupling between vaginal fluid and mucosal transport is needed. One potential is to use Linear Time Invariance systems theory for the one-dimensional transport problem which results in a simple functional response of the mucosal concentration with any arbitrary input to the tissue surface. This coupling will enable a better understanding of the exact effect on protective concentrations in the stroma after complex luminal activities such as coitus. Model of a rectal enema can be improved by introducing enema fluid distribution. This will be strongly dependent on the shape of the rectum as well as how each enema is applied. The result should gave a better understanding of the location which is coated versus uncoated by the enema.

Knowledge gained here in the model can also be extended to other novel dosage forms. These include vaginal and rectal tablets, vaginal films, rectal gels, and fiber meshes. The key properties to drug delivery are the release rate of each dosage form, the area for which it is being released to, and whether such release is aided by local fluid flow or biological functions such as water absorption. The models of transport for gels, rings, and enemas can be easily adapted to these new dosage forms since the difference between them is primarily in the luminal distribution of the drug and not mucosal transport. With the exception in some cases where tonicity of the dosage forms can be a factor.

The models here focused primarily on the drug Tenofovir. However the experience gained can be applied to other drugs as well. Other reverse transcriptase inhibitors work similarly to Tenofovir in that it needs to be delivered to infectible host cells before being able to prevent HIV infections. The difference between these drugs is then their transport properties such as the release rate, diffusion coefficient, and the hydrophilicity of each drug manifested in its partition coefficient. Other drugs such as Griffithsin and Cyanovirin-N are entry inhibitors that need to be in contact with the virus before their entry to host cells to be effective. These drugs are then most likely active in the lumen instead of the mucosa. The model will also need to include the transport and distribution of the HIV virus in order to compute the drug's ability to prevent viral entry.

Viral dynamics are important not only for entry inhibitors, but also useful in the model of reverse transcriptase inhibitors discussed earlier. The pharmacodynamics measure used before is the Percent Protected, which does not account for the time and space distribution of the virus. This measure might over estimate drug efficacy since the distribution of viral attack regions is more likely to be concentrated near the surface of the tissue than the deeper areas. Incorporating viral dynamics will give a more accurate picture of how the virus and protective drug molecules interact. One caveat is that although data on drug distribution and transport are plentiful, the same cannot be said

with the virus. In addition, data on the kinetics of viral attack is scarce. This means care will be needed in estimating parameters of the viral dynamics model.

Appendix A: Fluid Flow in a Rectal Cylindrical Geometry

Rectal gels are another form of delivery vehicle being developed for microbicides. Spreading of a rectal gel is the first important step in understanding the extent of drug delivery. The rectal environment is very different from the vaginal environment, not only in terms of dimensions but also the geometry. In the vaginal environment, the walls in the collapsed state forms a thin approximately rectangular cross section, while in the rectum the walls are cylindrical with a much larger opening in the regular state.

In this model the gel is being squeezed by a cylindrical tube with the z direction being the axis of flow and the radial direction is the wall with applied squeezing force. A Carreau-like constitutive model with yield stress is used for analysis since it is the most advanced model of rheology. The method for finding the solution is similar to the vaginal model, in fact the boundary conditions from Equation 20 can be used simply by exchanging z for x, and r for y.

$$\frac{\partial P}{\partial z} = \frac{1}{r}\frac{\partial}{\partial r}\left(-r\tau\right)$$

Equation 54

The Navier-Stokes equation in a cylindrical coordinate system for the z dimension is in Equation 54. Again due to lubrication theory the pressure gradient in the radial dimension is assumed to be zero. The result is a pressure gradient in the direction

of flow and this pressure gradient is a function of z only. This expression can be integrated once to give the expression for shear stress in Equation 55.

$$\tau = -\frac{1}{2} r \frac{\partial P}{\partial z}$$

Equation 55

The continuity equation in radial coordinate system assuming symmetry in the radial direction is Equation 56.

$$\frac{\partial v_r}{\partial r} + \frac{v_r}{r} + \frac{\partial v_z}{\partial z} = 0$$

Equation 56

And the general rheological equation relating stress and strain is in Equation 57.

$$f(\tau) = -\frac{\partial v_z}{\partial r}$$

Equation 57

Starting with Equation 56, first take a partial derivative of the equation with respect to radius. After changing the order of differentiation (assuming continuity) the last expression contains the term for shear rate in Equation 57. This expression is then integrated twice with respect to the radius to give an integral that equals to the wall velocity in Equation 58.

$$z\dot{R}R = \int_{R_{crit}}^{R} r(r - R_{crit}) f\left(-\frac{1}{2} r \frac{\partial P}{\partial z}\right) dr$$

Equation 58

Here the value R is the radius at the walls, and R_{crit} is the critical radius for which the gel starts to move. This is defined in Equation 59.

$$R_{crit} = \frac{2\tau_0}{\frac{\partial P}{\partial z}}$$

Equation 59

The constitutive model for a Carreau-like equation can be plugged into Equation 58, the result after a series of algebraic steps is an inverse function relating the pressure gradient to position Equation 60.

$$f^{-1}(y) = g(y) = z = \frac{1}{\dot{R}R}\left[\frac{\frac{\partial P}{\partial z}}{m_0}\left(\frac{1}{8}R^4 - \frac{1}{6}R^3 R_{crit} + \frac{1}{24}{R_{crit}}^4\right)\right.$$
$$+\frac{\tau_0}{m_0}\left(-\frac{1}{3}R^3 + \frac{1}{2}R^2 R_{crit} - \frac{1}{6}{R_{crit}}^3\right)$$
$$\left.+\left(\frac{\frac{1}{2}R\frac{\partial P}{\partial z} - \tau_0}{m}\right)^{\frac{1}{n}}\left(\frac{n}{n+1}\right)(R - R_{crit})^2\left(3R - \frac{3n+2}{2n+1}R_{crit}\right)\right]$$

Equation 60

This equation can then be plugged into the integral for total force applied by the wall in Equation 61.

$$\frac{F}{4\pi R} = \int_0^{\frac{\partial P}{\partial z}(z=L)} \frac{1}{2}L^2 - \frac{1}{2}[g(y)]^2\,dy$$

Equation 61

Appendix B: Model of Franz Cell and Gel/Tissue Permeability Assays

Franz cell and permeability assays are often used in the design process of microbicide products. However the results in most experiments are simply the concentration or transport rate observed without any further analysis. Interpretation of the results is typically that the formulation is able to deliver adequate amount of drug under these conditions, but with modeling key transport parameters such as the diffusion coefficient and partition coefficient could be estimated. This information for a variety of drugs and dosage forms can then be used in transport models defined in the previous chapters.

In the Franz cell assay, a gel or other dosage form containing the drug is placed over a membrane separating it from a sink with volume several orders of magnitude larger than the applied dosage. Measurements are then made for the concentration in the sink as a function of time. For the tissue permeability assay, the setup is similar to a normal Franz cell, except the dosage form is placed on top of the tissue which is then separated on the other side by a membrane and the sink. The sink concentrations are measured as well as the tissue concentration which could be taken at select times.

The geometry of the problem can be reduced to one-dimension because the rate limiting step in transport is approximately homogeneous through the membrane. The volume of each compartment can be divided by the area of the membrane to yield their

length in one-dimensions. For a sink this approximation can be made because generally the sink is well stirred so the transport within the compartment can be assumed as instantaneous.

Transport in both tissue and gel compartments follow a simple diffusive process with a constant diffusion coefficient. Without a convective force, natural thermal driven diffusion should be the predominant method of transport. Spatial variations in the tissue should be small compared to the thickness of tissue explants. The previous model of the tissue includes separate epithelial and stromal layers, but in this problem such differentiation cannot be measured, thus only an effective diffusion coefficient for the entire mucosal layer can be calculated.

This model is solved by an explicit finite difference method. With diffusion equation defined in Equation 7. The boundary conditions are no flux at the top end of the model with numerical solution defined by Equation 9, internal boundaries with partition coefficients are defined in Equation 10. The boundary between the gel/tissue and the membrane is more complex, the membrane is assumed to be in quasi steady state. The boundary at the gel or tissue side is defined in Equation 62.

$$C_{i+1} = \frac{C_{i-1} + \frac{2dxD_m\phi\Phi_2}{D_g h_m} C_b}{1 + \frac{2dxD_m\phi\Phi_1}{D_g h_m}}$$

Equation 62

In the above equation, a phantom point C_{i+1} beyond the grid is defined by another concentration C_{i-1} two steps before, the concentration in the sink or bath compartment C_b, the physical spacing dx, area fraction of pores ϕ, diffusion coefficient for the gel D_g, diffusion coefficient for the membrane D_m, the membrane thickness h_m, partition coefficient between membrane and the gel Φ_1, and the partition coefficient between membrane and the bath Φ_2. This equation is derived by equating the flux on both side of the membrane and solving for the effective concentration on each side assuming a steady state linear concentration profile within the membrane. In the equation, if assuming the two partition coefficients are similar, then a dimensionless number emerges which is independent of the concentration. This dimensionless number represents the value between two extremes. If it is close to zero then the membrane is impermeable or no flux, and if the value is very large, then it is effectively a concentration boundary.

Results for the Franz Cell model include concentration in the bath compartment over time under variation of different parameters in Figure 57. The plots are normalized by the total mass of drug applied. The variations are in gel diffusion coefficient, partition coefficient between gel and the bath, size of the gel, and size of the bath compartments. These four parameters represent the common factors that can vary in a Franz Cell experiment.

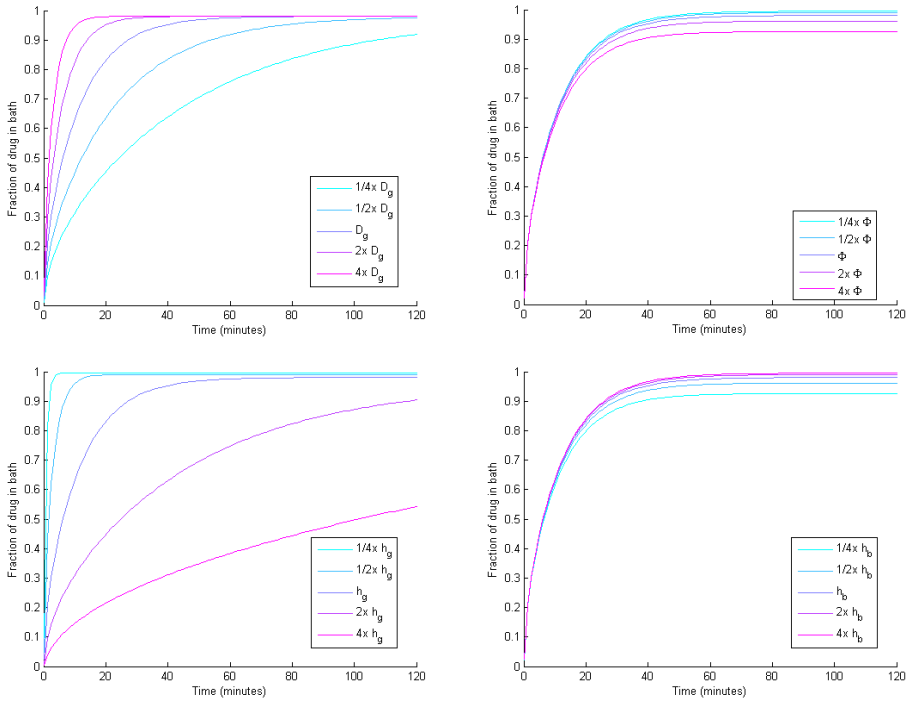

Figure 57: Fraction of drug found in the bath compartment of Franz cell assay, with variation in gel diffusion coefficient, partition coefficient, size of gel, and size of bath compartment over 2 hours.

Both diffusion coefficient in the gel and the size of the gel strongly influences the transport to the bath compartment. The size of the bath and the partition coefficient has negligible effects, especially at short times. This is due to the fact that the bath is already large enough to contribute a negligible amount of concentration even when saturated, so a size variation from a quarter to four times the original will not make a significant difference. The parameters gel size, partition coefficient, and bath size do however contribute to the steady state concentration measured. This steady state is simply a ratio of the size of the two compartments modified by the partition coefficient.

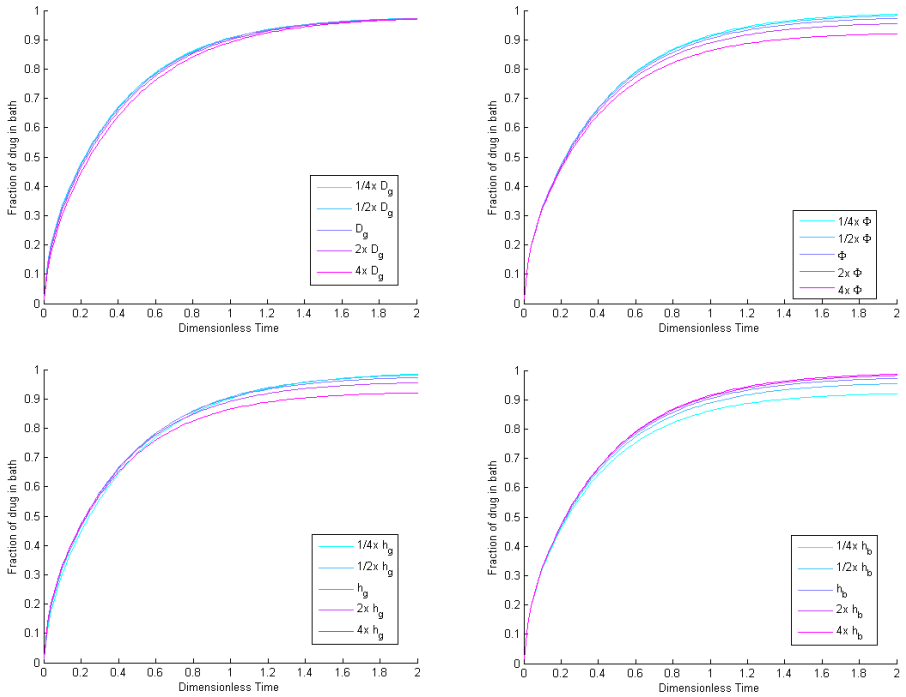

Figure 58: Fraction of drug found in the bath compartment of Franz cell assay, with variation in gel diffusion coefficient, partition coefficient, size of gel, and size of bath compartment over 2 hours non-dimensionalized by h_g^2/D_g.

The results of concentration versus time can also be plotted in terms of the dimensionless time in Figure 58. This time is the ratio of the gel height squared divided by the gel diffusion coefficient, the gel compartment is chosen because it's the rate limiting factor in transport. The non-dimensionalized curves are all very similar to each other, which gave further indication that the transport is dominated by the gel compartment. Like the dimensionalized version, steady state concentration is slightly altered by changing the partition coefficient and the size of each compartment.

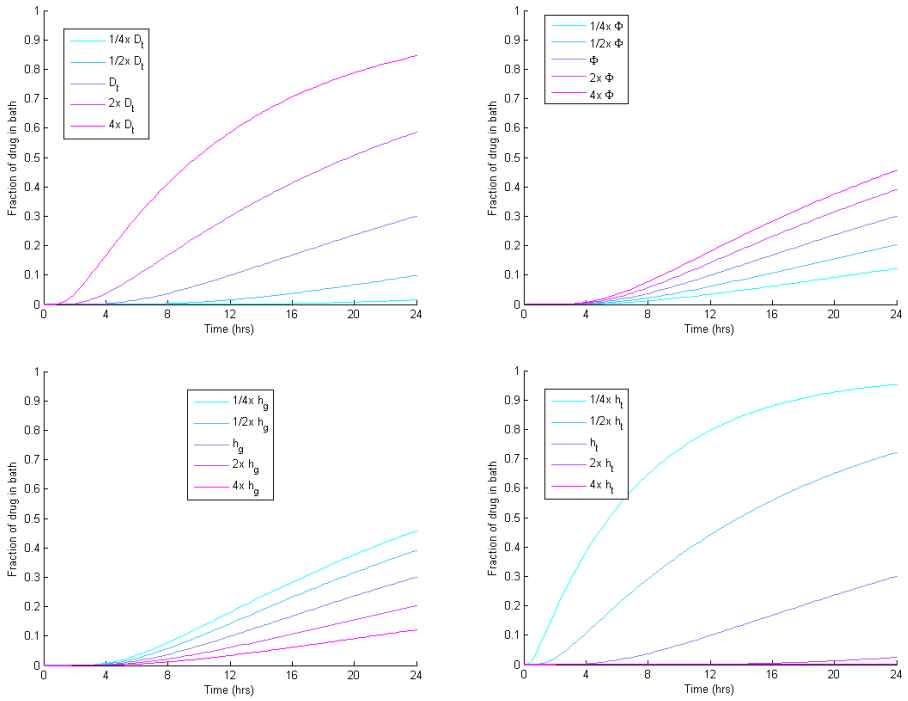

Figure 59: Fraction of drug found in the bath compartment of Gel/Tissue assay, with variation in tissue diffusion coefficient, partition coefficient, size of gel, and size of tissue compartment over 24 hours.

In the Gel/Tissue assay (Figure 59), all four variables, the diffusion in tissue, partition coefficient between gel and tissue, the size of the gel and tissue compartments all have a big effect on transport. Diffusion coefficient in the gel now is negligible since it's not the rate limiting step. Unlike the plots for the basic Franz Cell model where transport is dependent primarily on gel thickness and diffusion coefficient, here all four factors are important, which means there is no straightforward non-dimensionalization involving all four variables. The results indicate tissue thickness and diffusion coefficient are more important than gel thickness and the partition coefficient.

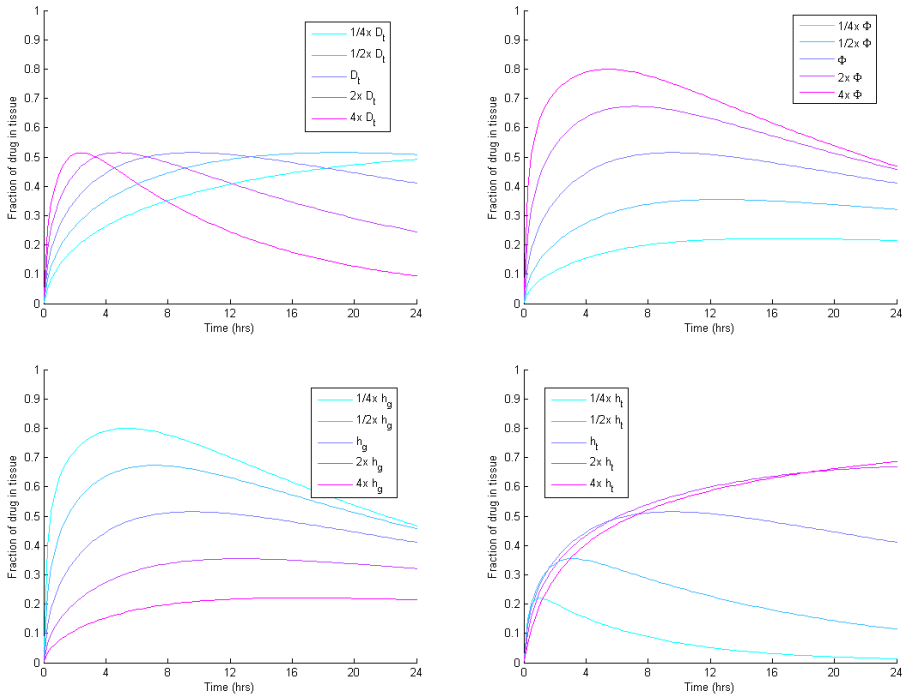

Figure 60: Fraction of drug found in the tissue compartment of Gel/Tissue assay, with variation in tissue diffusion coefficient, partition coefficient, size of gel, and size of tissue compartment over 24 hours.

Proportion of drug found in the tissue compartment is plotted in Figure 60. Once again all four factors are important to transport. Interestingly tissue diffusion coefficient and tissue thickness both alter the shape of the curve, with a slower diffusion or thicker tissue retaining the most drug even after 24 hours. While the parameters for partition coefficient and gel thickness changes the maximum height of the tissue curve. Experimentally the unknowns are tissue diffusion coefficient and the partition coefficient. Contribution by those two factors can be separated by using the shape of the curve to approximate the diffusion coefficient and then using the maximum concentration to find the partition coefficient.

Model of Franz Cell and Tissue Permeability assays is able to compute the key parameters in drug delivery in the diffusion coefficient and the partition coefficient. This information can enhance the interpretation of these assays and together with mechanic models of drug delivery created earlier, is able to predict drug delivery and efficacy of new microbicide formulations. Due to the destructive nature of the measurement, tissue concentrations are usually performed at a predetermined time. Models of concentration profile in the tissue can gave information on how to best pick the time to take biopsy measurements. Ideally one time point should be picked near the expected maximum concentration, while both the rise and decline of the concentration profile should be included as well. Overall this method can greatly enhance the information gained from Franz Cell and Tissue Permeability assays, which leads to a more efficient process in microbicide design.

References

1. Akil, A., M. A. Parniak, C. S. Dezzutti, B. J. Moncla, M. R. Cost, M. Li and L. C. Rohan. *Development and characterization of a vaginal film containing dapivirine, a non-nucleoside reverse transcriptase inhibitor (NNRTI), for prevention of HIV-1 sexual transmission*. Drug Delivery and Translational Research. 1:209-222, 2011.

2. Amico, K. R., L. Mansoor, A. Corneli, K. Torjesen and A. Straten. *Adherence Support Approaches in Biomedical HIV Prevention Trials: Experiences, Insights and Future Directions from Four Multisite Prevention Trials*. AIDS Behav. 17:2143-2155, 2013.

3. Anderson, P. L., J. J. Kiser, E. M. Gardner, J. E. Rower, A. Meditz and R. M. Grant. *Pharmacological considerations for tenofovir and emtricitabine to prevent HIV infection*. The Journal of antimicrobial chemotherapy. 66:240-50, 2011.

4. Baeten, J. M., T. Palanee-Phillips, E. R. Brown, K. Schwartz, L. E. Soto-Torres, V. Govender, N. M. Mgodi, F. Matovu Kiweewa, G. Nair, F. Mhlanga, S. Siva, L.-G. Bekker, N. Jeenarain, Z. Gaffoor, F. Martinson, B. Makanani, A. Pather, L. Naidoo, M. Husnik, B. A. Richardson, U. M. Parikh, J. W. Mellors, M. A. Marzinke, C. W. Hendrix, A. van der Straten, G. Ramjee, Z. M. Chirenje, C. Nakabiito, T. E. Taha, J. Jones, A. Mayo, R. Scheckter, J. Berthiaume, E. Livant, C. Jacobson, P. Ndase, R. White, K. Patterson, D. Germuga, B. Galaska, K. Bunge, D. Singh, D. W. Szydlo, E. T. Montgomery, B. S. Mensch, K. Torjesen, C. I. Grossman, N. Chakhtoura, A. Nel, Z. Rosenberg, I. McGowan and S. Hillier. *Use of a Vaginal Ring Containing Dapivirine for HIV-1 Prevention in Women*. New England Journal of Medicine. 2016.

5. Ball, C., E. Krogstad, T. Chaowanachan and K. A. Woodrow. *Drug-Eluting Fibers for HIV-1 Inhibition and Contraception*. PLoS One. 7:e49792, 2012.

6. Balzarini, J. and L. Van Damme. *Microbicide drug candidates to prevent HIV infection*. Lancet. 369:787-797, 2007.

7. Barnhart, K. T., A. Izquierdo, E. S. Pretorius, D. M. Shera, M. Shabbout and A. Shaunik. *Baseline dimensions of the human vagina*. Human Reproduction. 21:1618-1622, 2006.

8. Barnhart, K. T., K. Timbers, E. S. Pretorius, K. Lin and A. Shaunik. *In vivo assessment of NuvaRing® placement*. Contraception. 72:196-199, 2005.

9. Bessinger, R., P. Akwara and D. Halperin. *Sexual behavior HIV and fertility trends: a comparative analysis of six countries. Phase I of the ABC study*. 2003.

10. Billich, C. O. and R. Levitan. *Effects of sodium concentration and osmolality on water and electrolyte absorption from the intact human colon*. Journal of Clinical Investigation. 48:1336, 1969.

11. Blakney, A. K., C. Ball, E. A. Krogstad and K. A. Woodrow. *Electrospun fibers for vaginal anti-HIV drug delivery*. Antivir Res. 100:S9-S16, 2013.

12. Blakney, A. K., E. A. Krogstad, Y. H. Jiang and K. A. Woodrow. *Delivery of multipurpose prevention drug combinations from electrospun nanofibers using composite microarchitectures*. International journal of nanomedicine. 9:2967, 2014.

13. Choy, Y. B. and M. R. Prausnitz. *The rule of five for non-oral routes of drug delivery: ophthalmic, inhalation and transdermal*. Pharmaceutical Research. 28:943-948, 2011.

14. Chuchuen, O., M. H. Henderson, M. G. Sandros, A. D. M. Kashuba and D. F. Katz. *Transport and Transport Properties of Tenofovir from Microbicide Gels into Vaginal Tissue: Analysis Using Raman Spectroscopy*. Aids Research and Human Retroviruses. 30:A59-A60, 2014.

15. Chuchuen, O., M. H. Henderson, C. Sykes, M. S. Kim, A. D. Kashuba and D. F. Katz. *Quantitative analysis of microbicide concentrations in fluids, gels and tissues using confocal Raman spectroscopy*. PLoS One. 8:e85124, 2013.

16. Clark, J. T., M. R. Clark, N. B. Shelke, T. J. Johnson, E. M. Smith, A. K. Andreasen, J. S. Nebeker, J. Fabian, D. R. Friend and P. F. Kiser. *Engineering a segmented dual-reservoir polyurethane intravaginal ring for simultaneous prevention of HIV transmission and unwanted pregnancy*. 2014.

17. Clark, M. R., M. M. Peet, S. Davis, G. F. Doncel and D. R. Friend. *Evaluation of Rapidly Disintegrating Vaginal Tablets of Tenofovir, Emtricitabine and Their Combination for HIV-1 Prevention*. Pharmaceutics. 6:616-631, 2014.

18. Cutler, D. J. *Linear systems analysis in pharmacokinetics*. Journal of pharmacokinetics and biopharmaceutics. 6:265-282, 1978.

19. das Neves, J., R. Palmeira-de-Oliveira, A. Palmeira-de-Oliveira, F. Rodrigues and B. Sarmento. *Vaginal mucosa and drug delivery*. Mucoadhesive Materials and Drug Delivery Systems, John Wiley & Sons Inc, New York. 99-131, 2014.

20. Devlin, B., J. Nuttall, S. Wilder, C. Woodsong and Z. Rosenberg. *Development of dapivirine vaginal ring for HIV prevention*. Antivir Res. 100:S3-S8, 2013.

21. Dezzutti, C. S., L. C. Rohan, L. Wang, K. Uranker, C. Shetler, M. Cost, J. D. Lynam and D. Friend. *Reformulated tenofovir gel for use as a dual compartment microbicide*. Journal of Antimicrobial Chemotherapy. 67:2139-2142, 2012.

22. Fan, M., L. Ferguson, L. Rohan, L. Meyn and S. Hillier. *P2-S9. 06 Vaginal film microbicides for HIV prevention: a mixed methods study of women's preferences*. Sexually Transmitted Infections. 87:A263-A263, 2011.

23. Faundes, A., V. Brache and F. Alvarez. *Pros and cons of vaginal rings for contraceptive hormone delivery*. Am J Drug Deliv. 2:241-250, 2004.

24. Fetherston, S. M., P. Boyd, C. F. McCoy, M. C. McBride, K.-L. Edwards, S. Ampofo and R. K. Malcolm. *A silicone elastomer vaginal ring for HIV prevention containing two microbicides with different mechanisms of action*. European Journal of Pharmaceutical Sciences. 48:406-415, 2013.

25. Gao, Y. and D. F. Katz. *Multicompartmental Pharmacokinetic Model of Tenofovir Delivery by a Vaginal Gel*. PLoS One. 8:e74404, 2013.

26. Gao, Y., A. Yuan, O. Chuchuen, A. Ham, K. Yang and D. Katz. *Vaginal deployment and tenofovir delivery by microbicide gels*. Drug Delivery and Translational Research. 1-16, 2015.

27. Geonnotti, A. R., M. J. Furlow, T. Wu, M. G. DeSoto, M. H. Henderson, P. F. Kiser and D. F. Katz. *Measuring macrodiffusion coefficients in microbicide hydrogels via postphotoactivation scanning*. Biomacromolecules. 9:748-751, 2008.

28. Geonnotti, A. R. and D. F. Katz. *Compartmental Transport Model of Microbicide Delivery by an Intravaginal Ring*. Journal of Pharmaceutical Sciences. 99:3514-3521, 2010.

29. Geonnotti, A. R. and D. F. Katz. *Dynamics of HIV neutralization by a microbicide formulation layer: Biophysical fundamentals and transport theory*. Biophys J. 91:2121-2130, 2006.

30. Gómez, C. A. and B. V. Marin. *Gender, culture, and power: Barriers to HIV‐prevention strategies for women*. Journal of Sex Research. 33:355-362, 1996.

31. Grobler, A. and S. Abdool Karim. *Declining adherence is a more likely explanation than frailty of the apparent decline in efficacy in the CAPRISA 004 trial*. Aids. 26:2261; author reply 2262-3, 2012.

32. Gupta, G. R. *How men's power over women fuels the HIV epidemic: It limits women's ability to control sexual interactions*. BMJ: British Medical Journal. 324:183, 2002.

33. Haaland, R. E., T. Evans-Strickfaden, A. Holder, C.-P. Pau, J. M. McNicholl, S. Chaikummao, W. Chonwattana and C. E. Hart. *UC781 Microbicide Gel Retains Anti-HIV Activity in Cervicovaginal Lavage Fluids Collected following Twice-Daily Vaginal Application*. Antimicrob Agents Ch. 56:3592-3596, 2012.

34. Hacker, M., W. S. Messer II and K. A. Bachmann. *Pharmacology: principles and practice*. Academic Press. 2009.

35. Ham, A., W. Lustig, S. Nugent, J. Peters, D. Katz, C. Shelter, C. Dezzutti, A. Boczar, K. Buckheit and R. Buckheit. *Formulation development of the DuoGel: a dual chamber vaginal/rectal anti-HIV microbicide gel*. 2013.

36. Ham, A. S., L. C. Rohan, A. Boczar, L. Yang, K. W. Buckheit and R. W. Buckheit Jr. *Vaginal film drug delivery of the pyrimidinedione IQP-0528 for the prevention of HIV infection*. Pharmaceutical Research. 29:1897-1907, 2012.

37. Hawkins, T., W. Veikley, R. L. St Claire, B. Guyer, N. Clark and B. P. Kearney. *Intracellular pharmacokinetics of tenofovir diphosphate, carbovir triphosphate, and lamivudine triphosphate in patients receiving triple-nucleoside regimens*. Jaids-Journal Of Acquired Immune Deficiency Syndromes. 39:406-411, 2005.

38. Hawkins, T., W. Veikley, R. L. I. St. Claire, B. Guyer, N. Clark and B. P. Kearney. *Intracellular Pharmacokinetics of Tenofovir Diphosphate, Carbovir Triphosphate, and Lamivudine Triphosphate in Patients Receiving Triple-Nucleoside Regimens*. JAIDS Journal of Acquired Immune Deficiency Syndromes. 39:406-411, 2005.

39. Hendrix, C. W., Y. J. Cao and E. J. Fuchs. *Topical Microbicides to Prevent HIV: Clinical Drug Development Challenges*. Annual Review of Pharmacology and Toxicology. 49:349-375, 2009.

40. Hendrix, C. W., B. A. Chen, V. Guddera, C. Hoesley, J. Justman, C. Nakabiito, R. Salata, L. Soto-Torres, K. Patterson, A. M. Minnis, S. Gandham, K. Gomez, B. A. Richardson and N. N. Bumpus. *MTN-001: Randomized Pharmacokinetic Cross-Over Study Comparing Tenofovir Vaginal Gel and Oral Tablets in Vaginal Tissue and Other Compartments*. PLoS One. 8:e55013, 2013.

41. HIV/AIDS, J. U. N. P. o. *Global Report: UNAIDS Report on the Global AIDS Epidemic 2013. Geneva: UNAIDS, 2013*. According to the UNAIDS'estimate the number of new infections in the region increased from. 21:22,000-47,000, 2013.

42. Hladik, F. and T. Hope. *HIV infection of the genital mucosa in women*. Current HIV/AIDS Reports. 6:20-28, 2009.

43. Johnson, T. J., M. R. Clark, T. H. Albright, J. S. Nebeker, A. L. Tuitupou, J. T. Clark, J. Fabian, R. T. McCabe, N. Chandra and G. F. Doncel. *A 90-day tenofovir reservoir intravaginal ring for mucosal HIV prophylaxis*. Antimicrob Agents Ch. 56:6272-6283, 2012.

44. Karim, Q. A., C. Baxter and S. A. Karim. *Topical Microbicides—What's New?* JAIDS Journal of Acquired Immune Deficiency Syndromes. 63:S144-S149, 2013.

45. Karim, Q. A., S. S. A. Karim, J. A. Frohlich, A. C. Grobler, C. Baxter, L. E. Mansoor, A. B. Kharsany, S. Sibeko, K. P. Mlisana and Z. Omar. *Effectiveness and safety of tenofovir gel, an antiretroviral microbicide, for the prevention of HIV infection in women*. Science. 329:1168-1174, 2010.

46. Karim, Q. A., S. S. A. Karim, J. A. Frohlich, A. C. Grobler, C. Baxter, L. E. Mansoor, A. B. M. Kharsany, S. Sibeko, K. P. Mlisana, Z. Omar, T. N. Gengiah, S. Maarschalk, N. Arulappan, M. Mlotshwa, L. Morris, D. Taylor and C. T. Grp. *Effectiveness and Safety of Tenofovir Gel, an Antiretroviral Microbicide, for the Prevention of HIV Infection in Women*. Science. 329:1168-1174, 2010.

47. Kearney, B. P., J. F. Flaherty and J. Shah. *Tenofovir disoproxil fumarate - Clinical pharmacology and pharmacokinetics*. Clin Pharmacokinet. 43:595-612, 2004.

48. Kieweg, S. L. and D. F. Katz. *Interpreting properties of microbicide drug delivery gels: Analyzing deployment kinetics due to squeezing*. Journal of Pharmaceutical Sciences. 96:835-850, 2007.

49. Kieweg, S. L. and D. F. Katz. *Squeezing flows of vaginal gel formulations relevant to microbicide drug delivery*. Journal of Biomechanical Engineering-Transactions of the Asme. 128:540-553, 2006.

50. Kiser, P. F., T. J. Johnson and J. T. Clark. *State of the art in intravaginal ring technology for topical prophylaxis of HIV infection*. Aids Rev. 14:62-77, 2012.

51. Kreiss, J., E. Ngugi, K. Holmes, J. Ndinya-Achola, P. Waiyaki, P. L. Roberts, I. Ruminjo, R. Sajabi, J. Kimata and T. R. Fleming. *Efficacy of nonoxynol 9 contraceptive sponge use in preventing heterosexual acquisition of HIV in Nairobi prostitutes*. Jama. 268:477-482, 1992.

52. Lai, B. E., M. H. Henderson, J. J. Peters, D. K. Walmer and D. F. Katz. *Transport Theory for HIV Diffusion through In Vivo Distributions of Topical Microbicide Gels*. Biophys J. 97:2379-2387, 2009.

53. Leriche, M., G. Devroede, G. Sanchez and J. Rossano. *Changes in the rectal mucosa induced by hypertonic enemas*. Dis Colon Rectum. 21:227-236, 1978.

54. Louissaint, N. A., Y. J. Cao, P. L. Skipper, R. G. Liberman, S. R. Tannenbaum, S. Nimmagadda, J. R. Anderson, S. Everts, R. Bakshi, E. J. Fuchs and C. W. Hendrix. *Single Dose Pharmacokinetics of Oral Tenofovir in Plasma, Peripheral Blood Mononuclear Cells, Colonic Tissue, and Vaginal Tissue*. Aids Research and Human Retroviruses. 29:1443-1450, 2013.

55. Magnin, A. and J. Piau. *Cone-and-plate rheometry of yield stress fluids. Study of an aqueous gel*. J Non-Newton Fluid. 36:85-108, 1990.

56. Maisel, K., S. Chattopadhyay, T. Moench, C. Hendrix, R. Cone, L. M. Ensign and J. Hanes. *Enema ion compositions for enhancing colorectal drug delivery*. J Control Release. 209:280-287, 2015.

57. Malcolm, R. K., A. D. Woolfson, C. F. Toner, R. J. Morrow and S. D. McCullagh. *Long-term, controlled release of the HIV microbicide TMC120 from silicone elastomer vaginal rings*. Journal of Antimicrobial Chemotherapy. 56:954-956, 2005.

58. Mansoor, L. E., Q. A. Karim, L. Werner, B. Madlala, N. Ngcobo, D. H. Cornman, K. R. Amico, J. Fisher, W. A. Fisher, K. M. Macqueen and S. S. Karim. *Impact of an adherence intervention on the effectiveness of tenofovir gel in the CAPRISA 004 trial*. AIDS Behav. 18:841-8, 2014.

59. Marrazzo, J., G. Ramjee, G. Nair, T. Palanee, B. Mkhize, C. Nakabiito, M. Taljaard, J. Piper, K. Gomez Feliciano and M. Chirenje. *Pre-exposure prophylaxis for HIV in women: daily oral tenofovir, oral tenofovir/emtricitabine, or vaginal tenofovir gel in the VOICE Study (MTN 003)*. 3-6, 2013.

60. Mathworks. *MATLAB*. MathWorks Inc. 2010.

61. Minnis, A. M., S. Gandham, B. A. Richardson, V. Guddera, B. A. Chen, R. Salata, C. Nakabiito, C. Hoesley, J. Justman and L. Soto-Torres. *Adherence and acceptability in MTN 001: a randomized cross-over trial of daily oral and topical tenofovir for HIV prevention in women*. AIDS Behav. 17:737-747, 2013.

62. Minoguchi, R., T. Osborn, H. Hong, S. Owens and B. Haridas. *Reverse finite element analysis and modeling of biomechanical properties of internal tissues*. Google Patents. 2007.

63. Morrow, K. M., J. L. Fava, R. K. Rosen, S. Vargas, J. G. Shaw, E. M. Kojic, P. F. Kiser, D. R. Friend, D. F. Katz and P. L. S. Team. *Designing Preclinical Perceptibility Measures to Evaluate Topical Vaginal Gel Formulations: Relating User Sensory Perceptions and Experiences to Formulation Properties*. Aids Research and Human Retroviruses. 30:78-91, 2014.

64. Moss, J. A., A. M. Malone, T. J. Smith, I. Butkyavichene, C. Cortez, J. Gilman, S. Kennedy, E. Kopin, C. Nguyen and P. Sinha. *Safety and pharmacokinetics of intravaginal rings delivering tenofovir in pig-tailed macaques*. Antimicrob Agents Ch. 56:5952-5960, 2012.

65. Nagasawa, M. *Schrödinger equations and diffusion theory*. Springer. 2012.

66. Nel, A., S. Smythe, K. Young, K. Malcolm, C. McCoy, Z. Rosenberg and J. Romano. *Safety and Pharmacokinetics of Dapivirine Delivery From Matrix and Reservoir Intravaginal Rings to HIV-Negative Women*. JAIDS Journal of Acquired Immune Deficiency Syndromes. 51:416-423 10.1097/QAI.0b013e3181acb536, 2009.

67. Nivatvongs, S., H. S. Stern and D. S. Fryd. *The length of the anal canal*. Dis Colon Rectum. 24:600-601, 1981.

68. Ovalle, W. K. and P. C. Nahirney. *Netter's essential histology*. Elsevier Health Sciences. 2013.

69. Owen, D. H. and D. F. Katz. *A vaginal fluid simulant*. Contraception. 59:91-95, 1999.

70. Owen, D. H., J. J. Peters and D. F. Katz. *Rheological properties of contraceptive gels*. Contraception. 62:321-326, 2000.

71. Patton, D. L., S. S. Thwin, A. Meier, T. M. Hooton, A. E. Stapleton and D. A. Eschenbach. *Epithelial cell layer thickness and immune cell populations in the normal human vagina at different stages of the menstrual cycle*. American Journal of Obstetrics and Gynecology. 183:967-973, 2000.

72. Pendergrass, P. B., M. W. Belovicz and C. A. Reeves. *Surface area of the human vagina as measured from vinyl polysiloxane casts*. Gynecologic and obstetric investigation. 55:110-113, 2003.

73. Rees, H., S. Delany-Moretlwe, D. Baron, C. Lombard, G. Gray, L. Myer, R. Panchia, J. Schwartz and G. Doncel. *FACTS 001 Phase III Trial of Pericoital Tenofovir 1% Gel for HIV Prevention in Women* 26LB, 2015.

74. Ritschel, W. A. *Handbook of basic pharmacokinetics*. 1976.

75. Robbins, B. L., R. V. Srinivas, C. Kim, N. Bischofberger and A. Fridland. *Anti-Human Immunodeficiency Virus Activity and Cellular Metabolism of a Potential Prodrug of the Acyclic Nucleoside Phosphonate 9-R-(2-Phosphonomethoxypropyl)adenine (PMPA), Bis(isopropyloxymethylcarbonyl)PMPA*. Antimicrob Agents Ch. 42:612-617, 1998.

76. Rohan, L. C., B. J. Moncla, R. P. Kunjara Na Ayudhya, M. Cost, Y. Huang, F. Gai, N. Billitto, J. D. Lynam, K. Pryke, P. Graebing, N. Hopkins, J. F. Rooney, D. Friend and C. S.

Dezzutti. *In Vitro and Ex Vivo Testing of Tenofovir Shows It Is Effective As an HIV-1 Microbicide*. PLoS One. 5:e9310, 2010.

77. Saltzman, W. M. *Drug delivery : engineering principles for drug therapy*. Oxford University Press. xi, 372 p., 2001.

78. Schwartz, J. L., W. Rountree, A. D. M. Kashuba, V. Brache, M. D. Creinin, A. Poindexter and B. P. Kearney. *A Multi-Compartment, Single and Multiple Dose Pharmacokinetic Study of the Vaginal Candidate Microbicide 1% Tenofovir Gel*. PLoS One. 6:e25974, 2011.

79. Semmelink, H. J. F., P. C. M. de Wilde, J. C. van Houwelingen and G. P. Vooijs. *Histomorphometric study of the lower urogenital tract in pre- and post-menopausal women*. Cytometry. 11:700-707, 1990.

80. Shattock, R. J. and J. P. Moore. *Inhibiting sexual transmission of HIV-1 infection*. Nat Rev Micro. 1:25-34, 2003.

81. Shaw, J.-P., C. Sueoka, R. Oliyai, W. Lee, M. Arimilli, C. Kim and K. Cundy. *Metabolism and Pharmacokinetics of Novel Oral Prodrugs of 9-[(R)-2-(phosphonomethoxy)propyl]adenine (PMPA) in Dogs*. Pharmaceutical Research. 14:1824-1829, 1997.

82. Singer, R., P. Mawson, N. Derby, A. Rodriguez, L. Kizima, R. Menon, D. Goldman, J. Kenney, M. Aravantinou, S. Seidor, A. Gettie, J. Blanchard, M. Piatak, J. D. Lifson, J. A. Fernández-Romero, M. Robbiani and T. M. Zydowsky. *An Intravaginal Ring That Releases the NNRTI MIV-150 Reduces SHIV Transmission in Macaques*. Science Translational Medicine. 4:150ra123, 2012.

83. Smith, J. M., R. Rastogi, R. S. Teller, P. Srinivasan, P. M. Mesquita, U. Nagaraja, J. M. McNicholl, R. M. Hendry, C. T. Dinh and A. Martin. *Intravaginal ring eluting tenofovir disoproxil fumarate completely protects macaques from multiple vaginal simian-HIV challenges*. Proceedings of the National Academy of Sciences. 110:16145-16150, 2013.

84. Stone, A. *Microbicides: A new approach to preventing HIV and other sexually transmitted infections*. Nat Rev Drug Discov. 1:977-985, 2002.

85. Szeri, A. J., S. C. Park, S. Verguet, A. Weiss and D. F. Katz. *A model of transluminal flow of an anti-HIV microbicide vehicle: Combined elastic squeezing and gravitational sliding*. Phys Fluids. 20:083101, 2008.

86. Tanaka, E., T. Noguchi, K. Nagai, Y. Akashi, K. Kawahara and T. Shimada. *Morphology of the epithelium of the lower rectum and the anal canal in the adult human*. Medical molecular morphology. 45:72-79, 2012.

87. Tasoglu, S., D. F. Katz and A. J. Szeri. *Transient spreading and swelling behavior of a gel deploying an anti-HIV topical microbicide*. J Nonnewton Fluid Mech. 187-188:36-42, 2012.

88. Tasoglu, S., S. C. Park, J. J. Peters, D. F. Katz and A. J. Szeri. *The consequences of yield stress on deployment of a non-Newtonian anti-HIV microbicide gel*. J Non-Newton Fluid. 166:1116-1122, 2011.

89. Tasoglu, S., J. J. Peters, S. C. Park, S. Verguet, D. F. Katz and A. J. Szeri. *The effects of inhomogeneous boundary dilution on the coating flow of an anti-HIV microbicide vehicle*. Phys Fluids. 23:093101, 2011.

90. Thurman, A. R., M. R. Clark, J. A. Hurlburt and G. F. Doncel. *Intravaginal rings as delivery systems for microbicides and multipurpose prevention technologies*. Int J Womens Health. 5:695-708, 2013.

91. Truskey, G. A., F. Yuan and D. F. Katz. *Transport phenomena in biological systems*. Pearson/Prentice Hall Upper Saddle River NJ:. 2004.

92. Van Niekerk, N., J. Nuttall, S. Zeiser and A. Nel. *Population Pharmacokinetic Modelling of Dapivirine*. Aids Research and Human Retroviruses. 30:A38-A39, 2014.

93. Vermund, S. H. and L. Van Damme. *HIV Prevention in Women: Next Steps*. Science. 331:284, 2011.

94. Vourvahis, M., H. L. Tappouni, K. B. Patterson, Y. C. Chen, N. L. Rezk, S. A. Fiscus, B. P. Kearney, J. E. Rooney, J. Hui, M. S. Cohen and A. D. M. Kashubal. *The pharmacokinetics and viral activity of tenofovir in the male genital tract*. Jaids-Journal Of Acquired Immune Deficiency Syndromes. 47:329-333, 2008.

95. Weber, J., K. Desai, J. Darbyshire and P. on behalf of the Microbicides Development. *The Development of Vaginal Microbicides for the Prevention of HIV Transmission*. Plos Med. 2:e142, 2005.

96. Yang, K.-H., J. L. Schwartz, C. Sykes, G. F. Doncel and A. D. Kashuba. *Population Pharmacokinetic Model of Vaginal Tenofovir 1% Gel in the Cervicovaginal Fluid*. Aids Research and Human Retroviruses. 30:A38-A38, 2014.

Biography

Yajing Gao was born on November 16th, 1986 in Beijing China. After living for a few years in the city he moved around to a number of places including Vancouver Canada, Odense Denmark, and Rostock Germany before settling in Chapel Hill North Carolina.

He attended high school at East Chapel Hill High and then the North Carolina School of Science and Mathematics before moving down Ninth Street to Duke University. Graduated in 2009, he earned a degree in Bachelor of Science in Engineering with majors in Biomedical Engineering, Mechanical Engineering, Chemistry, and Mathematics. During his undergraduate career he worked on a number of research projects in chemistry and mathematics.

While enrolled in the PhD program at Duke, he enjoyed watching the Men's Basketball team winning two national championships. In addition to being a member of Duke's yearbook team as Managing Editor and a photographer, he also volunteers for the annual Duke Math Meet in addition to maintaining the website and database as a part of Duke University Math Union. He was a member of the Engineering Graduate Student Council and the Biomedical Engineering Society.

His hobbies include cooking (particularly dumpling making), photography, and trip planning. His spare time is often spent pondering philosophical questions and logical paradoxes.

Publications:

1. Jarrett AM, Gao Y, Katz DF, Cogan NG, Hussaini MY *Sensitivity Analysis of a Pharmacokinetic Model of Vaginal Anti-HIV Microbicide Drug Delivery*. Journal of Pharmaceutical Sciences: In press, 2016.

2. Katz DF, Yuan A, Gao Y *Vaginal Drug Distribution Modeling*. Advanced Drug Delivery Reviews: 2-13, 2015.

3. Gao Y, Yuan A, Chuchuen O, Ham A, Yang K, et al. *Vaginal deployment and Tenofovir Delivery by Microbicide Gels*. Drug Delivery and Translational Research: 1-16, 2015.

4. Gao Y, Katz DF *Multicompartmental Pharmacokinetic Model of Tenofovir Delivery by a Vaginal Gel*. PLoS One 8: e74404, 2013.

5. Katz DF, Gao Y, Kang M *Using Modeling to Help Understand Vaginal Microbicide Functionality and Create Better Products*. Drug Delivery and Translational Research 1: 256-276, 2011.